Ultrasonic metal welding

ULTRASONIC METAL WELDING

J. L. HARTHOORN

ULTRASONIC METAL WELDING

PROEFSCHRIFT

TER VERKRIJGING VAN DE GRAAD VAN DOCTOR
IN DE TECHNISCHE WETENSCHAPPEN
AAN DE TECHNISCHE HOGESCHOOL EINDHOVEN
OP GEZAG VAN DE RECTOR MAGNIFICUS,
PROF. DR. P. VAN DER LEEDEN,
VOOR EEN COMMISSIE AANGEWEZEN DOOR HET
COLLEGE VAN DEKANEN IN HET OPENBAAR
TE VERDEDIGEN OP VRIJDAG 14 APRIL 1978 TE 16.00 UUR

DOOR

JOHANNES LEENDERT HARTHOORN

GEBOREN TE 'S-HEERENHOEK

DIT PROEFSCHRIFT IS GOEDGEKEURD DOOR DE PROMOTOREN

PROF. DR. P.C. VEENSTRA EN PROF. IR. B.L. TEN HORN

CONTENTS

LIST OF SYMBOLS

a	ratio ξ/ξ_s	(–)
a	acceleration	($m\,s^{-2}$)
A	area (cross section)	(m^2)
A_n	nominal area of contact	(m^2)
A_m	area of a microweld	(m^2)
A_r	area of real contact	(m^2)
A(t)	welded area after welding time t	(m^2)
$A(\infty)$	final value of the welded area	(m^2)
B	weighted sum of characteristic impedance (see eq. 3.21)	($kg\,s^{-1}$)
c	propagation velocity of longitudinal waves	($m\,s^{-1}$)
c	thermal capacity	($J\,kg^{-1}\,°K^{-1}$)
C	capacitance of the transducer	(F)
C	effective stress at $\bar{\delta} = 1$	(Nm^{-2})
D	diameter	(m)
E	energy dissipation per unit volume per oscillation	(Jm^{-3})
E	Young's modulus	(Nm^{-2})
F	force	(N)
F_a	alternating tangential force in subsonic welding	(N)
F_a	adhesion force	(N)
$F_b(t)$	breaking force in the tensile-shear test, of a weld produced in t sec.	(N)
$F_b(\infty)$	final value of the breaking force	(N)
F_c	clamping force	(N)
F_l	alternating force exerted on the load by the welding tip	(N)
F_n	force, normal to the plane of contact	(N)
F_s	force, tangential to the plane of contact	(N)
F_w	alternating tangential force in the welded interface	(N)
$F(\beta)$	error function	(–)
H_v	Vickers hardness	(Nm^{-2})
H	strength of a heat source; amount of heat	(J)
i	electric current (complex quantity)	(A)
j	imaginary unit	(–)
k	wave number	(m^{-1})
K	constant of the model	($m^{-1}\,s^{-1}$)
l	length of a waveguide section	(m)
l	average length of microwelds	(m)
L	inductance	(H)
m	work hardening exponent	(–)
M	mechanical transformation ratio	(–)
n	density of microwelds (per unit area)	(m^{-2})
N	number of microwelds	(–)
N	electromechanical transformation ratio	(Asm^{-1})

p	pressure, tensile stress, hardness	(Nm^{-2})
p_o	yield pressure	(Nm^{-2})
P	power	(W)
r	radius vector	(m)
R_e *)	electrical resistance	(Ω)
R_m *)	real part of mechanical impedance	($kg\,s^{-1}$)
R_d	dielectric loss resistance of the transducer	(Ω)
t	welding time	(s)
T	temperature	(°K)
T_w	temperature in the welding zone	(°K)
T_m	melting temperature	(°K)
U	energy dissipation per unit volume	(Jm^{-3})
v_l	velocity at the load (complex quantity)	($m\,s^{-1}$)
V	voltage at the transducers terminals (complex quantity)	(V)
W	intensity of a heat source	($W\,m^{-2}$)
W_{ab}	surface energy	(Jm^{-2})
x	ratio between the actual frequency ν and the resonance frequency ν_r	(–)
X *)	imaginary part of an impedance	($kg\,s^{-1}$)
Y	yield stress	(Nm^{-2})
z	axial coordinate	(m)
Z_e *)	electrical impedance (complex quantity)	(Ω)
Z_m *)	mechanical impedance (complex quantity)	($kg\,s^{-1}$)
γ	shear angle	(–)
$\underline{\gamma}$	surface energy	($J\,m^{-2}$)
$\bar{\delta}$	effective strain	(–)
λ	thermal conductivity	($Wm^{-2}\,°K^{-1}$)
λ	wavelength	(m)
λ_r	wavelength at resonance	(m)
ν	frequency	(s^{-1})
ν_r	resonant frequency (unloaded)	(s^{-1})
ν_{rl}	resonant frequency (under loaded conditions)	(s^{-1})
ξ	vibrational amplitude (of the welding tip)	(m)
ξ_s	relative vibrational displacement (slip) amplitude between the weld members	(m)
ρ	specific mass	($kg\,m^{-3}$)
σ	tensile stress	(Nm^{-2})
$\bar{\sigma}$	effective stress	(Nm^{-2})
σ_n	necking stress	(Nm^{-2})
τ	tangential or shear stress	(Nm^{-2})
τ_b	breaking stress	(Nm^{-2})
τ_n	stress at the onset of plastic instability in tensile shear testing	(Nm^{-2})

τ_W	alternating tangential stress amplitude in the welding zone	(Nm^{-2})
ω	angular frequency	(s^{-1})
ω_r	angular frequency at resonance	(s^{-1})

---

*) This quantity can have the following suffixes
- l : the quantity is related to the load
- w : the quantity is related to the waveguide system
- t : the quantity is related to the transducer.

1. INTRODUCTION

1.1. Ultrasonic metal welding

Ultrasonic metal welding is a technique suitable for joining both similar and dissimilar metal work pieces (1.1) or welding a piece of metal to a metallized substrate (1.2, 3) (ceramics or glass). The weld formation is caused by the application of external pressure and ultrasonic vibrations.

In order to give a general idea of the technique a short description is given of the fundamental parts of the welding equipment and the parameters involved. This is followed by a list of special characteristics of the process and finally some fields of application are mentioned.

Ultrasonic metal welding equipment consists of 3 fundamental parts (see fig. 1.1).

1. *The electrical part*
   a. a generator, producing an electrical signal (in general a sine wave), being the input signal for the amplifier
   b. a timing circuit, by which the required welding time can be preset
   c. an automatic frequency adjustment system, in order to maintain resonance conditions during the welding operation
   d. an amplifier, able to supply sufficient electrical power (to the electromechanical transducer).

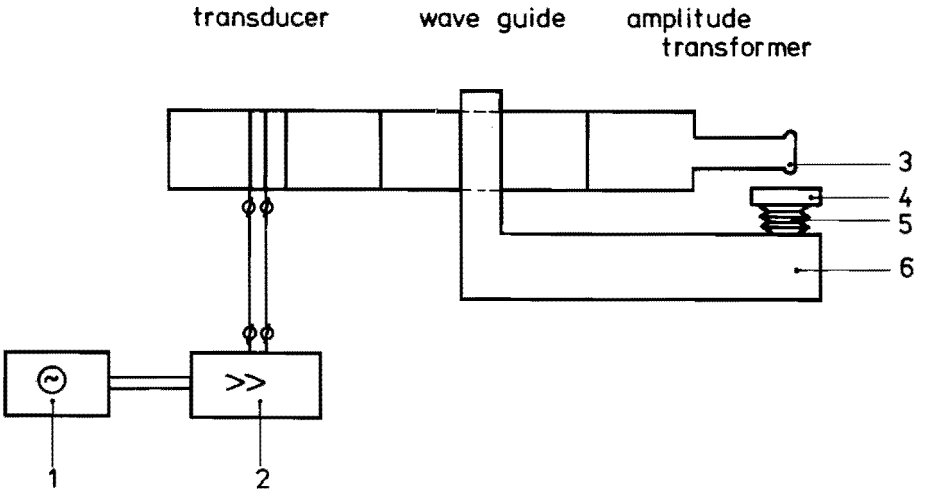

Fig. 1.1. Ultrasonic metal welding equipment, including
1. The electrical part: generator (1) and amplifier (2)
2. The electromechanical transducer
3. The mechanical part: wave guide and amplitude transformer with welding tip (3); an anvil (4); bellow (5) for applying the clamping force by air pressure; frame (6).

2. *The electromechanical transducer*
   This transducer converts the electrical power into mechanical vibrations. The transducer can be either of the magnetostrictive or the piezo-electric (1.4) type. The transducer is coupled to the waveguide system.
3. *The mechanical part*
   a. a waveguide system with an amplitude transformer. This system guides the mechanical vibration from the transducer to the work piece
   b. a welding tool or welding tip contracting the upper work piece. The welding tool is situated at one end of the waveguide system
   c. an anvil. The work pieces to be welded are clamped between the welding tool and the anvil
   d. a mechanical frame, on to which all parts are mounted.
      This includes a mechanism to clamp the work pieces between welding tool and anvil.

The most important parameters of the welding process are
1. The vibrational frequency, ranging between 10 kHz and 150 kHz. At the operating frequency the transducer and waveguide system (with welding tool) must be in resonance.
2. The vibrational amplitude ξ of the welding tip. This quantity ξ ranges roughly between 0.5 and 30 μm. The direction of vibration of the welding tool is parallel to the interface to be welded.
3. The duration of the welding operation, the welding time, ranges from 10 ms up to several seconds.
4. The clamping pressure in the weld area. This pressure equals approximately 0.1 to 0.3 times the Vickers hardness of the material to be welded.

The required values of the welding parameters (vibrational amplitude, welding time, clamping pressure) depend upon
1. The thickness of the work piece contacting the welding tip, i.e. the upper work piece.
2. The material properties (e.g. tensile strength, hardness) of the materials to be welded.

As to the geometry of the work pieces some remarks can be made. The upper work piece may be a wire, a foil, sheet or strip (thickness up to several millimeters). With regard to the lower work piece contacting the anvil there are no special requirements or limitations as to shape or dimensions, provided it can be positioned properly to the anvil.

The different types of welds, which can be produced are spot welds, line welds or ring welds (1.5). Using rotating discs as welding tool and anvil continuous seam welds can be made (1.5).

According to the Welding Handbook of the American Welding Society (1.6) almost any metal and alloy can be welded ultrasonically. This reference mentions: Al and its alloys; Cu and its alloys; iron and various types of steel; Ni, Ti, Zr and their various alloys; Au, Ag, Pt and alloys, refractory metals as Mo, Nb, Ta, W; Be, Re. *) In the literature most attention is paid to the welding of Al and Cu; for microelectronic applications Au and Al are used frequently.

Special characteristics of ultrasonic metal welding are
1. Metals with widely different melting points can be welded (e.g. Al to Cu).
2. Thin foils or wires can be welded to much thicker parts.
3. Temperature in the weld area is below the melting point of the welded material.
4. No fluxes or protective gas are needed.

The main applications are at present (1.7)
1. In microelectronics, wires and ribbons of Au, Al and Cu with a thickness ranging from 25 μm to 500 μm are welded ultrasonically to metallized substrates (1.8, 9);
2. Welding of Al and Cu in various applications, e.g. electrical leads, closure welds of tubes and cans, containing volatile or explosive substances.

1.2 Historical background

Initially ultrasound was applied to resistance spot welding, in order to refine the grain structure of the weld zone (1.10).
The first German patent in this field is from 1938 (1.11). The first author to report on welding by mechanical vibrations alone is Willrich (1950) (1.12). He mentions that using equipment designed to apply low frequency vibration to the welding zone of a resistance weld, a kind of cold welding occurred in the absence of any welding current.

Research workers in the U.S.A. followed the same trail. Starting with the application of ultrasound to resistance welding, they occasionally found that the application of ultrasonic energy alone could produce a weld (1.13, 14). The first report on "the application of ultrasonic energy to cold welding" appeared in 1953 (1.14).

---

*) The data from which weldability has been determined are not mentioned in the Welding Handbook. From our own experience we know that weldability of Mo and W is very poor. This list of materials should therefore be treated with caution.

1.3. Aim and contents of the present study

The central question of this study is: What kind of processes cause the formation of a weld in ultrasonic welding?
This question is asked in an industrial laboratory in order to understand e.g. the influence of process parameters and material properties on the strength (or quality) of an ultrasonic weld. This basic knowledge of the welding process is required for a better control of weld quality, which is important in highly mechanized mass production in order to assure a reproducible quality.

We will now give a description of the contents and the background thoughts of this thesis.

After the introduction in the present chapter, literature will be reviewed in chapter 2. This chapter will deal with

1. A description of the phenomena associated with ultrasonic metal welds (sec. 2.1 – 3).
2. Quantities measured during welding, including temperature and vibrational amplitude of the welding tip (sec. 2.4).
3. Mechanism of ultrasonic welding (sec. 2.5).

From the initial sections of chapter 2 it is evident that experimental data, available from the literature, are mainly related to mechanical strength of ultrasonic welds (tensile shear tests) and metallographic sections of welds. All these data refer to the final stage of a full grown weld; information about phenomena during the welding period is rare and no unanimous opinion exists as to the process of weld formation.

A discussion of the welding mechanism in ultrasonic welding is given in section 2.5. Welding by melting can be excluded on the basis of data from literature. Hence the remaining possibilities are either a thermal or a non-thermal (cold) solid state welding process. As to this no conclusion can be drawn from the literature.
As we are of the opinion that thermal processes do not primarily contribute to the formation of an ultrasonic weld (see chap. 5 and 6), we did not pay much attention to the literature concerning the temperature in the welding zone. Instead of this we studied the literature on metallic adhesion, as this is a cold solid state bonding process (sec. 2.5).

In chapter 3 welding and testing equipment will be described. This chapter includes a detailed theory of the ultrasonic vibrating system. The purpose of this theory is to find relationships between the mechanical impedance of the load at the welding tip and the electrical impedance at the transducer terminals. The mechanical impedance at the welding tip is the ratio of the alternating force exerted by the welding tip on the weld members and the velocity of the welding tip. The electrical impedance is the ratio of the current flowing through the transducer and the

voltage. The impedances are in general complex. This approach has the advantage that electrical measurements give information about mechanical quantities, which are difficult to measure in a direct way.

Chapter 4 deals with experiments concerning ultrasonic welding. The ultrasonic experiments were carried out in order to observe the phenomena during the welding period.
The first group of experiments was set up to study the growth of a weld from a few milliseconds after the beginning until the completion. This was done for aluminium, copper, nickel and steel, the vibrational amplitude being an experimental parameter (sec. 4.2).
In the second group of experiments the alternating force exerted by the welding tip was determined. This gives information about the area of real contact between the weld members (sec. 4.3).
In the last group of experiments the relative vibrational displacement between the welding surfaces was studied (sec. 4.4).

Chapter 5 deals with experiments concerning subsonic welding. Subsonic welding is a slow motion model for ultrasonic welding; relative motion (vibrational amplitude) and contact pressure being the same as in ultrasonic welding. In subsonic welding the vibrational frequency is 30 Hz instead of 20 kHz in ultrasonic welding. The idea of subsonic welding emerged after a study of fretting. *)
Welds produced by subsonic welding are very similar to ultrasonic welds. Therefore we assume that the welding mechanism of both subsonic and ultrasonic welding is the same. As temperature rise is negligible in subsonic welding, ultrasonic welding may also be a non thermal solid state welding process.

In chapter 6 a model, based on the present experiments and information from the literature, is described. The model deals with the phenomena in the contact area between the weld members. In this area weld formation occurs. Mechanics of the process outside the contact area and welding zone are not discussed in this thesis.

---

*) Fretting occurs when two metallic surfaces are in contact and perform a vibrational relative movement. Hurricks (1.15) describes that in this process adhesion junctions are initially formed. In the next stage these junctions are broken and wear debris is formed.

In the model the following subjects are discussed

1. The real contact in the welding zone.
2. The formation of microwelds, as a consequence of the relative vibrational motion of the contacting surfaces. Microwelds are small welded areas in the contact surface between the two weld members.
3. The increase in the number of microwelds, resulting in welding over the entire contact area.

An outline of the model is given in section 6.1. Finally a verification of the model and a discussion will be given.

Results and conclusions are summarized in chapter 7.

2. A REVIEW OF THE LITERATURE ON THE PHENOMENA ASSOCIATED WITH ULTRASONIC WELDS AND MECHANISMS OF WELD FORMATION

2.1. Mechanical properties of ultrasonic welds

2.1.1. Tensile shear strength

In a tensile shear test a weld, made between two overlapping strips, is broken. The direction of the tensile force acting on the sheets is parallel to the plane of the strips; the weld is being sheared by this action (fig. 2.1).

Several investigators only mention the total breaking force of a weld in a specified strip material (2.1, 2, 3, 4, 10, 15, 22, 36), which for design purposes might be sufficient. However, in order te define weld quality in terms of the ratio of weld breaking stress and strength of the parent material, the total welded area must be known.
In ref. (2.5) the total breaking force of welds in aluminium, copper, nickel, steel and titanium is given: failure usually occurs in thin specimens by fracture of the base material and in intermediate specimens by fracture of the base material or by tear-out of a weld button. Ol'skanskii (2.6) reports that the tensile shear stress in Al and Cu welds is almost equal to the shear strength of the parent material.

The tensile shear test was chosen as testing method for our experiments (sec. 3.4); the results show that weld strength is comparable to the strength of the parent material (sec. 4.2.1.4).

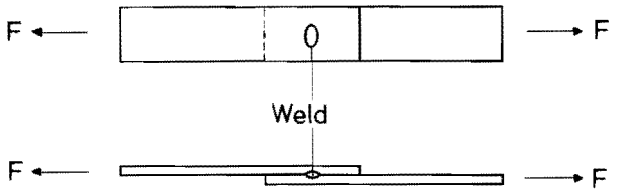

Fig. 2.1. Overlapping strips with an ultrasonic weld for the tensile shear test. F is the pulling force.

2.1.2. *Cross-tension strength*

A second method of testing ultrasonic welds is the cross-tension test in which the weld is broken by pulling perpendicular to the weld interface. The value of the breaking force measured in this test is usually within the range of 20% to 40% of the tensile shear strength (2.5). A Russian author mentions that the cross-tension strength is never less than 30% of the tensile shear strength for Al alloys (2.7). Weare et al. (2.34) state that the cross tension strength is about 20% of the tensile shear strength (also for Al). The cross-tension test is rarely used for testing ultrasonic welds.

2.1.3. *Fatigue strength*

Koziarski (2.8) reports that ultrasonic welds in Al (2024-T3 alloy) have a fatigue strength equal to or slightly better than resistance welds. This was determined from S-N *) curves of both types of welds. Sillin (2.7) comes to a similar conclusion. Drews (2.2) determined S-N curves of Al and Cu. He concluded that the fatigue strength for Cu is 20% of the tensile shear strength and for Al 20% to 30%. Detailed data on the fatigue experiments have not been listed in the literature cited.

2.1.4. *Leak tightness*

An example of hermetic sealing of aluminium tubes by ultrasonic welding is given by Estes and Turner (2.9). Helium leak rates of the welds proved to be much less than the required value of 10^{-6} mbar-liter/sec. In reference 2.5 it is reported that ultrasonic ring welds have reproducibly shown no leakage within the sensitivity of 10^{-9} mbar-liter/sec. We may conclude therefore that leaktight welds can be made by ultrasonic welding.

2.1.5. *Reproducibility*

The reproducibility of welds has only been tested using tensile shear tests. The Welding Handbook (2.5) gives 5% as scatter for welds in Al-alloys, Ni-alloys and Cu; the scatter amounts to 10% for Ti and some steels **). From data by Drews (2.2) the scatter for Al, Cu and stainless steel can be estimated as 15% to 25%. Sillin (2.7) gives data from which the scatter can be determined as 5% to 20% for different Al-alloys. From the present experiments we have found a similar scatter (see sec. 4.2.1.2).

---

*) In an S-N curve, the breaking strength S is plotted versus the number of fatigue cycles N.

**) Scatter means half the distance between the 90% confidence limits.

2.2. The influence of machine settings on tensile shear strength

Many authors investigated the influence of the machine settings (2.1, 2, 3, 4, 10, 15, 22, 32, 36) on the tensile shear strength. The most important settings in ultrasonic welding are

1. The clamping force or clamping pressure. This is the force applied to clamp the specimen between the anvil and the welding tip.
2. The electrical power delivered to the vibrator.
3. The welding time.

The clamping force has, for a specified geometry of both welding tip and anvil, an optimum value (see sec. 4.2.1.1). At this value welds can be made using minimum electrical power (2.10).

The electrical power determines the vibrational amplitude of the welding tip. In general increasing vibrational amplitude results in increasing tensile shear strength (2.15, 36). Chang and Frisch (2.41) used a spherical welding tip directly in contact with a flat anvil and the tip was welded to the anvil. In this experiment vibrational amplitudes above a critical value caused damage of the welds.
Another general fact is that the thicker the upper work piece and the harder the material to be welded, the more power is required for welding. *)
In our sheet welding experiments we did not observe a decrease in the weld strength at larger vibrational amplitudes (see sec. 4.2.1.2). The observations of Chang and Frisch are affirmed by our own experiments (see sec. 4.4.2).

The welding time depends on the power used for welding. The higher the power, the shorter the required welding time. Some authors state that excessively long welding times may cause cracking in the weld zone (see sec. 2.3.2). Consequently weld strength decreases. Others, however, report that long weld times do not affect the initially obtained maximum strength (2.13, 36).

In literature other parameters of the equipment, influencing weld strength, are described only in a qualitative way. These are: material properties, geometry and surface conditions of both the welding tip and the anvil (2.5, 33, 34, 45).

---

*) Jones states (2.23) that the vibrational power required to make a weld is proportional to the thickness of the upper workpiece to the power 3/2. A similar empirical relation is proposed for the acoustic power as a function of material hardness: i.e. acoustic power $\sim$ (hardness)$^{3/2}$.

2.3. Metallographic studies

In the literature the study of metallographic sections of ultrasonic welds is directed towards the following phenomena

1. Thermal effects, such as cast zones as signs of melting, recrystallization and diffusion.

2. Plastic deformation in the weld zone; interpenetration of welded specimens and formation of cracks.

3. Surface film rupture and dispersion.

2.3.1. Thermal effects

From the present experiments we have found that ultrasonic welding is not a thermal process (see chap. 5 and 6). Therefore we will not review the literature on thermal effects in metallographic sections of ultrasonic welds. The extensive amount of literature on this subject is discussed elsewhere (2.60). Summarizing the literature no evidence was found for melting in ultrasonic metal welding and the observations regarding recrystallization and diffusion are contradictory.

2.3.2. Plastic deformation and hardness measurements in the weld zone; cracks

Many authors observed severely deformed interfacial layers in metallographic sections of ultrasonic welds.
Baladin (2.25) reports a plastic flow zone with a thickness of about 200 μm in Cu welds. Beyer (2.22) has shown a surface layer of Al-oxide is dispersed by plastic deformation within an interfacial zone, 20 μm thick. Chang and Frisch (2.41) observed a deformed interfacial layer of 60 μm in thickness, whilst Jones (2.10) and Ol'shanskii (2.6) only mention the occurrence of deformation in the interface. Joshi (2.17) found localized deformation present at all interfaces examined, in similar and dissimilar bonds of Al, Cu and Au. Heymann and Pusch (2.43) and Weare et al. (2.34) observed plastic flow in the form of curls at the welded interface. Heymann and Heymann (2.44) conclude that plastic deformation is a necessary condition for ultrasonic welding.
In fact, severe plastic deformation of the interfacial layer has been reported in all cases of ultrasonic weld formations. Our own observations are in accordance with this fact (see sec. 4.2.2). A calculation of the energy dissipation by plastic deformation in the interfacial layer of an ultrasonic weld is in reasonable agreement with the experimental results (see appendix A5).

In order to investigate whether work hardening occurs in the weld zone, measurements of hardness on metallographic sections of ultrasonic welds have been carried out. The results are summarized from the literature.

In a number of experiments it is found that the hardness in the weld zone is higher than the hardness of the parent material. Beyer (2.22) reports that this difference amounts to 50 to 130% for Al welds and in Cu welds it amounts to 50 to 80%. Heymann and Heymann (2.44) measured an increase of the hardness in the weld zone of 20 to 40% compared with the hardness of the base material (copper). For ultrasonic seam welds in Al Stemmer (2.20) observed an increase in hardness of about 20% in the weld zone (Similar increase of hardness is reported from cold welding investigations e.g. Pranch (2.40) measured an increase of 15 – 40% in the cold welded zone of Al). Ginzburg (2.21) has also observed work hardening. All the observations mentioned above indicate that work hardening occurs in ultrasonic welding.

The presence of cracks both inside and outside (2.11) the weld zone is mentioned in literature. High power levels and long weld times seem to enhance this phenomenon. Sillin (2.16) describes that long welding times (longer than 1 or 2 seconds) often result in internal and external cracking of the metal. These welds usually break at the perimeter of the weld during testing, resulting in low values of the breaking force. Weare (2.34) also reports cracks after excessive welding times. Weare and Monroe (2.12) observed severe cracking at the edge of the weld zone during welding of hard materials (Mo, Ti, Nb, AISI 316 stainless steel). Metallographic examination showed that the degree of cracking increased with both vibrational amplitude and welding time but was independent of the clamping pressure. The quality of the welds, in terms of cross tensile strength, proved to be very poor.

2.3.3. Contaminating surface layers

A generally accepted point is that contaminating layers on the metal surface (such as oxide layers, adsorbed gases, grease and oil) are disrupted during ultrasonic welding. The contaminants are thought to be dispersed in the plastically deformed parent material (2.25, 10, 34, 15) or to be transported (or partly transported) to the periphery of the weld (2.14). Harman and Leedy (2.35) suppose that in wire welding deformation of the wire is sufficient to break the contaminating layer and "sweep it aside".
Evidence for the behaviour of the contaminating layer is obtained from experiments with anodized aluminium. The Al-oxide layers (thickness 1 – 10 μm) are clearly visible in sections of the welds. Rupture and dispersion of these layers have been shown by Beyer (2.22), Johnson (2.36), Lehfelt (2.37) and Bruk (2.38). A similar rupture of anodized layers is reported by Cantelajos (2.39) in roll bonding of Al sheets. Bruck studied the dispersion of the anodized layer in detail. He observed that in a small central region of the weld the layer is only cracked, the dispersion being most severe at the perimeter of the weld zone.
Welding of Al and Cu in vacuum has been performed by Chang and Frisch (2.41, 42). The pressure in their vacuum systeem was about 10^{-5} N/m^2, hence formation

of a monolayer of adsorbed gas occurs in about 10 seconds. Consequently reoxidation of the areas cleaned by ulstrasonic action is ruled out because the welding time was only one second. No clear difference was observed between welds made in vacuum and welds made under atmospheric conditions.
A special class of surface contaminants is formed by films of oil and grease. Most authors advise removal of these lubricants by degreasing before welding (2.1, 5, 15, 36, 45), as they are not easily removed during the welding process.

2.4. Quantities measured during welding

In this section we review literature on the measurement of quantities during welding, such as temperature, acoustic power and vibrational amplitude.

2.4.1. Temperature

Although we are of the opinion that ultrasonic metal welding is not a thermal process (chap. 5 and 6), the large amount of experimental data on temperature measurements during welding cannot be overlooked (2.10, 13, 14, 17, 18, 19, 21, 25, 26, 45).
Usually temperature is measured by insserting thermocouples into the weld zone (2.24). Other methods are (2.10) observation of metallographic changes in the weld zone or using melting wire inserts or foils in the weld zone. The following is a summary of the factors determining the temperature in the weld zone.

1. The applied power density.
2. The welding time and the clamping force.
3. Material properties of the weld members: thermal conductivity, specific heat and acoustic loss factor.
4. Thermal conductivity of the anvil and welding tip.
5. Geometry of the work pieces (e.g. thickness of the sheet or wire) and the geometry of the welding tip and anvil.

In the references quoted in this section temperature values measured show large differences. As a comparison we took from the references the maximum temperature observed in the weld zone (T_w) and the melting temperature of the material having the lowest melting point (T_m). The ratio T_w/T_m varies from 0.3 to 0.95 *).

Because the factors determining temperature in the welding zone, mentioned above, are often unspecified in the references, the different observations of temperature are not necessarily contradictory.

---

*) A more detailed description of these differences is found in Harthoorn (2.60).

Apart from the fact that no melting occurs, no conclusion as to the role of temperature in the weld zone can be drawn from literature.

2.4.2. Acoustic power and vibrational amplitude

Monitoring of ultrasonic welding by measuring any relevant quantity during the welding period is a target of many investigations; until now this has not been acieved. Several quantities have been studied during welding but none of them showed a clear relation with the quality of the weld (i.e. weld strength).
The measurement of acoustic power delivered to the work pieces has been reported by Jones (2.23), Dippe (2.27), Kholopov (2.28) and Bello (2.29) but none of these authors found a relation between acoustic power and weld strength suitable for monitoring the process. Bechert and Dippe (2.30) measured the amplitude of the welding tip during welding (loaded condition) as well as in the unloaded situation. They conclude that the difference between these two measurements is related to the shear strength of the weld. They indicate a possibility of quality control during welding. Equipment to apply this principle to the welding process is described by Wendler (2.31). However, no results of a controlled welding experiment are given.

2.5. Welding mechanism

2.5.1. Welding mechanism and possible welding operations

According to the Welding Handbook (2.61) welding 'is the process of joining two or more pieces of material, often metallic, by a localized coalescence or union across the interface'. Coalescence or union means that the atoms of the welded pieces are brought so close, that the distance between two adjacent atoms, belonging to different weld pieces, is approximately equal to the interatomic distance in the base material of one weld piece (atomic contact). Further the atoms of the two weld pieces must exhibit mutual attractive forces (adhesion) comparable to the binding forces of the atoms in one weld piece. This coalescence must take place over an area of the interface which is large compared to the interatomic distances (macroscopic area).
From this it is clear that a welding operation must bring the weld pieces into mutual atomic contact over a macroscopic area. In order to achieve adhesion, contamination layers must be removed by the welding operation. In short: a clean metallic contact over a macroscopic area must be created by the welding operation.

There are three types of welding operations (2.61)

1. *Welding by fusion of an interfacial zone.*
   When the interface of the weld members is in a liquid state, clean metallic contact is made because contaminating surface layer can be dissolved in the molten zone. Consequently the requirements for making a weld are fulfilled.

2. *Welding in the solid state*
   We can distinguish
   a. Welding by heating without fusion
   b. Welding by mechanical force alone (cold welding).

When the two metal surfaces are brought into contact by normal pressure and the interfacial temperature is increased to between 0.5 T_m and T_m (T_m is the melting temperature of the weld member having the lowest melting point) a weld can develop without fusion. At the elevated temperature the atoms of the contaminant surface layer can diffuse into the material of the weld pieces and the atoms of the material at the interface can rearrange themselves in such a way that the required clean atomic contact is created over a macroscopic area. In other words: diffusion can cause welding. Such a welding operation is called diffusion welding or pressure bonding.

Atomic contact between two surfaces can also be created by applying mechanical force only. A clean contact can be achieved when the contaminating layer can be ruptured or dispersed by the action of the force. This can happen when the surface area of the contacting interface is stretched, due to deformation of the weld members. This welding operation is called 'cold welding' (2.61, 62).

2.5.2. Mechanism of ultrasonic metal welding

In the literature no generally accepted theory dealing with the formation of a joint in ultrasonic metal welding can be found. From the previous sections it appears that three facts are undeniable
1. No melting occurs during ultrasonic welding (see sec. 2.3.1).
2. In the welded interface a severely deformed layer exists (see sec. 2.3.2).
3. Contaminating layers are disrupted during ultrasonic welding (see sec. 2.3.3).

In order to explain the formation of a joint in ultrasonic welding a number of physical phenomena is mentioned in the literature.
Many authors consider heating of the interface as a relevant phenomenon (2.18, 25, 26, 46). Heating facilitates plastic deformation which ruptures or disperses the contaminating layer. Diffusion is mentioned as the main phenomenon by Drews (2.45) and Genscoy (2.15). Chang and Frisch (2.41) describe the mechanism of ultrasonic welding as 'basically solid state bonding, such as adhesion, mechanical interlocking, recrystallization and possibly diffusion'. Finally Joshi (2.17) and Harman (2.35) are of the opinion that 'the process leading to formation of intimate contacts at the interface can best be described as that of structural softening as a direct consequence of ultrasonic excitation'.
On basis of our own experiments we exclude thermal effects from the explanation of the mechanism of joint formation. Hence the only possible mechanism left is metallic adhesion, brought about by the action of mechanical force (as mentioned in sec. 2.5.1). Adhesion will be discussed in the next section.

In appendix A1 we will review literature on acoustic softening and diffusion under the influence of ultrasound. It will be shown that the contribution of these phenomena to joint formation is not established.

2.5.3. Metallic adhesion

When metal parts are brought into close contact by the action of normal forces or a combination of normal and tangential forces, welded junctions can come into existence. The occurrence of these welds (having a strength comparable to that of the parent material) is called adhesion. This phenomenon is important for the explanation of friction, wear and cold welding.
The factors influencing the adhesion of metals (2.48, 49, 50) are

1. *The area of real contact.*
   To permit adhesion the distance between the parts must be roughly equal to the interatomic distances in the metal(s). The area where this demand is fulfilled is called the area of real contact.
2. *Surface contaminants.*
   In the area of real contact contaminant layers (such as lubricants, oxide layers and adsorbed gas layers) must be removed or disrupted in order to permit clean metal to metal contact.
3. *Formation of metal to metal bonds.*
   When the former conditions are satisfied a further requirement for adhesion is that the atoms of the contacting parts are able to attract one another i.e. to form a bond. For similar metals this is possible because such a bond equals the binding forces at the grain boundary or within the solid. For dissimilar metals formation of a bond is also possible, but the strength depends on the structure of the different metals.
4. *Residual stresses.*
   When the external forces for contacting are removed, the elastically deformed zones will recover. This can cause tensile stresses in the welded areas resulting in breaking of the adherent junctions. Hence adhesion strength may be reduced by elastic recovery.

Several workers have tried to correlate adhesion properties of metals with the physical or chemical properties of the material. We will review literature on this subject in appendix A2. The conclusion is that, up to now, no quantitative relationship between the adhesion of a metal and its physical or chemical properties could be found; only general tendencies can be given.

In the following sections each of the factors mentioned above will be discussed.

2.5.3.1. The area of real contact

On real surfaces asperities are to be found. When two surfaces are brought into

contact these asperities touch one another. Assuming that the contacting asperities are deformed by plastic flow under the action of the external normal force F_n the area of real contact is given by

$$A_r = \frac{F_n}{p_o} \tag{2.1}$$

where p_o is the plastic yield pressure (2.50).

It is well established that under the combined action of normal and tangential forces the real contact area increases. This is known as the theory of junction growth. According to Bowden and Tabor (2.50) the area of real contact A_r under the action of an external normal force F_n and a tangential force F_s can be found from

$$p^2 + \alpha\tau^2 = \beta Y^2 \tag{2.2}$$

With $p = F_n/A_r$ and $\tau = F_s/A_r$, Y is the yield stress of the material and α and β are constants *).
Equation (2.2) can be written

$$A_r = \left(\frac{F_n^2 + \alpha F_s^2}{\beta Y^2}\right)^{\frac{1}{2}} \tag{2.3}$$

When only a normal force F_n acts eq. (2.3) reduces to (2.1) and consequently $p_o^2 = \beta Y^2$. The value of α can be determined experimentally. Measurements by McFarlane and Tabor (2.15) using indium gave a value $\alpha = 3.3$; a value $\alpha = 12$ was found by Courtney-Pratt and Eisner (2.52) from measurements using platinum.

Equation (2.3) shows that the area of real contact increases more effectively under the action of a tangential force than under the action of a similar normal force, provided that α is considerably larger than one.

---

*) This relation is assumed to be valid for the complex stress situation in a real asperity contact. Its form is analogous to the relation obtained by application of von Mises criterion, assuming a plane stress situation in the asperity contact. The constants α and β are used to match the relation to the real situation; they can be determined experimentally only.

2.5.3.2. Surface contaminants

The influence of contaminant surface layers on adhesion of metals is clearly demonstrated in adhesion experiments in ultrahigh vacuum (pressure 10^{-8} – 10^{-9} N/m^2). In such experiments contacts are made under light loads, i.c. the deformation in the contact region is mainly elastic. When surface contaminants are present no, or very weak, adhesion is observed. In ultrahigh vacuum, surface contaminants can be removed by degassing, heating by electron bombardment or argon ion bombardment (2.55).
After cleaning the samples are brought into contact under a load normal to the contacting surfaces. Next the samples are separated by a tensile force. This force is a measure of the strength of the adhesion bond. In these experiments strong adhesion (i.e. adhesion strength is comparable with the strength of the bulk material) has been observed for Cu-Cu and Au-Au by Gane et al. (2.53), for Ag-Ag, Ag-Ni and Ag-Cu by Johnson et al. (2.54), for Fe-Fe and stainless steel-stainless steel by Aldrich (2.56), for Au-Au, Au-Ag, Au-Al and Au-Cu by Buckley (2.58). Ti-Ti couples showed adhesion to a strength of about half the bulk strength of the material and Mo-Mo to one quarter of the bulk strength (2.57).
Controlled contamination of the cleaned surfaces with oxygen or undried air prevented adhesion (2.53, 54). Adhesion of Ti-Ti and Mo-Mo couples was reduced significantly by the admittance of ultrapure N_2 with a pressure of 10^{-4} – 10^{-7} N/m^2 (2.57).

From these data the conclusion can be drawn that surface contaminant films form a barrier which inhibits adhesion (2.54). Consequently, the adhesion properties of metal couples are largely determined by the extent to which these layers can be removed. Johnson (2.57) concludes that the normally observed difficulty in forming adhesion junctions between couples of harder metals (such as Mo) or between couples of hexagonal structure (such as Ti) is not an intrinsic property of these metals, but a consequence of the presence of contaminants even after the cleaning procedure. He suggest that contact resistance measurement is a useful tool in ascertaining the degree of contamination present at a conducting interface.

Under atmospheric conditions surface contaminants can effectively be disrupted and dispersed by relative sliding of the contacting surfaces. This is one reason why this sliding can increase adhesion (2.59); the second reason is the growth of the area of real contact brought about by the tangential forces associated with sliding (see sec. 2.5.3.1).

2.5.3.3. Formation of metal to metal bonds

For similar metals the bonding between atoms in two specimens is the same as the bonding at the grain boundaries. Thus the strength of the adhesion junctions must be comparable to the strength of the parent material. This is affirmed by the experiments with Cu, Au (2.53), Ag (2.54) and Fe (2.56).

However, there is a factor which limits adhesion strength. Gane et al. (2.53) studied adhesion of Co. They found that the contact resistance was 2 to 4 times higher than the value to be expected on theoretical grounds *). This might be due to imperfect cleaning. The adhesion force (= force to pull the speciment apart) of Co proved to be 5 to 10 times lower than the expected value **).
Gane c.s. ascribe this additional decrease of adhesion to 'the embrittling effect produced by the notch geometry of the junctions on a material of low ductility'.
In another experiment (2.53), the adhesion of Ge was studied as a function of temperature. It appeared that the adhesion strength was almost zero for contacts made and tested below 400 °C, but it increased rapidly at higher temperatures. An adhesion junction was made at 700 °C and cooled to 100 °C, with the compressive load still applied (hence it is certain that adhesion junctions have been formed). At this lower temperature very little or no adhesion was retained compared with adhesion at 700 °C. Therefore it was concluded that the ductility of the interfacial junctions (which is much lower at 100 °C than at 700 °C) determined the adhesion strength of the junctions. (During cooling considerable care was taken to assure that no rupture took place due to thermal contractions).
The final conclusion of Gane et al. (2.53) is quoted here: 'These experiments show that, in the absence of surface contaminants, a major factor determining the strength of adhesion between solids is the ductility of the junctions formed at the interface. For ductile materials such as metals, even if the loading produces only elastic deformation, the rupturing of the junctions when the adhesive strength is measured involves the plastic flow of metal. The stronger the metal the higher the adhesive strength. There is, however, a limit to this since an increase in hardness is usually accompanied by a reduction in ductility. As the ductility decreases the force required to break the junctions decreased. In the limit the strength of adhesion between brittle solids becomes very small indeed. Experiments with germanium suggest that this is due to the lack of ductility and not to the need to activate interfacial bonds.'

---

*) Consequently the real contact area was 2 to 4 times smaller than the expected value. The theoretical value was deduced by assuming that the contact was elastic, hence the Hertzian contact area (radius a) could be calculated. The contact resistance was obtained from $R = \rho/2a$, where ρ is the electrical resistivity of the metal (2.63). The theoretical values showed good agreement with the experimental values for Au and Cu.

**) The expected value was based on total adhesion over the Hertzian contact area.

The preceding facts indicate that adhesion for similar metal couples can be decreased because of
1. the difficulty of removing contaminant layers,
2. the low ductility of the adhesion junctions formed.

Adhesion of dissimilar couples (cleaned in ultrahigh vacuum) was studied quantitatively by Buckley (2.58). Het observed that the higher the misfit between the adhering surfaces (i.e. the difference in lattice parameters) the lower the adhesion strength. The experiments included 15 metal combinations. We conclude that strong adhesion between dissimilar metal couples can occur. It seems that too little experimental evidence is available to give precise rules for the adhesion of dissimilar metals.

From the preceding facts we expect that ductility might be a factor determining ultrasonic weldability.

2.5.3.4. Residual stresses

The breaking of adhesion junctions by recovery of the residual stresses in the contacting parts was described theoretically by Bowden and Tabor (2.50). The theory was supported by experiments on large-scale model junctions.

Ainbinder et al. (2.47) assume that ' . . . the adhesion which originates under plastic deformation is ruptured by the residual stresses upon removal of the loading'. Ainbinder discussed adhesion of 'metals tending to brittle fracture' in connection with the cold-weldability of such metals. To make his hypothesis plausible, he puts forward: 'Under combined plastic deformation all these metals adhere excellently in a pair with any other metal possessing a sufficient reserve of plasticity. Thin foils, fabricated from such metals, also adhere with considerable strength under deformation. Adhesion nodes form on the surfaces of these metals under the joint effect of normal and tangential loading'.

For ductile metals (Ag, Cu, Ni) Johnson and Keller (2.54, 57) found that during unloading of contacts, cleaned in ultrahigh vacuum, no rupture of junctions took place.

It is clear that rupture of adhesion junctions by residual stresses is determined mainly by the ductility of the junctions.

2.5.3.5. Conclusion

From the preceding sections we can draw the following tentative conclusions, concerning the factors influencing adhesion

1. Adhesion occurs when metal parts are brought into real contact over a clean area. Thermal effects are not required for the explanation of adhesion.
2. Atomic contact between two surfaces can be created by the plastic deformation of asperities (junction-growth).
3. The removability of the surface contaminants determines to a large extent the adhesion strength of contacting surfaces.
4. The lower the ductility of the adhesion junctions, the lower the force required to break the junctions (assuming a constant material strength) and consequently the lower the adhesion strength.
5. Junctions may already be ruptured by recovery of elastic stresses in the contacting surfaces.

3. WELDING AND MEASURING EQUIPMENT

In this chapter a description of both the ultrasonic welding equipment and the subsonnic welding equipment is given. A detailed analysis of the electromechanical vibrating system is included. The aim of this analysis is the determination of the alternating force excerted by the welding tip on the work pieces.

3.1. Ultrasonic welding equipment

3.1.1. The generator and power amplifier

The generator consists of three main parts

1. *The oscillator*
   This is a voltage controlled oscillator in order to regulate the frequency, see 2. The nominal frequency can be set to a multiple of 20 kHz. The output voltage is sinusoidal and the voltage amplitude can be preset. In the present experiments a nominal frequency of 20 kHz is used.
2. *The automatic frequency adjustment unit*
   This unit controls the frequency of the oscillator in such a way that the phase difference between voltage and current – at the transducer terminals – is less than 10°. The transient time is less than 5 msec.
3. *The timing circuit*
   This circuit switches the oscillator. Welding times from 1 msec to 10 sec can be preset.

The oscillator is connected to a power amplifier. According to the specification the amplifier can feed 400 W into a matched load. The output impedance of the amplifier is switchable to 220Ω, 490Ω, 880Ω and 1350Ω.

3.1.2. The vibrating system

The vibrating system is outlined in fig. 3.1. The power amplifier drives a piezoelectric transducer which generates a mechanical vibration (nominal frequency 20 kHz). For a description of the transducer we refer to Hulst (3.1). The transducer is coupled (plane 5 in fig. 3.1), by means of a stud, to a mechanical waveguide (parts c and d in fig. 3.1). This is a 50 mm diameter rod, 124 mm long, which equals half a wavelength for longitudinal waves with a frequency of 20 kHz. In the middle of the waveguide a flange is provided and by this means the whole system can be mounted into a frame. The amplitude transformer (part a and b, fig. 3.1) is fastened to the end of the waveguide. At the end of the amplitude transformer a thicker part acts as the welding tip.
The vibrating system is made out of a titanium alloy. *) The system vibrates

---

*) 318 A, manufactured by Imperial Metal Industries Ltd.
Composition: Al: 5.5–6.5%; Va: 3.5–4.5%; Fe ≤ 0.2%; H ≤ 0.015%; Ti: remainder.

longitudinally. In the unloaded condition a standing wave pattern is present with nodes of the vibration amplitude in the planes 2, 4 and the plane between the two piezoelectric discs (fig. 3.1).

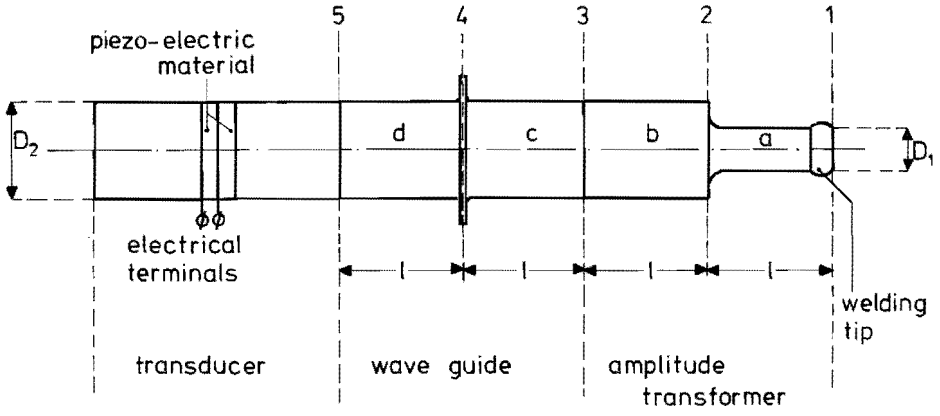

Fig. 3.1. The ultrasonic vibrating system. The radius of the welding tip is 20 mm. The mechanical load impedance $\bar{Z}_{ml}$ is situated in plane 1.
D_1 = 22.5 mm; D_2 = 50.0 mm; $l = \frac{1}{4}\lambda_T$ = 62 mm (see 3.2.1.2).

3.1.3. The anvil and the clamping mechanism

The sheets to be welded (see fig. 3.2) are put on an anvil. The anvil is a hardened steel block (dimensions 80 mm x 80 mm x 20 mm) with a ground upper surface.

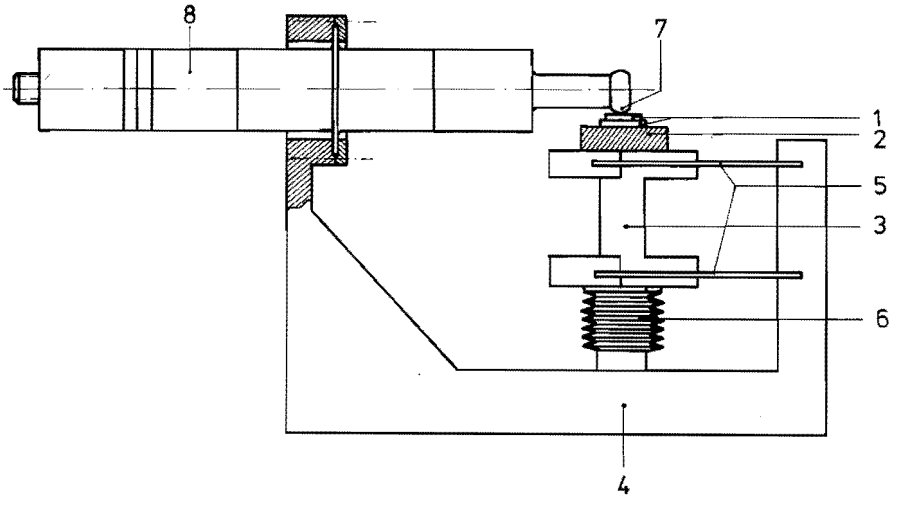

Fig. 3.2. The welding apparatus.
1. Sheets to be welded; 2. anvil; 3. support; 4. mechanical frame; 5. plate springs; 6. bellow; 7. welding tip; 8. transducer.

This anvil is mounted on an aluminium support (see fig. 3.2). The support is connected to the frame of the equipment using 4 thick plate springs. These springs are mounted in such a way that the support can move a few millimeters in the vertical direction. This movement is frictionless; the stiffness for the vertical movement is 20 N/mm. Under the support is placed a coil spring (not drawn in fig. 3.2) to compensate for the weight both of the anvil and the support.
The work pieces can be clamped between the welding tip and the anvil by means of a force excerted by air pressure in a bellow under the support (fig. 3.2). The clamping force ranges from 100 N. to 1500 N. and is kept constant during welding.

3.2 Theoretical description of the vibrating system *)

In this section relations between the electrical quantities at the transducer terminals and the mechanical quantities at the end of the ampitude transformer (welding tip) will be derived. At the transducer terminals we will consider the electric current $\bar{I}$ and the voltage $\bar{V}$; the mechanical quantities at the welding tip are the force $\bar{F}_1$ and velocity $\bar{v}_1$. Such relations are useful because electrical measurements then can give information about the mechanical load at the welding tip.
The quantities $\bar{I}$, $\bar{V}$, $\bar{F}_1$ and $\bar{v}_1$ are complex, as they must account for phase differences; they contain a term which is varying harmonically in time. The complex mechanical load impedance $\bar{Z}_{m1}$ of the vibrating system is defined as the ratio of the force $\bar{F}_1$ exerted in plane 1 of fig. 3.1 and the velocity $\bar{v}_1$ in the same plane. Hence

$$\bar{Z}_{m1} = R_{m1} + j\,X_{m1} = \frac{\bar{F}_1}{\bar{v}_1} \qquad (3.1)$$

The quantities R_{m1} and X_{m1} are the real and imaginary part of $\bar{Z}_{m1}$.

We will describe how a mechanical load impedance is transformed by the transformer waveguide system (fig. 3.1). Next, the electrical impedance $\bar{Z}_e$ at the terminals of the transducer will be expressed as a function of the mechanical load impedance; a relation between the current through the transducer and the velocity at the welding tip will be found.

---

*) This section will be part of a separate publication by J.L. Harthoorn and A.P. Hulst.

3.2.1. The mechanical transformer

3.2.1.1. The cylindrical rod as a transformer

Consider the cylindrical rod with cross-sectional area A and length l, which is loaded at its end face (z = 1) by a complex mechanical load

$$\bar{Z}_{ml} = \frac{\bar{F}_l}{\bar{v}_l} \tag{3.2}$$

The forces and velocities are as defined in Fig. 3.3.

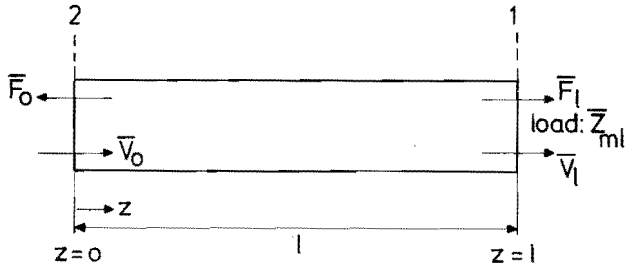

Fig. 3.3. Cylindrical rod, loaded by a mechanical impedance $\bar{Z}_{ml}$.

The wave equation for longitudinal waves propagating in the axial direction is:

$$\frac{\partial^2 \xi}{\partial t^2} = c^2 \frac{\partial^2 \xi}{\partial z^2} \tag{3.3}$$

where ξ is the displacement in the z direction and t is the time. The quantity c is the propagation velocity for longitudinal waves in the rod.
A solution of eq. (3.3) for harmonic vibrations is:

$$\xi = (C_1 e^{-jkz} + C_2 e^{jkz}) e^{j\omega t} \tag{3.4}$$

with ω = angular frequency of the vibrations
k = wave number = $\frac{\omega}{c}$
C_1 and C_2 are constants.

The stress in the z direction is as follows

$$\sigma_z = E \frac{\partial \xi}{\partial z} \tag{3.5}$$

where E is Young's modulus of the material.

Using $c = \sqrt{\frac{E}{\rho}}$, where ρ is the specific mass of the rod material, the tensile force in the axial direction is *)

$$\bar{F}_z = A\,\sigma_z = A\,E\frac{\partial \xi}{\partial z} = A\rho c^2\,\frac{\partial \xi}{\partial z} \tag{3.6}$$

The particle velocity in the axial direction is

$$\bar{v}_z = \frac{\partial \xi}{\partial t} = j\omega\xi \tag{3.7}$$

The impedance in plane z = 0 is

$$\bar{Z}_{mo} = \frac{\bar{F}_0}{\bar{v}_0} \tag{3.8}$$

Using eqs. (3.2), (3.6), (3.7), (3.8) and (3.4) we can express $\bar{Z}_{ml}$ and $\bar{Z}_{mo}$ in $A\rho c$, kl, C_1 and C_2. By elimination of C_1 and C_2 we obtain:

$$\bar{Z}_{mo} = \frac{\bar{Z}_{ml} + j\,A\rho c \tan k\,l}{1 + j\,\frac{\bar{Z}_{ml}}{A\rho c}\tan k\,l} \tag{3.9}$$

Equation (3.9) expresses how the load $\bar{Z}_{ml}$ is transformed by a transmission line with length l and characteristic impedance $A\rho c$.

3.2.1.2. The bi-cylindrical transformer

We will now apply eq. (3.9) to the amplitude transformer and the waveguide of the system shown in fig. 3.1. First we consider the bar between the planes 1 and 2. Its length is ¼ λ_r and the cross-sectional area is A_1. The mechanical impedance in plane 1 is $\bar{Z}_{ml}$ and the impedance in plane n is $\bar{Z}_{mn}$ **).
Using eq. (3.9) we obtain

$$\bar{Z}_{m2} = \frac{\bar{Z}_{ml} + j\,A_1\rho c \tan ¼\,k\lambda_r}{1 + j\,\frac{\bar{Z}_{ml}}{A_1\rho c}\tan ¼\,k\lambda_r} \tag{3.10}$$

---

*) The stress σ_z is assumed to be uniform in a cross-section of the rod.
**) Stress and velocity are assumed to be uniform in the cross-section planes.

For a vibration, having wavelength λ_r and frequency ν_r, the propagation velocity is $c = \lambda_r \nu_r$. The corresponding angular frequency is $\omega_r = 2\pi\nu_r$. When the actual vibration frequency of the bar is ν (with $\omega = 2\pi\nu$) we can write:

$$\tan \tfrac{1}{4} k\lambda_r = \tan \tfrac{1}{2} \pi x \qquad (3.11)$$

$$\text{with } x = \frac{\omega}{\omega_r} = \frac{\nu}{\nu_r}$$

In our experiments ω differs less than a few percent from ω_r, therefore $x \approx 1$ and we can approximate:

$$\tan \tfrac{1}{2} \pi x = \frac{1}{\tfrac{1}{2} \pi (1 - x)} \qquad (3.12)$$

Hence eq. (3.10) can be written as

$$\bar{Z}_{m2} = \frac{\bar{Z}_{ml} + \dfrac{j A_1 \rho c}{\tfrac{1}{2} \pi (1 - x)}}{1 + j \dfrac{\bar{Z}_{ml}}{\tfrac{1}{2} \pi (1 - x) A_1 \rho c}} \qquad (3.13)$$

If $| \bar{Z}_{ml} (1 - x) | \ll A_1 \rho c$, we obtain as an approximation

$$\bar{Z}_{m2} = \frac{j A_1 \rho c}{\tfrac{1}{2} \pi (1 - x) + j \dfrac{\bar{Z}_{ml}}{A_1 \rho c}} \qquad (3.14)$$

Since in practical cases *)

$$| \bar{Z}_{ml} | \ll A_1 \rho c$$

it appears from eq. (3.14) that

$$| \bar{Z}_{m2} | \gg A_1 \rho c \qquad (\text{for } x \approx 1) \qquad (3.15)$$

---

*) The value of $| \bar{Z}_{ml} |$ in the present experiments varies between 200 and 400 kg s^{-1} (see e.g. table 6.1). The value of $A_1 \rho c$ is 8.64×10^3 kg s^{-1}.

This inequality is used in the next approximation, after the application of eq. (3.9) to the rod between the planes 2 and 3 of Fig. 3.1 (length ¼ λ_r and cross-sectional area A_2), which yields the relation

$$\bar{Z}_{m3} = \frac{\bar{Z}_{m2} + \dfrac{j A_2 \rho c}{\frac{1}{2}\pi (1-x)}}{1 + j \dfrac{\bar{Z}_{m2}}{\frac{1}{2}\pi (1-x) A_2 \rho c}}$$

This formula can be simplified to

$$\bar{Z}_{m3} = \frac{(A_2 \rho c)^2}{\bar{Z}_{m2}} - j \frac{\pi}{2} A_2 \rho c (1-x) \qquad (3.16)$$

if $|\bar{Z}_{m2}| \gg A_2 \rho c (1-x)$, which is apparent from eq. (3.15). Combination of the eqs. (3.14) and (3.16) finally yields

$$\bar{Z}_{m3} = M^2 \bar{Z}_{m1} - j \frac{\pi}{2} (1-x) \left\{ A_2 \rho c + M^2 A_1 \rho c \right\} \qquad (3.17)$$

$$M^2 = \left(\frac{A_2}{A_1}\right)^2 \qquad (3.18)$$

where M^2 is the transformation ratio of the half-wave transformer in resonance.

The power dissipation in the load (in plane 1, fig. 3.1) is:

$\frac{1}{2} |\bar{v}_1|^2 \, \mathrm{Re}(\bar{Z}_{m1})$

The power that flows through the transformer (through plane 3, fig. 3.1) is:

$\frac{1}{2} |\bar{v}_3|^2 \, \mathrm{Re}(\bar{Z}_{m3})$

These two powers are equal if the transformer is assumed to be loss free. Hence

$$\frac{|\bar{v}_1|}{|\bar{v}_3|} = \sqrt{\frac{\mathrm{Re}(\bar{Z}_{m3})}{\mathrm{Re}(\bar{Z}_{m1})}}$$

and from eq. (3.17)

$$\mathrm{Re}(\bar{Z}_{m3}) = M^2 \, \mathrm{Re}(\bar{Z}_{m1})$$

it follows that

$$\frac{|\bar{v}_1|}{|\bar{v}_3|} = M \qquad (3.19)\ *)$$

From eqs. (3.18) and (3.19) we see that the ratio of the velocities at the endfaces of the bi-cylindrical transformer is the inverse of the ratio of the corresponding areas of the two cylindrical parts.

3.2.1.3. Series connection of a transformer and a waveguide

A waveguide consisting of the cylinderical rod between planes 3 and 5 is connected in series with a transformer (fig. 3.1). The impedance $\bar{Z}_{m5}$ (in plane 5, fig. 3.1) can be expressed in terms of $\bar{Z}_{m1}$ and the characteristic impedances of both the transformer and waveguide. Analoguous to eq. (3.17) we obtain:

$$\bar{Z}_{m5} = M^2\, \bar{Z}_{m1} + j\, X_{mw} \qquad (3.20)$$

where

$$X_{mw} = -\tfrac{1}{2}\pi (1 - x) \left\{ A_4 \rho c + A_3 \rho c + A_2 \rho c + M^2\, A_1 \rho c \right\} =$$

$$= -\tfrac{1}{2}\pi (1 - x)\, B \qquad (3.21)$$

The suffix of the area A refers to the part of the vibrating system as indicated in fig. 3.1. In conclusion, the load impedance after transformation $\bar{Z}_{m5}$ consists of a part resulting from the original load impedance $\bar{Z}_{m1}$ multiplied by the relevant transformation ratio and of an imaginary part resulting from the detuning of the applied halfwave transformer and waveguide.

3.2.2. Mechanical losses in the transformer and waveguide

Up till now the waveguide and the transformer have been assumed to be free of losses. In fact there are three dissipative factors present in the waveguide transformer system

1. Internal losses in the material
2. Losses in the contact planes and screw ends
3. Losses in the flange, which is clamped to the apparatus.

---

*) This relation can also be derived for a transformer with internal losses.

The first of these losses can be calculated analytically using the acoustic loss factor of the material. The two other factors cannot be calculated. To account for all three factors we add a resistive term R_{mw} to eq. (3.20) which can only be determined by experiment; it appears that R_{mw} is constant within the accuracy limits of the experiments. Equation (3.20) then becomes

$$\bar{Z}_{ms} = M^2 \bar{Z}_{ml} + R_{mw} + j\, X_{mw} \tag{3.22}$$

where X_{mw} is according to eq. (3.21). Hence, the load on the ultrasonic transducer can be characterized by means of its real and imaginary parts respectively,

$$R_{ms} = \mathrm{Re}\,(\bar{Z}_{ms}) = M^2\, R_{ml} + R_{mw} \tag{3.23}$$

$$X_{ms} = \mathrm{Im}\,(\bar{Z}_{ms}) = M^2 X_{ml} + X_{mw}$$

3.2.3. The complete vibrator

3.2.3.1. The ultrasonic transducer

We use the equivalent circuit for the transducer as described by Hulst (3.1). Fig. 3.4 shows the electrical substitute for the generator, transducer and load. R_d represents the dielectric losses of the piezoelectric discs in the transducer. C_o is the capacitance of the transducer. An external inductance L_o is connected in parallel to the transducer to compensate for C_o near the resonance frequency ν_r.
Hence $\omega_r^2\, L_o\, C_o = 1$ with $\omega_r = 2\pi\nu_r$.

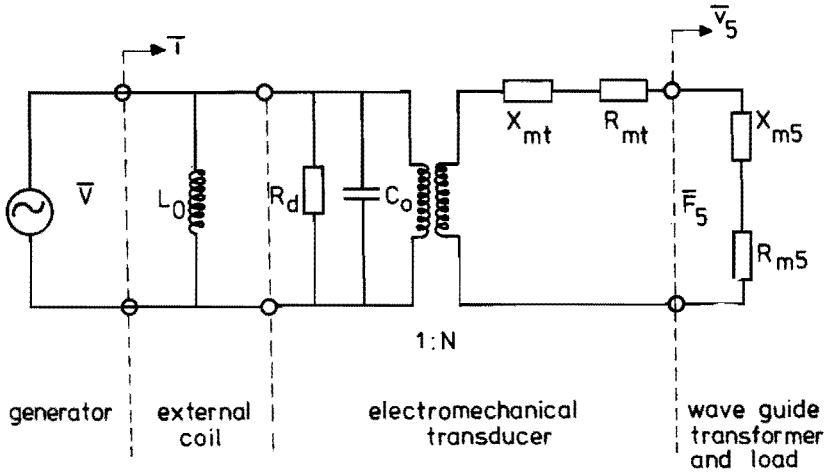

Fig. 3.4. The equivalent circuit of the vibrating system and the load.

The conversion of electrical vibrations into mechanical vibrations is symbolized by an electromechanical transformer with a non-dimensionless transformation ratio N. N is defined as the ratio of the current i and the velocity v_5 *) (see fig. 3.4). Hence

$$N = \frac{\bar{I}}{\bar{v}_5} \tag{3.23a}$$

At the input side of the transformer the quantities are of an electric nature; at the output side the quantities are mechanical. In the mechanical branch R_{mt} and X_{mt} represent the mechanical resistance and the mechanical reactance of the transducer respectively. The complex mechanical internal impedance is

$$\bar{Z}_{mt} = R_{mt} + j\,X_{mt}$$

The mechanical impedance of the waveguide, the amplitude transformer and the load is

$$\bar{Z}_{ms} = R_{ms} + j\,X_{ms}$$

Actually this impedance $\bar{Z}_{ms}$ is the total load of the transducer.
As the frequency varies less than 1% around the resonance frequency ν_r, the value of R_{mt} is assumed to be constant. Hulst (3.1) showed that R_{mt} varies about 2% under such conditions. It was also shown (3.1) that for the symmetrical transducer the value of X_{mt} is well approximated by

$$X_{mt} = \pi(A\rho c)_t \left(\frac{\omega}{\omega_r} - 1\right) = -\pi(A\rho c)_t\,(1 - x) \tag{3.24}$$

in the range $0.9 < x < 1.1$. In this expression $(A\rho c)_t$ stands for the characteristic mechanical impedance of the transducer. The total impedance in the mechanical branch of the circuit of fig. 3.4 is $\bar{Z}_{mt} + \bar{Z}_{ms}$. The electrical equivalent of this mechanical impedance is an electrical impedance (see fig. 3.5)

$$\bar{Z}_e = \frac{1}{N^2}\,(\bar{Z}_{mt} + \bar{Z}_{ms}) \tag{3.25}$$

which is connected parallel to R_d, L_o and C_o.

---

*) The transformation ratio is in principle a complex quantity, as it is the ratio of two complex quantities. Physically such a complex transformation ratio is the consequence of the presence of losses in the piezoelectric material. In the present transducer these losses can be neglected. Hence N is assumed to be real (in the frequency interval near resonance).

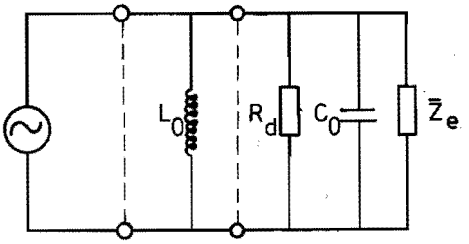

Fig. 3.5. Simplified equivalent circuit of the vibrating system and the load.

The dielectric loss resistance R_d can be estimated to be of the order of 10^5 Ω. The parallel conncection of L_0 and C_0 has a very high impedance near resonance. In our experiments it proves $|\bar{Z}_e| < 10^3$ Ω. Thus near resonance we can neglect R_d, L_0 and C_0 in the equivalent circuit of fig. 3.5 and conclude that the generator is loaded with Z_e only.

3.2.3.2. The frequency adjustment system

The electrical generator that feeds the transducer is equipped with an automatic frequency adjustment. The frequency is adjusted in such a way that no phase shift exists between current and voltage at the generator terminals.
Hence at the operating frequency ν (angular frequency ω) *)

$$\mathrm{Im}\,(\bar{Z}_e) = 0$$

or with eq. (3.25)

$$X_{mt} + X_{ms} = 0 \qquad (3.26)$$

Relation (3.26) gives the electrical and mechanical resonance condition for the loaded vibrating system during welding.

---

*) The operating frequency ν differs in the present experiments less than a few percent from the resonance frequency ν_r.

3.2.3.3. The real part of the load

With eq. (3.26) the electrical impedance $\bar{Z}_e$ becomes a resistance R_e

$$R_e = \mathrm{Re}\,(\bar{Z}_e) = \frac{1}{N^2}\,\mathrm{Re}\,(\bar{Z}_{mt} + \bar{Z}_{ms}) = \frac{1}{N^2}\,(R_{mt} + R_{ms}) =$$

$$= \frac{1}{N^2}\,(R_{mt} + R_{mw} + M^2 R_{ml}) =$$

$$= R_{et} + R_{ew} + \frac{M^2}{N^2}\,R_{ml} =$$

$$= R_{et} + R_{ew} + R_{el} \qquad (3.27)$$

The mechanical resistance R_{mt} is transformed into the electrical resistance R_{et} by

$$R_{et} = \frac{1}{N^2}\,R_{mt}$$

and analogous:

$$R_{ew} = \frac{1}{N^2}\,R_{mw}$$

Hence using (3.27) we obtain

$$R_{ml} = \frac{N^2}{M^2}\,\{R_e - (R_{et} + R_{ew})\} = \frac{N^2}{M^2}\,R_{el} \qquad (3.28)$$

Here, R_e is the total electrical resistance measured between the transducer terminals under load; $R_{et} + R_{ew}$ is the total electrical resistance measured when the system is not loaded. R_{el} is the electrical equivalent of the load *).

---

*) In our experiments R_e ranges between 400 Ω and 600 Ω. The value of $R_{et} + R_{ew}$ is (80 ± 5) Ω. The factors responsible for the magnitude of this resistance are mentioned in sec. 3.2.2.; the contribution of the internal losses of the materials is less than 10 Ω.

3.2.3.4. The imaginary part of the load

According to eqs. (3.21) and (3.23) the imaginary part of the load after transformation is

$$X_{ms} = \mathrm{Im}\,(\bar{Z}_{ms}) = M^2\, X_{ml} - \tfrac{1}{2}\pi\,(1 - x)\,B$$

Combining this with eqs. (3.24) and (3.26) we can express the imaginary part as

$$X_{ml} = \frac{\pi}{2M^2}\left\{B + 2\,(A\rho c)_t\right\}(1 - x) \tag{3.29}$$

where $1 - x = -\dfrac{\nu_{rl} - \nu_r}{\nu_r} = -\dfrac{\Delta\nu_r}{\nu_r}$ is the relative difference between the resonant frequency under load ν_{rl} and the resonant frequency in an unloaded situation ν_r.

Equations (3.28) and (3.29) express the real and imaginary part of the load in quantities which can be measured at the electrical terminals of the transducer and in quantities being physical properties of the vibrating system.

3.2.3.5. The force and the velocity at the load

The transformation ratio N is defined in section 3.2.3.1.

$$N = \frac{\bar{I}}{\bar{v}_5}$$

Applying eqs. (3.18) and (3.19) to the amplitude transformer and the waveguide (see fig. 3.1) we obtain

$$|\bar{v}_1| = M\,|\bar{v}_3| \quad \text{and} \quad |\bar{v}_3| = |\bar{v}_5|$$

Hence

$$|\bar{v}_1| = \frac{M}{N}\,|\bar{I}| \tag{3.30}$$

This expresses the velocity at the load in the electrical current $\bar{I}$. The value of the force exerted on the load can be calculated from eq. (3.2)

$$|\bar{F}_l| = |\bar{v}_l|\,|\bar{Z}_{ml}| \tag{3.31}$$

where $|\bar{Z}_{ml}|$ can be determined from eqs. (3.28) and (3.29).

3.3. Measuring equipment

For recording of quantities during the welding period a storage oscilloscope and a Polaroid camera were used. The following quantities were recorded: the current through the transducer $\bar{I}$, output voltage of the generator $\bar{V}$, the vibrational amplitude of the welding tip ξ and the frequency difference $\Delta\nu_r$ (see sec. 3.2.3.4.). For the measurement of the last two quantities special equipment was used as will be described in the next sections.

3.3.1. The 'Fotonic sensor'

A 'Fotonic sensor' is a non-contact optical proximity detector. *) A bundle of optical fibres guides light to a reflecting surface. The reflected light is transmitted, again through optical fibres, to a photodetector. The intensity of reflected light depends upon the distance between the end face of the optical fibre-bundle and the reflecting surface. Hence the electrical signal from the photodetector is a measure of this distance. After a separate calibration of the instrument, vibrational displacements up to a frequency of 60 kHz can be measured. The noise level of the instrument is equivalent to a distance variation of 0.1 μm.

3.3.2. The frequency deviation meter

The instrument measures the difference $\Delta\nu_r$ between the resonant frequency of the loaded vibrating systems ν_{rl} and the resonant frequency of the unloaded system ν_r. An analog output signal is produced, with a rise time of less than 6 ms., hence changes of $\Delta\nu_r$ can be followed. The resolution of the instrument is about 5 Hz. **)

3.4. Quality of a weld and the test method

We will discuss what is meant by the 'quality of a weld'. These remarks will only refer to welds produced by ultrasonic welding (as mentioned in sec. 1.1.).

First, we will list the testing methods used in testing ultrasonic welds

1. Measurement of mechanical strength
2. Measurement of fatigue strength
3. Determination of corrosion resistance
4. Metallurgical examination (such as cross-sectioning).

---

*) The instrument is manufactured by Mechanical Technology Inc., Latham, New York.

**) The instrument was designed by Mr. W. v. Liefland from the Philips Product Division Elcoma.

The problem is how to define the quality of a weld in terms of results of the testing methods. From a pragmatical point of view, a weld has a good quality when it does not fail during the lifetime of the device or construction where it is applied. The link between this definition and the measurable quantities can only be made by correlating the behaviour of welds under practical circumstances (life time tests) with the test results of equivalent welds.
In the case of ultrasonic welds it appears from experience that mechanical strength is a reasonable measure of quality. The tensile shear test is used to test the mechanical strength of the welds. An ultrasonic weld is made between two overlapping strips and then a tensile force is applied at the ends of the strips by a standard testing machine. The direction of the tensilde force is indicated in fig. 2.1. In the present experiments the pulling velocity during testing van 20 mm/min.

The reasons chosen for the tensile shear test, are as follows

1. The tensile shear test can be carried out quickly and no special preparation of the specimens is required. *)
2. In the literature this test is most frequently encountered. This makes it possible to compare our experimental results with data from the literature.
3. In a tensile shear test the welded area is loaded more uniformly than in an U-tension test or the cross-tension test. (The U-tension test and cross-tension tests are better measures for the notch sensitivity of a weld than a tensile-shear test, see ref. 3.2).

In conclusion the tensile shear test is considered to be the most relevant measurement in the study of the influence of process parameters on weld formation.

3.5. Subsonic welding equipment

As already mentioned in the introduction (sec. 1.3) welding esperiments using a vibrational frequency of 30 Hz were performed. For these experiments a simple apparatus was built. (fig. 3.6). The testpieces are made out of sheet material. The lower sheet 1 (dimensions 40 x 12 x 2 mm) is fastened to an anvil, the upper sheet (40 x 12 x 1 mm) is mounted on a lever rotating around the point P (fig. 3.6). The center of sheet 2 is situated over a rectangular hole in the lever. At one end of the lever a vibrator is mounted (not shown in fig. 3.6). By vibrating the lever, sheet 2

---

*) For tests like the cross-tension or U-tension test (see ref. 3.2) specimens with holes are required and bending of the specimens in a special shape is necessary for the latter test.

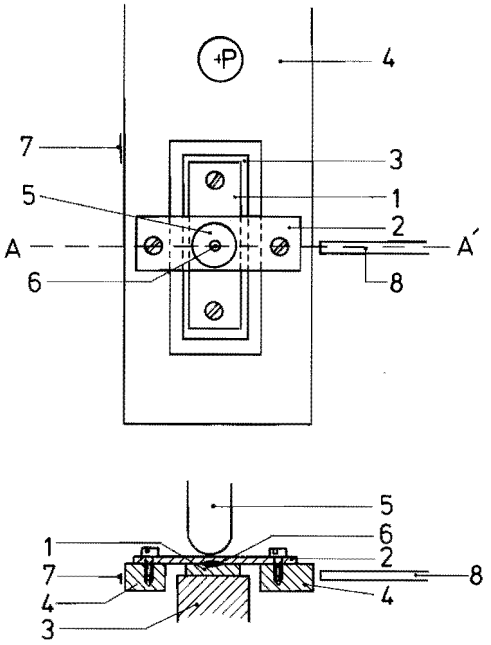

Fig. 3.6. The subsonic welding apparatus.
1. The lower sheet; 2. upper sheet; 3. anvil; 4. lever (rotating point P). 5. pin with spherical top, in order to press the center of the sheets together; 6. welding zone; 7. strain gauge; 8. 'Fotonic sensor'. The lower drawing is a section through AA'.

makes an almost linear vibrational movement in the direction AA'. The maximum amplitude is 40 μm. The center of sheet 2 is pressed onto the fixed sheet 1 by means of a pin, with a spherical top (radius 6 mm). The construction is such that only a normal force and no tangential force is exerted by the pin on the weld specimens.

The vibrational amplitude is measured at the position A' by means of a 'Fotonic Sensor' (see section 3.3.1). The force in the contact zone parallel to the interface of the two sheets is measured by means of a strain gauge on the lever, thus acting as a dynamometer.

4. ULTRASONIC WELDING EXPERIMENTS AND RESULTS

In order to be able to describe the ultrasonic welding process in a model, first of all experimental information must be available. Experimental data from the literature are mainly related to (see chap. 2)
1. Tensile shear tests of full-grown welds
2. Metallographic sections of welds
3. Temperature measurements in the welding zone.

All these data, except the temperature measurements, refer to the final situation of the full-grown weld.

In this chapter a number of experiments will be described, aimed at explaining the following phenomena not usually treated in the literature.
1. The initial stage of weld formation and the growth of the weld as a function of both welding time and vibrational amplitude.
2. The alternating force exerted by the welding tool on the workpieces and the relative displacement (slip) of the surfaces to be welded.

Hence, these experiments will give information about the phenomena during the formation of a weld.

4.1. The specimens

All welding experiments were carried out using strips, 10 mm x 50 mm x 0.5 mm, two of which were welded with an overlap of about 30 mm.

The materials used, are listed in tables 4.1, 2. Aluminium and copper were chosen because these materials are used as electrical conductors and are joined by ultrasonic welding in special cases (see sec. 1.1). In the literature it is mentioned that hardness determines weldability (2.3), therefore steel and nickel were chosen to study materials with a higher hardness than copper and aluminium.
Prior to welding the specimens were degreased in acetone, as recommended in literature (see sec. 2.3.3). Initial experiments did show that copper specimens, even after degreasing, have a very poor ultrasonic weldabbility. This was also observed by Leven (2.3). When the oxide layer is removed in a 2% HCl-solution, weldability is improved.

4.2. The development of a weld

The first experiments were designed to study the development of an ultrasonic weld. Measurements of the tensile shear force as a function of welding time and vibrational amplitude are reported; the appearance of the welded interface after peeling of the weld has been studied as well as microsections of the welds. Then, in the case of medium hard Al the length of the microwelds was measured. Microwelds are separate welded regions in the weld area. The influence of surface conditions, e.g. surface roughness or the presence of a lubricating layer is demonstrated.

TABLE 4.1.
Materials used in ultrasonic welding experiments.

Material	Contents	
Al (medium hard)	Si $\leqslant$ 1.00% Fe $\leqslant$ 1.00%	Cu + Zn $\leqslant$ 0.10% other impurities $\leqslant$ 0.10% Al : remainder
Al (hard)	Mg : 0.50 – 2.00% Si : 0.50 – 1.50% Mn : 0.20 – 1.50%	Fe $\leqslant$ 0.40% Cu $\leqslant$ 0.05% other impurities $\leqslant$ 0.10% Al : remainder
Cu	Cu $\geqslant$ 99.4% O and S $\leqslant$ 0.10% Al, Zn and Sn $\leqslant$ 0.10%	Si $\leqslant$ 0.20% Ni, Pb $\leqslant$ 0.10% As $\leqslant$ 0.05%
Ni	Ni and Co $\geqslant$ 98.5% Co $\leqslant$ 1.00% C $\leqslant$ 0.10% Al $\leqslant$ 0.04% Si $\leqslant$ 0.10%	S $\leqslant$ 0.02% Mn and Mg: 0.20 – 0.40% Mg $\leqslant$ 0.10% Fe $\leqslant$ 0.25% Cu $\leqslant$ 0.15%
Stainless steel	Cr $\geqslant$ 17.00% Ni $\geqslant$ 8.00% C $\leqslant$ 0.15% Si $\leqslant$ 0.75%	P $\leqslant$ 0.030% S $\leqslant$ 0.035% Mn $\leqslant$ 0.60% Fe : remainder
Mild steel	C $\leqslant$ 0.10% Si $\leqslant$ 0.20% Mn : 0.20 – 0.45%	P $\leqslant$ 0.050% S $\leqslant$ 0.050% Fe : remainder

4.2.1. The breaking force in a tensile shear test as a function of welding time and vibrational amplitude

4.2.1.1. The clamping force

Before discussing the welding experiments we will describe how the value of the clamping force F_C is chosen. This choice affects the matching of the load impedance to the ultrasonic vibrating system and generator. In principle this matching can be achieved by variation of: the clamping force F_C, the mechanical transformation factor M^2 of the amplitude transformer or the output impedance of the amplifier

TABLE 4.2
Several data of the materials

Material	Vickers hardness H_V [1] (N/mm²)	Work hardening exponent m	C (N/mm²)	Young's modules E (N/mm²)	Ductility δ	Clamping force F_c (N)	Base material fracture stress [2] τ_n (N/mm²)	Breaking stress of the welds τ_b (N/mm²)	τ_b/τ_n
Al (medium hard)	370±20	0.3	200	7 x10⁴	12	375	80	55±5	0.7
Al (hard)	910±20	0.2	420	6.8x10⁴	4	675	170	130±10	0.8
Cu	970±40	0.3	420	12.5x10⁴	11	375	170	150±20	0.9
Ni	2200±100	0.4	1100	21 x10⁴	34	1000	440	310±30	0.7
Stainless steel	1700±100	0.4	1300	21 x10⁴	30	1000	520	190±20	0.4
Mild steel	1320±70	0.2	1000	21 x10⁴	4	675	420	170±20	0.4

1) The indicated scattering is the standard deviation of a number of hardness measurements on different specimens.
2) See sec 4.2.1.4.

Z_{out}. The transformation factor is constant in the present experiments. The output impedance Z_{out} is switchable to 220 Ω, 490 Ω, 880 Ω and 1350 Ω. At the four values of Z_{out}, the clamping force F_c is varied; the higher F_c, the larger the contact area and hence the larger the load impedance Z_{ml}. The electrical impedance at the transducer terminals Z_e depends upon Z_{ml} and a number of constant quantities (see eqs. 3.22 and 3.25). Consequently matching of Z_e to the amplifier can be realized by adjusting F_c to an appropriate value.

The value of F_c was varied in steps of about 30%, starting at 100 N. and at each setting a number of welds was made. The setting of the amplifier and the welding time were kept constant. The tensile shear force of the welds was used as a criterion for determining an optimum value of the clamping force F_c. The optimum value was found – within the limits of the choice of parameters – for all materials at Z_{out} = 490 Ω. The values of the clamping force are listed in table 4.2.

4.2.1.2. Observations

The materials mentioned in table 4.1 were welded as similar metal couples. The welding time was varied from 10 ms to several seconds. Three different settings of the amplifier were used which resulted in three values of vibrational amplitude. The choice of the range of both welding time and vibrational amplitude is determined on one hand by the limitations of the equipment (maximum welding time: 10 seconds. nominal electric output power of amplifier: 400 W) and on the other by the first appearance of a weld. The clamping force used was determined as described in sec. 4.2.1.1.

For each combination of welding time and vibrational amplitude 10 welds were made. The breaking force $F_b(t)$ of 8 welds was determined by a tensile shear test (see sec. 3.4). The remaining 2 welds were peeled off in order to study the welded area (see sec. 4.2.2). In figs. 4.1 to 4.6 the average values of $F_b(t)$ are plotted as a function of the welding time t, for different values of vibrational amplitude ξ. The range indicated in the graphs is twice the standard deviation of the 8 observations. The 90% confidence interval is 1.7 times this range. The values of ξ mentioned in the graphs, are mean values for 10 welds; the value of ξ for a particular weld being a time average determined over the welding period. At any time the vibrational amplitude can deviate up to 10% from this time average. The time average values themselves show a scatter of up to 10% of the mean value mentioned in the graphs. Each mean value of ξ corresponds to a mean value of the electrical power P_e delivered by the amplifier, listed in table 4.3.
The strongest welds pull a nugget out of the base material in the tensile shear test. This occurred for: medium hard Al (ξ = 23 μm, t = 60 ms); hard Al (ξ = 25 μm, t = 200 ms) and Cu (ξ = 21 μm; t = 1000 ms). All the other welds fractured by shear at the weld interface.

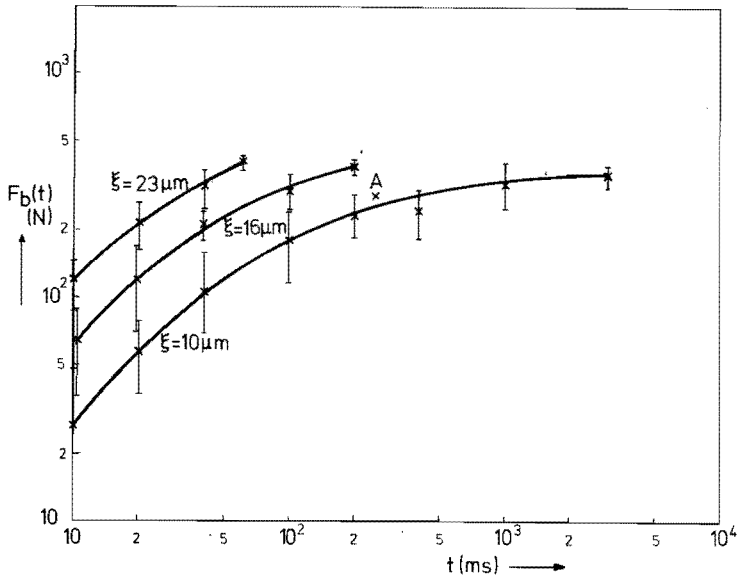

Fig. 4.1. Breaking force $F_b(t)$ of ultrasonic welds as a function of the welding time t, at different levels of the average vibrational amplitude ξ. The bars indicate twice the standard deviation of a series of 8 welds. Material: medium hard Al.

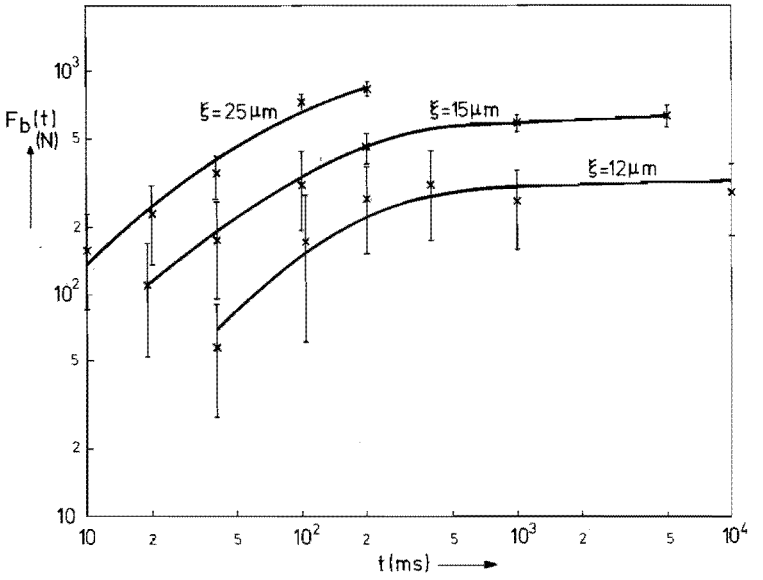

Fig. 4.2. Breaking force $F_b(t)$ for hard Al (see fig. 4.1).

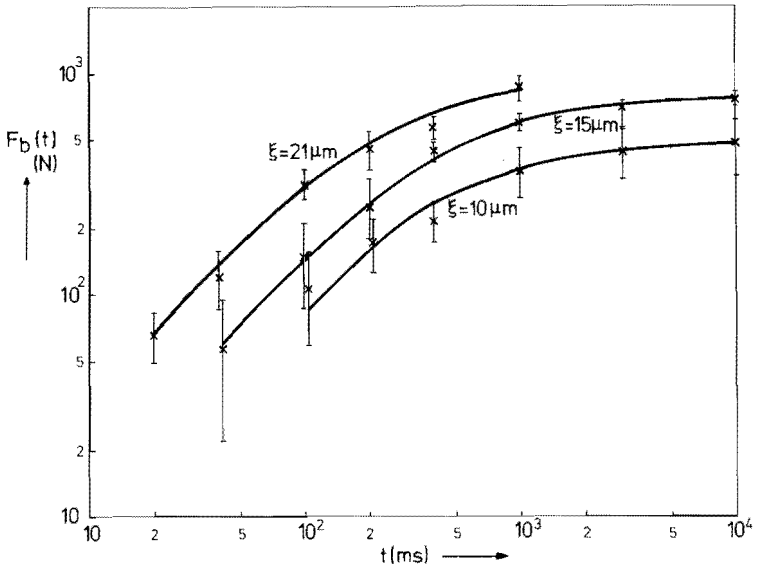

Fig. 4.3. Breaking force $F_b(t)$ for Cu (see fig. 4.1).

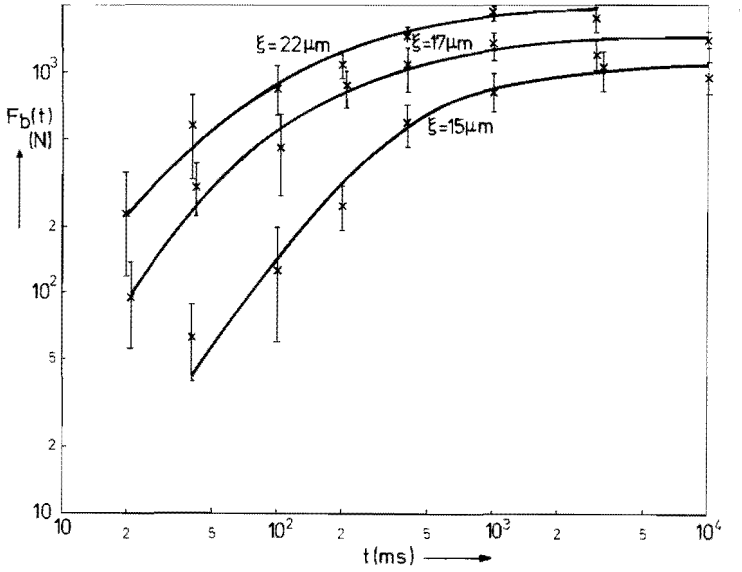

Fig. 4.4. Breaking force $F_b(t)$ for Ni (see fig. 4.1).

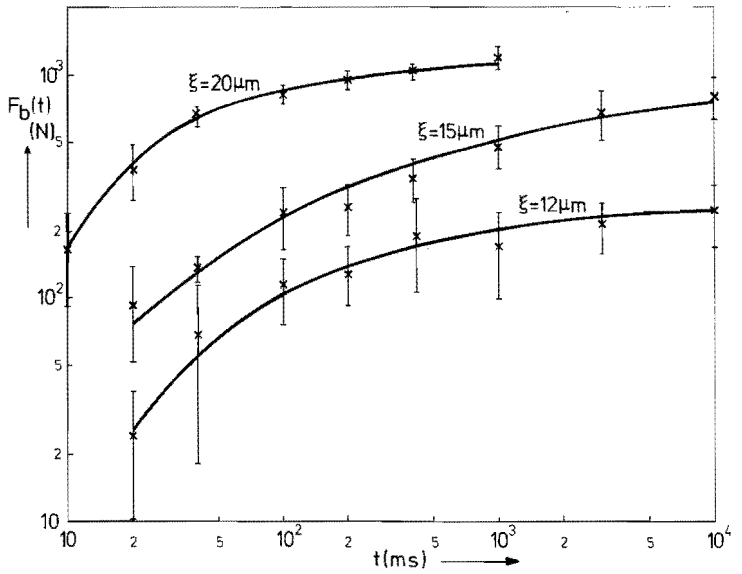

Fig. 4.5. Breaking force $F_b(t)$ for stainless steel (see fig. 4.1).

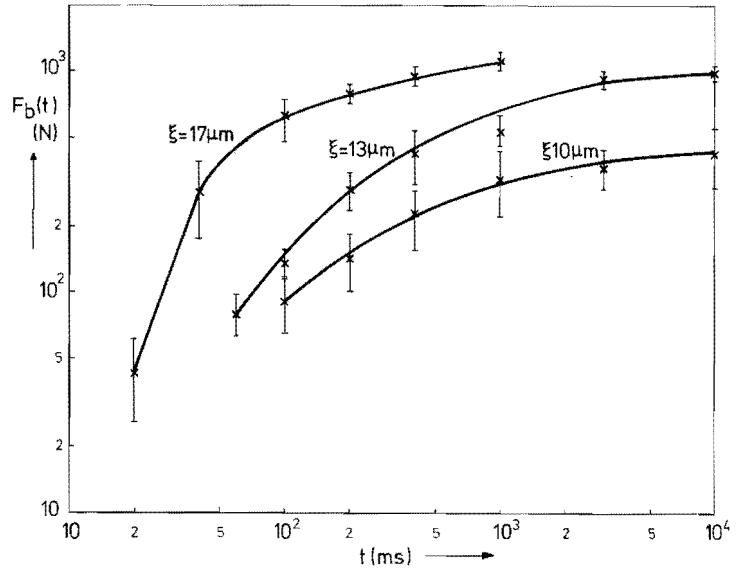

Fig. 4.6. Breaking force $F_b(t)$ for mild steel (see fig. 4.1).

TABLE 4.3.
Electrical power P_e (delivered by the amplifier) and vibrational amplitude ξ of the welding tip for different settings of welding equipment.

Al (medium hard)		Al (hard)		Cu	
P_e (W)	ξ (μm)	P_e (W)	ξ (μm)	P_e (W)	ξ (μm)
90	10	100	12	100	10
230	16	230	15	200	15
380	23	530	25	500	21
Ni		**stainless steel**		**mild steel**	
P_e (W)	ξ (μm)	P_e (W)	ξ (μm)	P_e (W)	ξ (μm)
130	15	110	12	110	10
220	17	200	15	210	13
440	22	400	20	380	17

From the experiments we conclude
1. The higher the vibrational amplitude ξ the faster the breaking force $F_b(t)$ increases with time.
2. The increase of the breaking force per unit time (the growth rate of the weld) decreases with increasing welding time.
3. There is a saturation strength of the weld; this saturation level increases with the amplitude of vibration.
4. The breaking force does not decrease even for long welding times.
5. In the initial stage of weld formation, the scatter of the values $F_b(t)$ is large. This scattering becomes relatively smaller as the saturation strength is approached.

The welded area of broken welds was measured by two different methods
1. The welded area was photographed and the area of the welded parts was measured by means of a planimeter.
2. The axes of the elliptical weld were measured using a microscope with a measuring eye piece and the area of the weld calculated. This method can only be used for welds having little or no unwelded regions (e.g. figs. 4.8c, 9e) whereas the first method is also applicable when the weld consists of a number of separated welded junctions (microwelds).

The average breaking stress (in the tensile shear test) τ_b of the welds was calculated from the breaking force and the welded area. The results are given in table 4.2.

In spite of the high breaking forces in the tensile shear test, the welds in stainless steel and mild steel could be peeled off by hand very easily, even for welding times of t = 1000 ms. (see fig. 4.12, 13).

Some further observations are

1. In some experiments using large vibrational amplitudes, sticking of the workpieces to the welding tip or to the anvil was observed. This is also reported by Genscoy (2.15) and Drews (2.45). During the welding of nickel and the two steels sticking to the tip was severe and after a few tens of welds caused considerable damage to the welding tip surface. In these cases the welding tip surface either had to be dressed or changed by rotating the vibrating system about its axis (see fig. 3.2). This severe wear of the tip during welding of nickel is also reported by Meriin (4.1).
2. For a welding time of 1 second and the highest amplitude of vibration, specimens of mild and stainless steel showed blue temper colours. Hence the surface temperature must have been about 300 °C (4.2).
3. In some cases the strips to be welded slid away under the welding tip, a simple clamping mechanism to hold the sheets in position avoided this.

4.2.1.3. The breaking stress

In medium hard Al strips (thickness 1 mm) 80 welds were made, using different welding times and vibrational amplitudes. In this way a large variation in weld strength was obtained, the breaking force ranging from 100 N to 1100 N. The weakest welds showed a number of clearly separated microwelds whereas in the strongest welds complete welding of the contact area occurred. The welded area was determined by using a planimeter. in fig. 4.7 the breaking force F_b is plotted versus the welded area A_w. Linear regression analysis shows that the relationship

$$F_b = \tau_b A_w \qquad (4.1)$$

is valid, where τ_b is the average breaking stress of the weld in a tensile shear test. *)

We conclude that the breaking stress of the weld is independent of its size and number of microwelds. Similar experiments with different materials gave the same result.

---

*) The line that fits the measurements best is $F_b = 55\ A_w - 15$; the coefficient of determination is 0.93. This line is drawn in fig. 4.7.

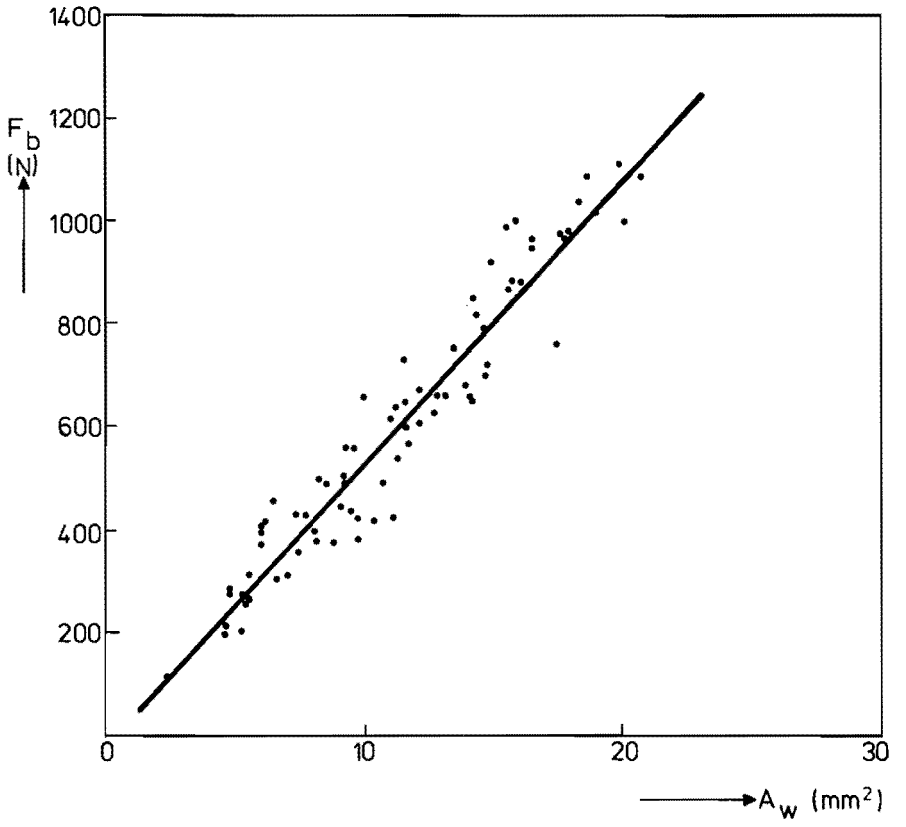

Fig. 4.7. Breaking force as a function of the welded area A_W for Al (medium hard).

4.2.1.4. Discussion

In this section we will compare the breaking stress τ_b of the welds to the base-material strength and then discuss some factores influencing ultrasonic weldability of metals.

The breaking stress τ_b should be derived from the real state of stress in the fracture zone which depends on geometrical configuration and the way of loading. However, we choose the necking stress in a tensile bar as a safe lower limit of the fracture stress, since necking is the onset of plastic instability in a tensile test. The necking equals

$$\sigma_n = C m^m \tag{4.2}$$

where C is a constant (effective stress at effective strain $\bar{\delta} = 1$) and m is the work

hardening exponent (see Kobayashi (4.3)). The estimated values of C and m are listed in table 4.2, based on data from Veenstra (4.4). The shear stress at fracture in a tensile shear test is $\tau_n = \sigma_n/\sqrt{3}$. This stress τ_n is also listed in table 4.2. When the weld strength is equal to that of the parent material the ratio τ_b/τ_n is equal to 1. The values of τ_b/τ_n for the different materials are listed in table 4.2. The values of τ_b/τ_n for Al, Cu and Ni range from 0.7 to 0.9 and thus the strength of the welds in Al, Cu and Ni approaches the strength of the parent material. The value τ_b/τ_n is 0.4 for the two kinds of steel, hence these welds are of inferior quality. This is confirmed by microsections of the welds (sec. 4.2.2) and by the fact that they could be peeled easily by hand (see sec. 4.2.1.2). This suggests that little metallurgical bonding occurred and that the strength is derived mainly from mechanical interlocking. Mild steel and stainless steel were not studied in further experiments because they proved difficult to weld ultrasonically.

The factor most likely to be responsible for the difference in weldability between the group: Al, Cu and Ni and the two kinds of steel is the ease with which the contaminating surface layers can be removed. This is in agreement with the conclusions in sec. 2.5.3.5. regarding the adhesion of metals.
The oxide layer on Al is much harder than the parent material and therefore easily ruptured and dispersed by deformation of the metal close to the interface. This is assumed to be the reason for the good weldability of Al.
Stainless steel is covered by a chromium/chromium oxide layer, having a high wear resistance (4.6, 7) and thus hard to remove by mechanical action. As to the oxide layer on mild steel no relevant information could be found. Microsections (see sec. 4.2.2) of the welds in the two types of steel show that the interface remains clearly visible. This indicates that the surface layer was not sufficiently removed by the ultrasonic welding operation.

In the literature a number of material properties are mentioned, which might influence the ultrasonic weldability of a material. We will consider crystal structure, ductility and hardness from which it will be seen that none of these properties shows a clear relationship with ultrasonic weldability in the present experiments.

1. *Crystal structure.*
   The structure of Al, Cu, Ni and stainless steel is face centered cubic (FCC). The structure of mild steel is BCC. From the results of the experiments we conclude that crystal structure is not primarily correlated with the ultrasonic weldability of the materials; the cubic structure may be favourable (compare appendix A2, fig. A2.1) but is certainly not sufficient.
2. *Ductility*
   Ductility is a measure of the amount of plastic deformation a material can withstanc before fracture. As plastic deformation occurs in the interfacial zone of an ultrasonic weld a relationship between weldability and ductility is suggested in

the literature (4.5), i.e. the higher the ductility the better the ultrasonic weldability. However, a quantitative definition of both ductility and welability is not given.
The ductility of a material is defined as (4.4)

$$\delta = \left(\frac{E}{C}\right)^{\frac{m}{1-m}}$$

where E is Young's modulus. The values of δ are listed in table 4.2. From this table we see that the metals with a good weldability (i.e. Al, Cu and Ni) have a ductility ranging from 4 to 34; both steel specimens showed poor weldability although the ductility is in the same range. Therefore a high ductility is not sufficient to explain ultrasonic weldability. A low ductility may be sufficient to prohibit ultrasonic weldability. *)

3. *Hardness*
Leven (2.3) stated that ultrasonic weldability depends on the hardness of the material: the lower the hardness the better the weldability. The experiments mentioned in this chapter show that there is certainly no univocal relationship between hardness and weldability. This is demonstrated by the fact, that nickel has a higher hardness than stainless steel and mild steel, yet Ni is the only weldable one of these three materials (see table 4.2).

4.2.2. The appearance of the welded interface

In order to follow the development of an ultrasonic weld, two of the welds, made during the experiment described in sec. 4.2.1.2., were peeled in such a way that smearing out of broken welds, as occurred in the tensile shear tests, was avoided. Peeling of the strongest welds (as mentioned in sec. 4.2.1.2) resulted in pulling a nugget out of the base material. Hence the welded interface could not be observed in these cases. Photographs of the peeled surfaces are shown in figs. 4.8 to 4.13. The bright spots on the photographs are the areas where welding occurred with no welding in the dark background. In these figures the direction of vibration during welding is indicated.

In the initial stage of the welding period we observed a number of small welded spots (microwelds) which were elongated in the direction of vibration. The average

---

*) From experiments not described in this thesis we know that the ultrasonic weldability of molybdenum is very poor. The ductility of Mo is very low. It is conceivable that because of the low ductility the welded junctions are ruptured by the relative movement of the weld members.

Fig. 4.8. Peeled welds. Material: Al (medium hard). Clampingforce F_c = 375 N. Amplitude of vibration ξ = 23 μm. The direction of vibration during welding is indicated.

⟷ direction of vibration ——— = 250 μm

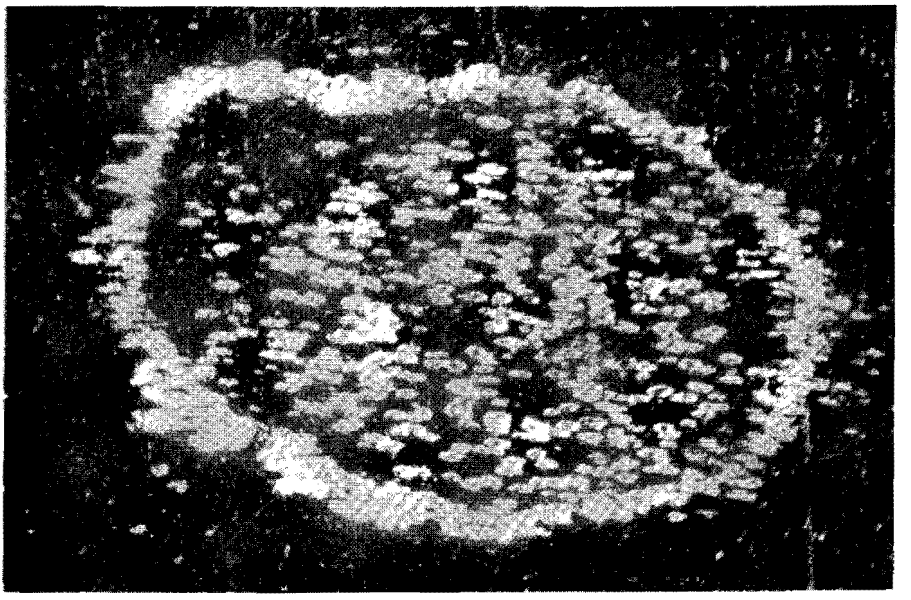

a. after welding time t = 5 ms.

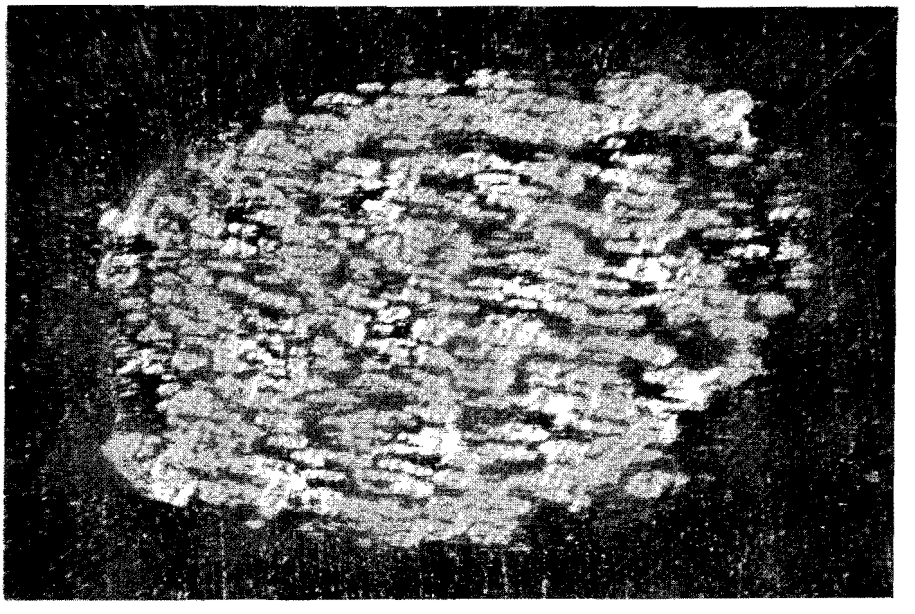

b. after welding time t = 10 ms.

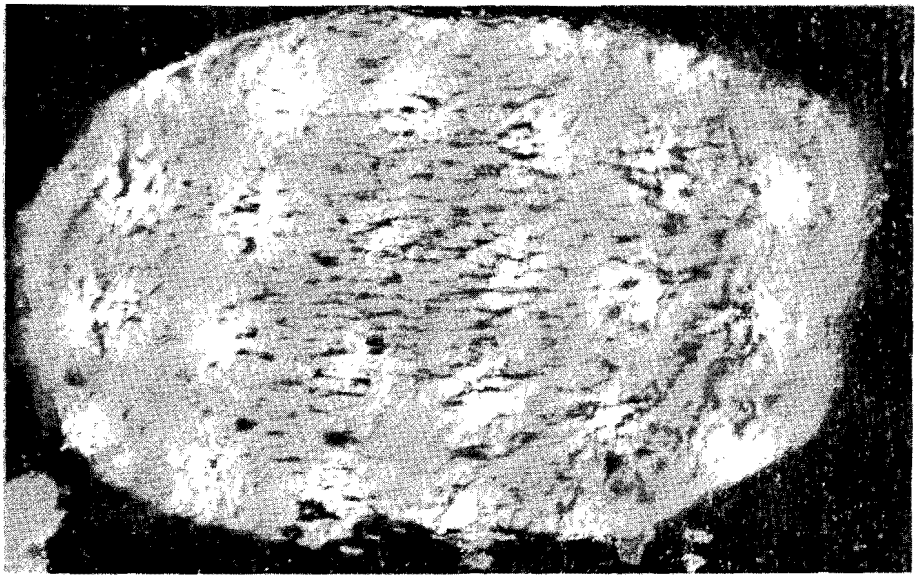

c. after welding time t = 40 ms.

Fig. 4.9. Peeled welds. Material: Al (hard). Clamping force F_c = 675 N. Amplitude of vibration ξ = 25 μm. The direction of vibration during welding is indicated.

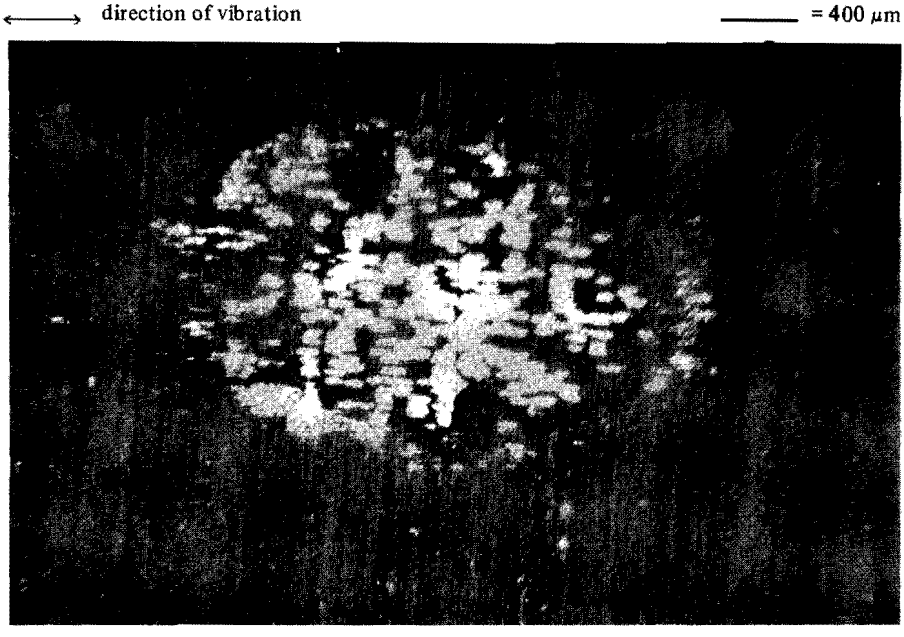

a. after welding time t = 5 ms.

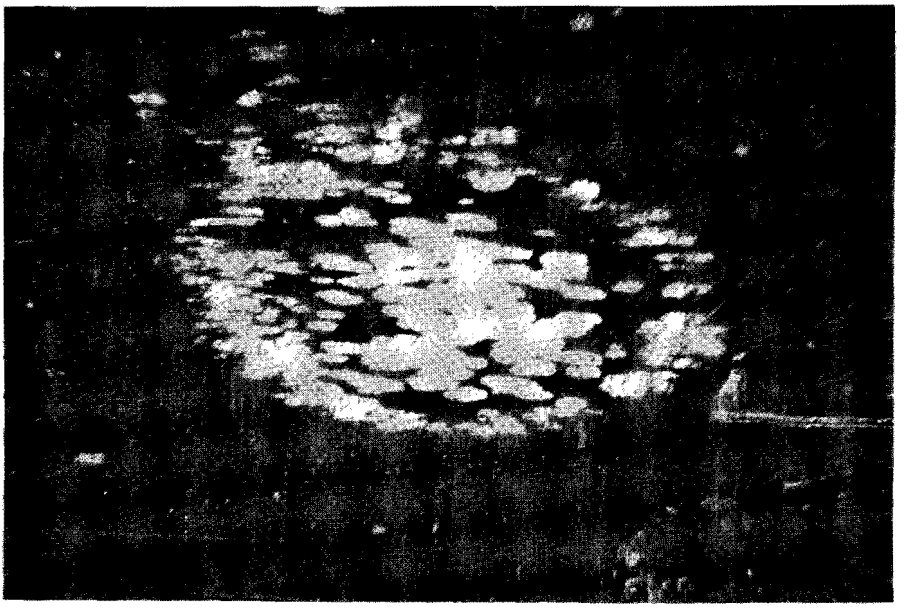

b. after welding time t = 10 ms.

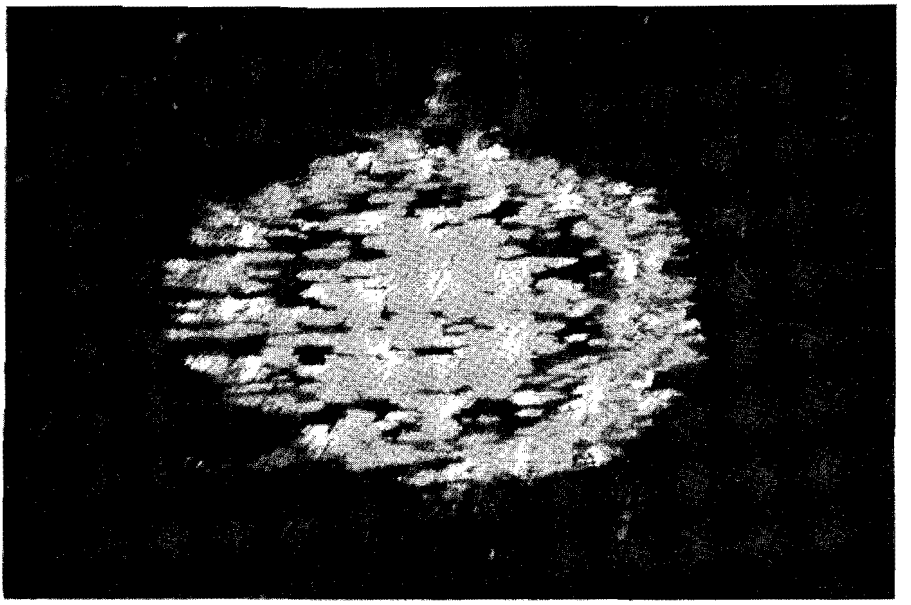

c. after welding time t = 20 ms

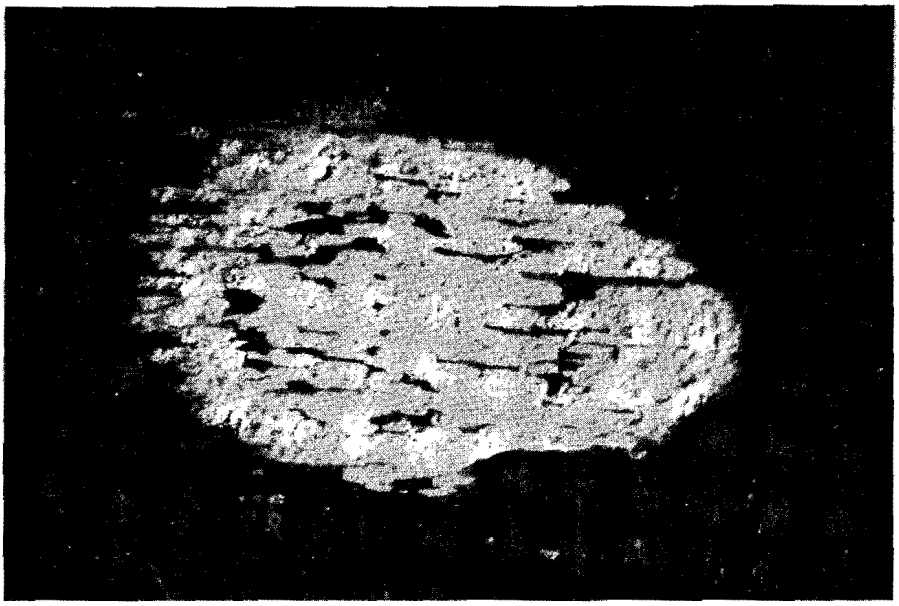

d. after welding time t = 40 ms.

e. after welding time t = 100 ms

Fig. 4.10. Peeled welds. Material: Cu. Clamping force F_c = 375 N. Amplitude of vibration ξ = 21 μm. The direction of vibration during welding is indicated.

$\longleftrightarrow$ direction of vibration ——— = 400 μm

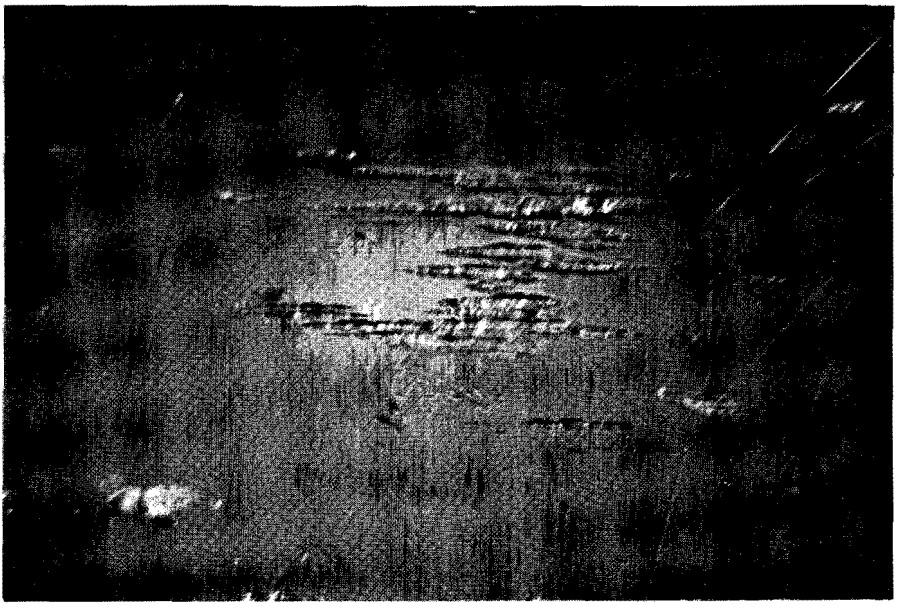

a. after welding time t = 20 ms.

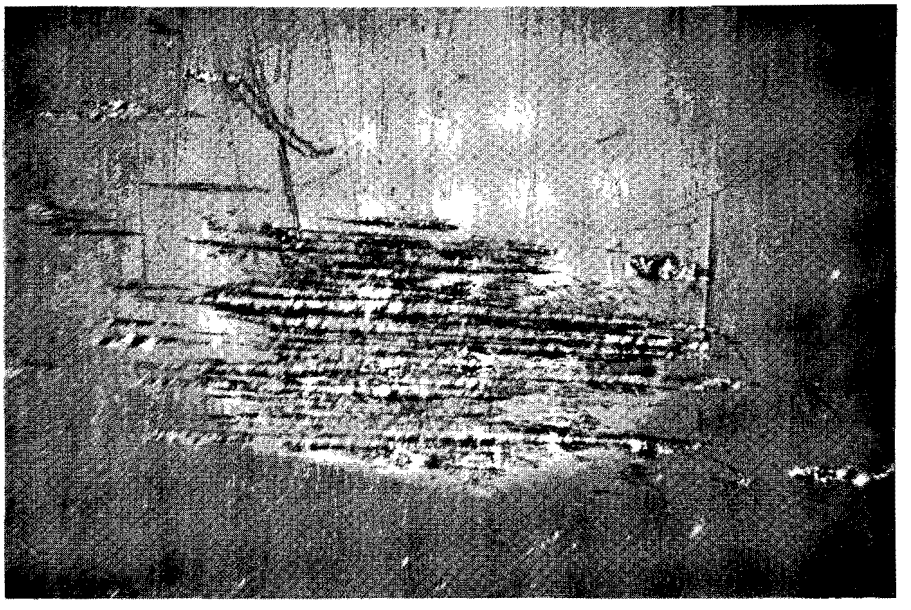

b. after welding time t = 40 ms.

c. after welding time t = 100 ms.

d. after welding time t = 400 ms

Fig. 4.11. Peeled welds. Material: Ni. Clamping force F_c = 1000 N. Amplitude of vibration ξ = 22 μm. The direction of vibration during welding is indicated.

$\longleftrightarrow$ direction of vibration ——— = 400 μm

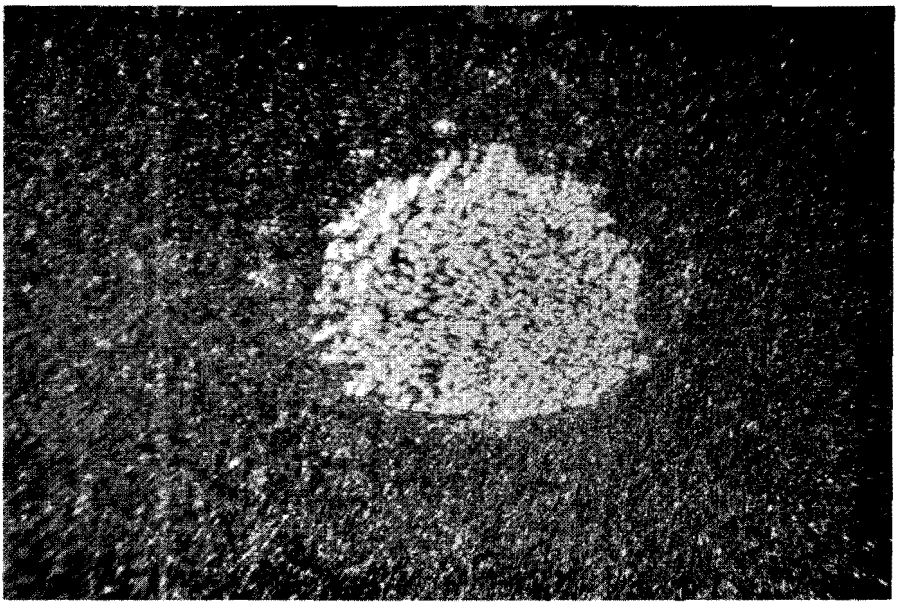

a. after welding time t = 20 ms.

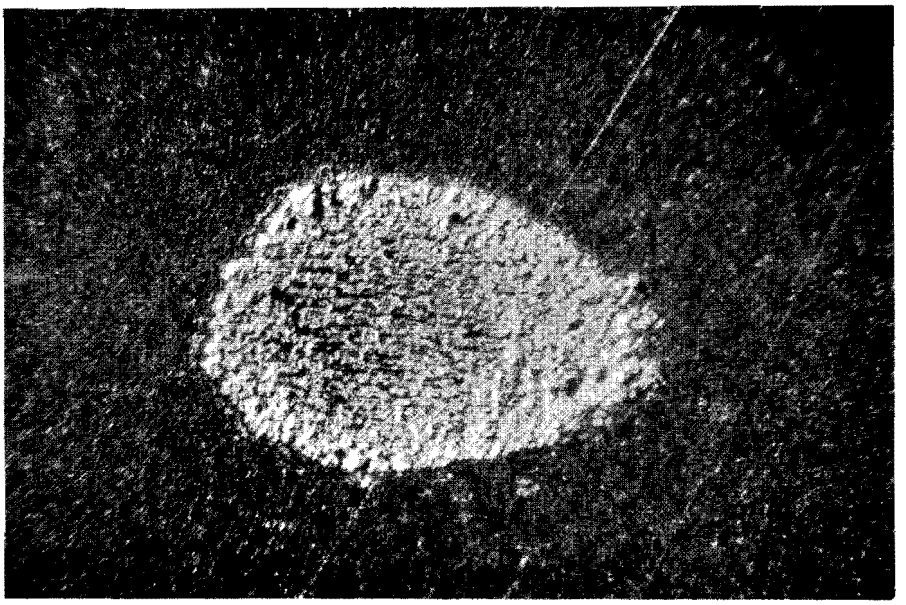

b. after welding time t = 40 ms.

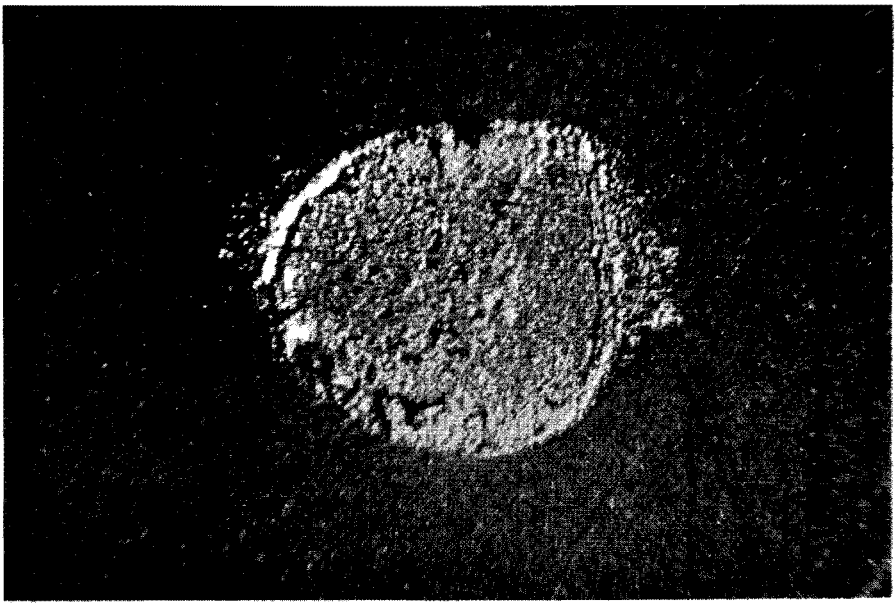

c. after welding time t = 100 ms.

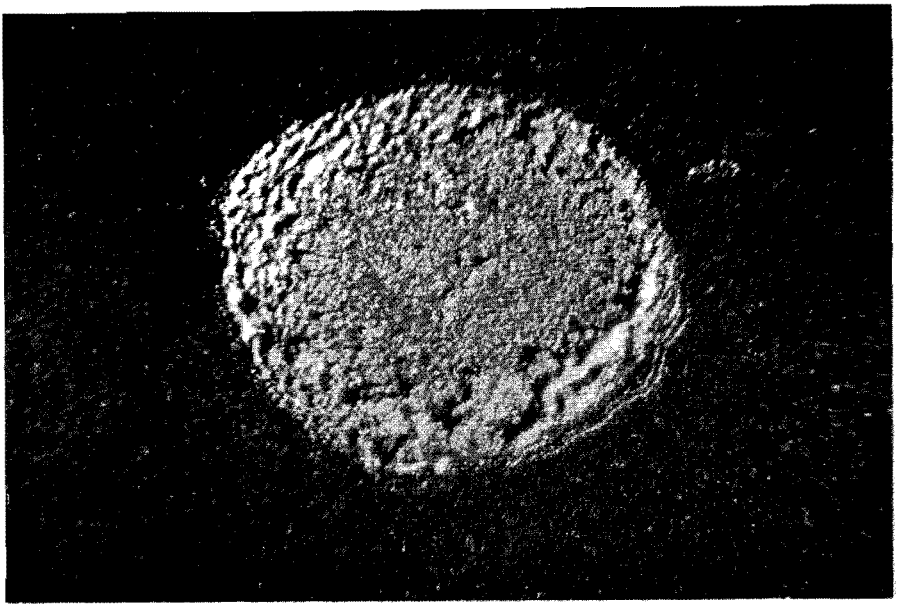

d. after welding time t = 200 ms

Fig. 4.12. Peeled welds. Material: stainless steel. Clamping force F_c = 1000 N. Amplitude of vibration ξ = 20 μm. The direction of vibration during welding is indicated.

$\longleftrightarrow$ direction of vibration ——— = 400 μm

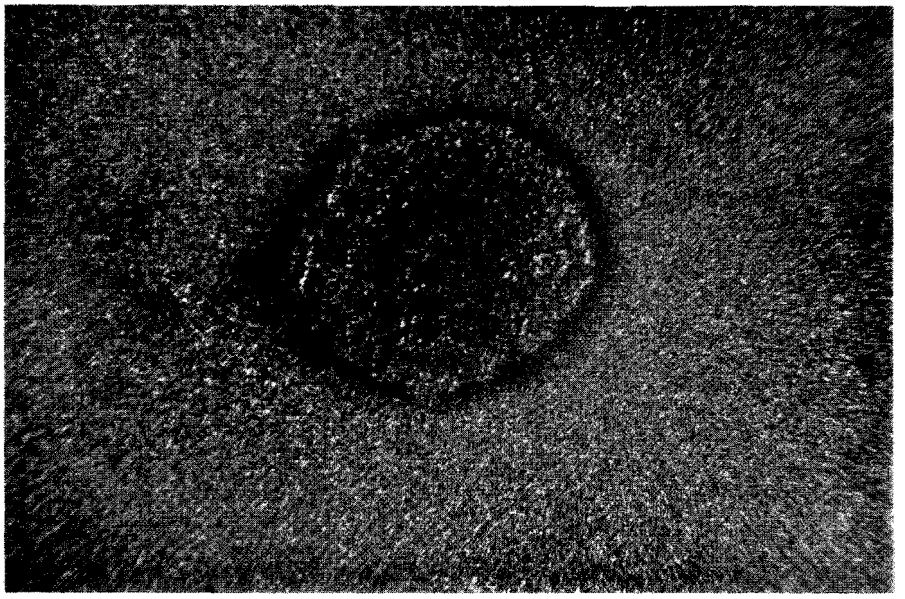

a. after welding time t = 10 ms.

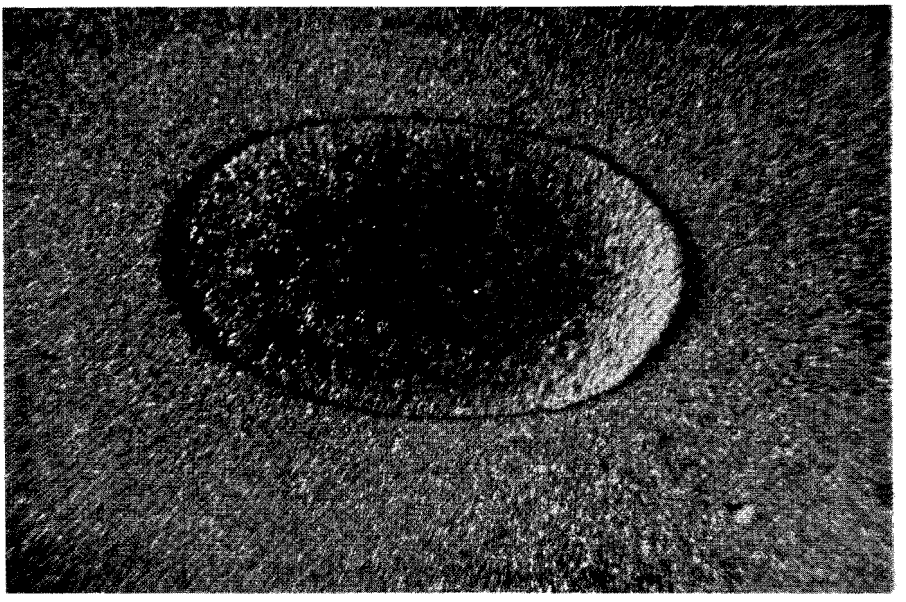

b. after welding time t = 40 ms.

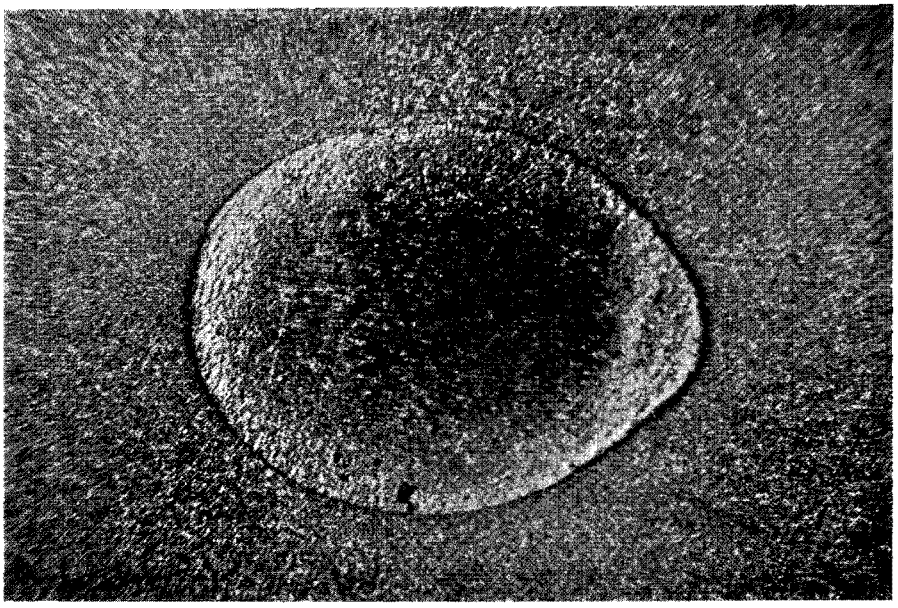

c. after welding time t = 100 ms.

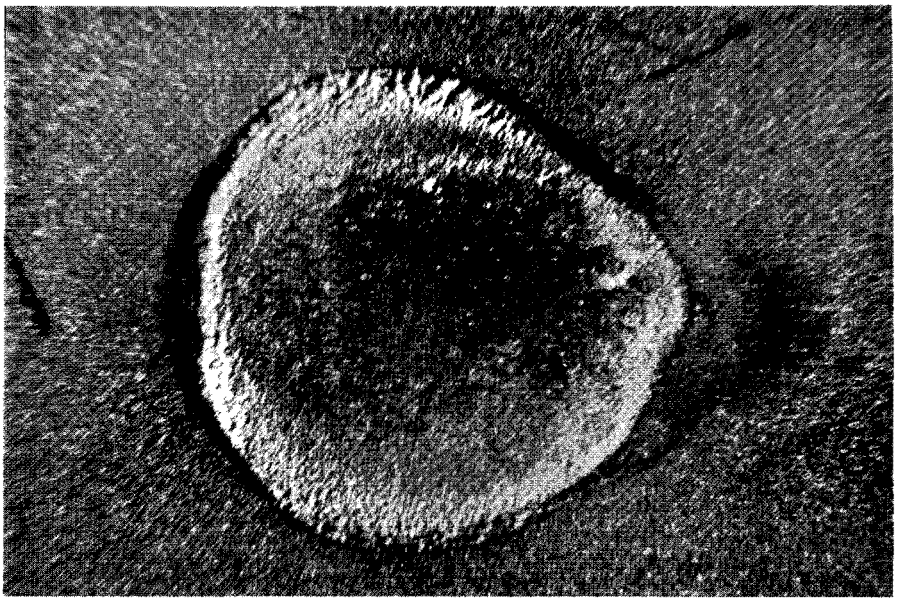

d. after welding time t = 400 ms

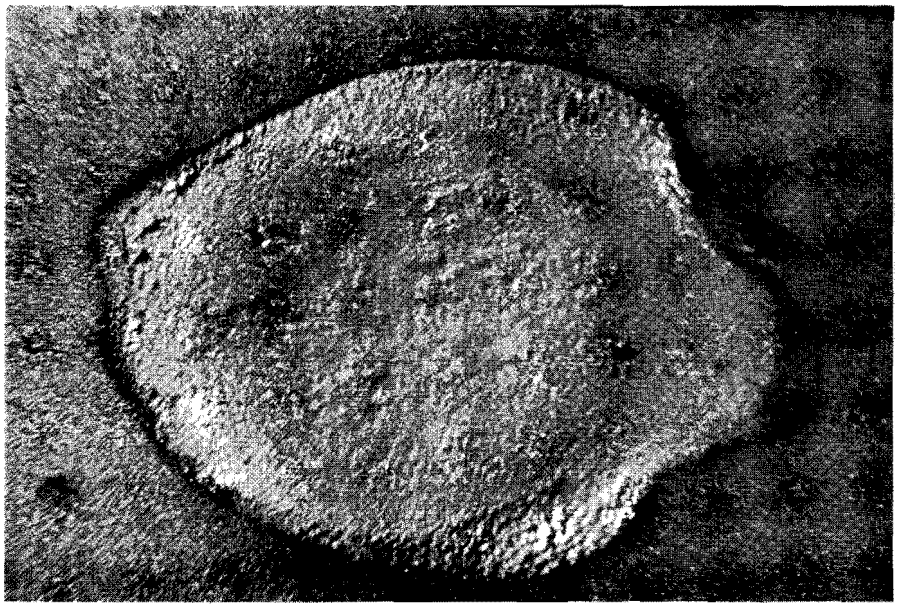

e. after welding time t = 1000 ms.

Fig. 4.13. Peeled welds. Material: mild steel. Clamping force F_c = 1000 N. Amplitude of vibration ξ = 17 μm. The direction of vibration during welding is indicated.

$\longleftrightarrow$ direction of vibration ——— = 400 μm

a. after welding time t = 20 ms.

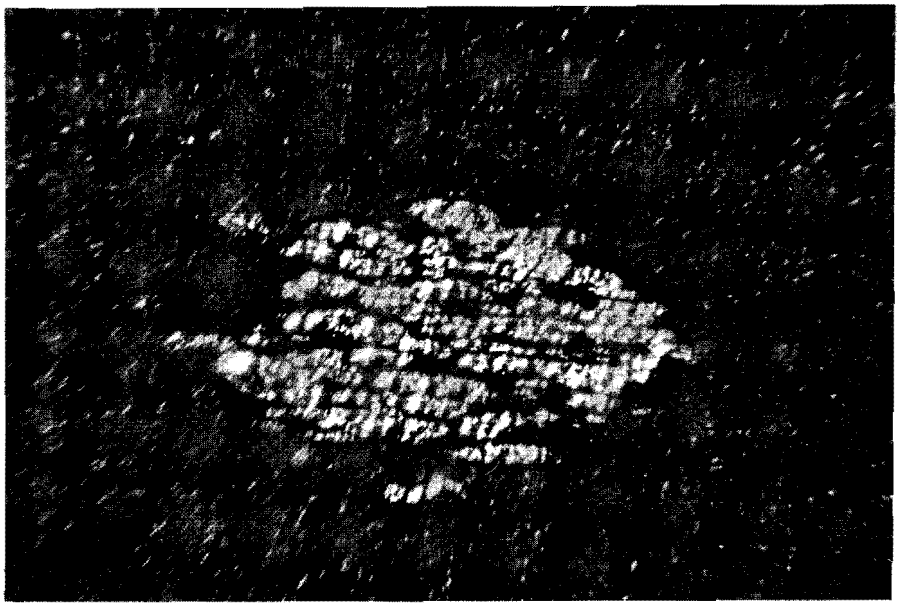

b. after welding time t = 40 ms.

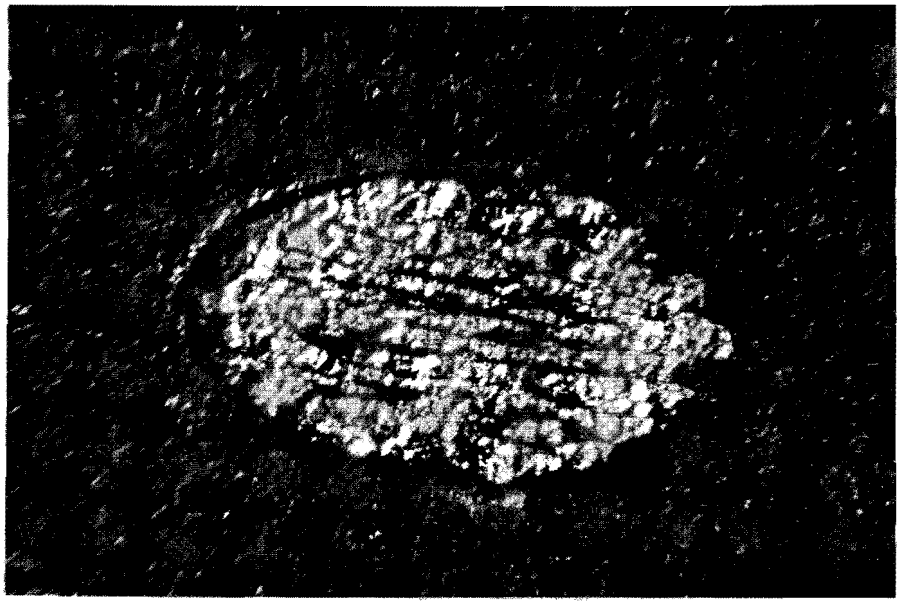

c. after welding time t = 100 ms

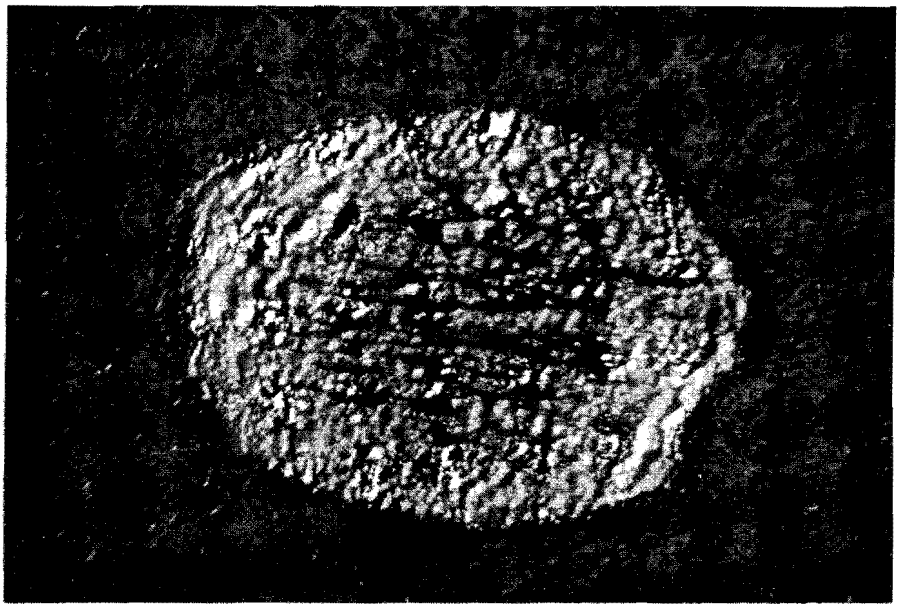

d. after welding time t = 400 ms.

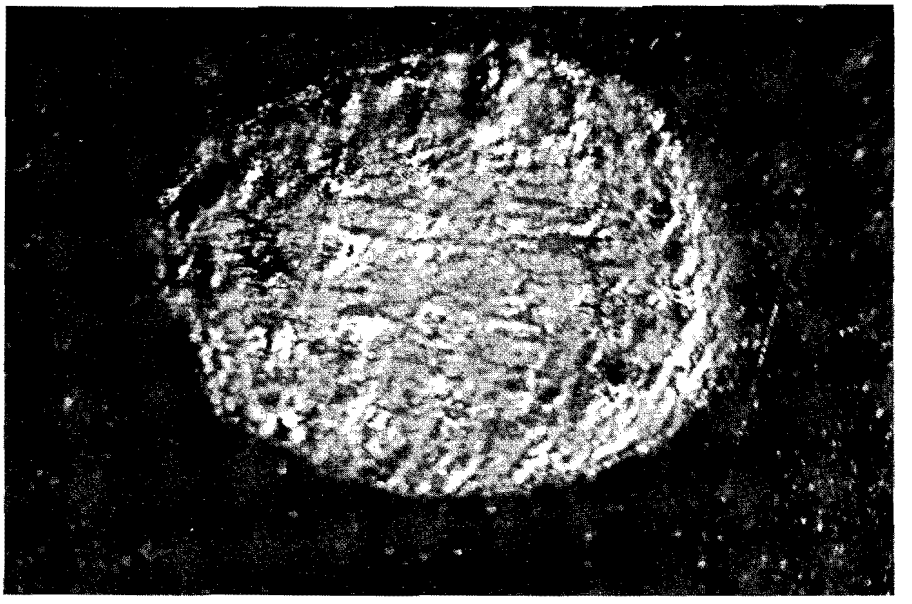

e. after welding time t = 1000 ms

length of these spots was different for different materials. For stainless steel (fig. 4.12) the length was less than 50 μm. For Ni and Al the length of the spots varied between 50 to 100 μm (figs. 4.8, 9, 11). The microwelds in Cu were initially up to 500 μm long, but in the later stages of weld formation they became so long that they could not be clearly distinguished (fig. 4.10).
As the welding period proceeded the number of microwelds increased.

At the periphery of the welded area the surface of the peeled welds has a more rough appearance (fig. 4.8c, 11d, 12c, 13e). In this zone the microwelds are being broken during welding. This point of view is supported by microsections (see below; fig. 4.17a). The occurrence of cracks at the periphery is reviewed in sec. 2.3.2. In the present experiments the average tensile shear strength is not significantly lowered by the occurrence of cracks.

The conclusion from observations on the peeled welds are as follows
1. An ultrasonic weld is built up by small welded areas (microwelds).
2. The number of microwelds increases with increasing welding time. The weld is completed when the whole area is covered with microwelds.
3. In most cases the microwelds are distributed at random over the welded area; sometimes their density is higher at the perimeter than in the central part of the weld.
4. The microwelds are oblong with their longest axes parallel to the direction of vibration. This suggests that the microweld has grown in this direction by the oscillatory relative movement of the contacting surfaces.
5. Near the end of the welding period some materials show cracks at the perimeter of the weld.

Microsections of welds were made with the direction of sectioning perpendicular to the direction of vibration during welding. Figs. 4.14 to 4.18 show the results for the different materials. In the contact area a zone of severely plastically deformed material exists. In the case of Al, Cu and Ni the interface (boundary line) between the weld members has partially disappeared. The thickness of the zone of plastic deformation is between 30 and 100 μm. Outside this area deformation of the material is not visible in the micrographs (except in the case of mild steel).
Micro-sections of stainless steel show heavy deformation at the periphery of the weld and in this region the parts clearly did not weld (fig. 4.17b). In the middle of the weld (fig. 4.17a) hardly any deformation can be observed; the interface stays clearly visible. This is in agreement with the observations of figs. 4.12d, e. Up to a welding time of 400 ms the central region of the weld shows no microwelds. Only after a welding time of 1000 ms did the central area show a rough surface. The weld in the microsection obviously did not reach the stage of fig. 4.12e. The mild steel specimens are plastically deformed over the whole thickness, The difference between deformed material and parent material is visible in fig. 4.18a. The interface stays clearly visible in the middle of the weld (fig. 4.18b) but disappears at the perifery.
No recrystallization or melting was observed in any of the microsections.

Fig. 4.14. Microsections of ultrasonic welds. Material: Al (medium hard).
→← weld interface ——— = 50 μm

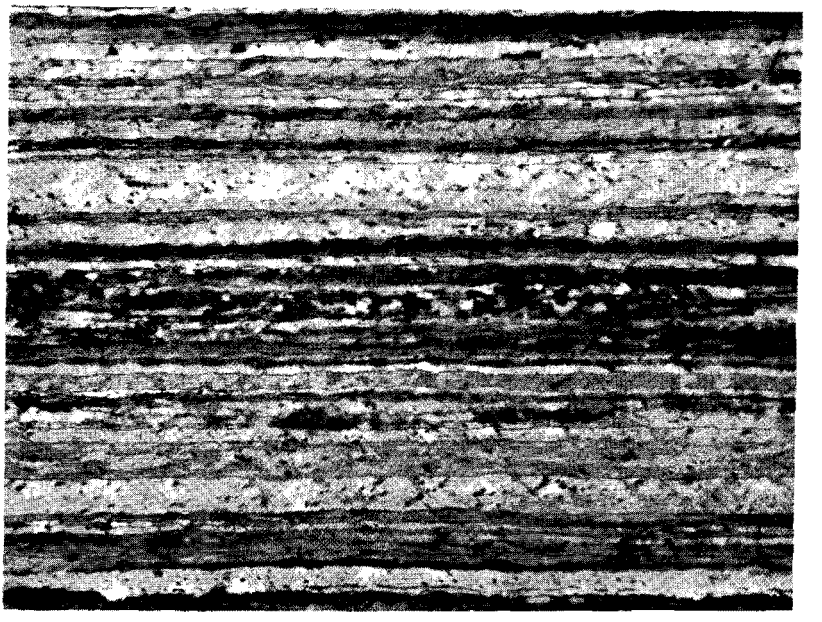

a. Centre of the welding zone.

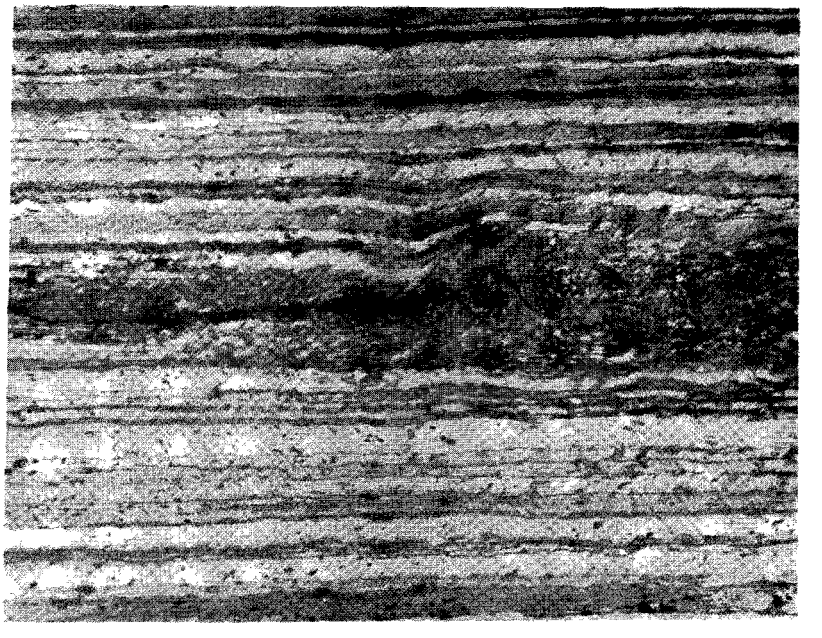

b. Periphery of the welding zone.

Fig. 4.15. Microsections of ultrasonic welds. Material: Cu.
→← weld interface ——— = 100 μm

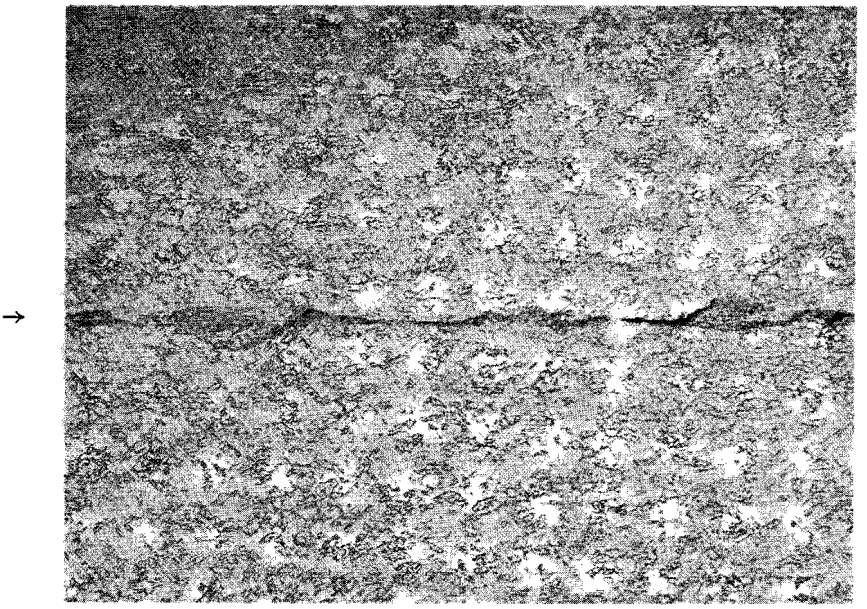

a. Centre of the welding zone. ——— = 50 μm

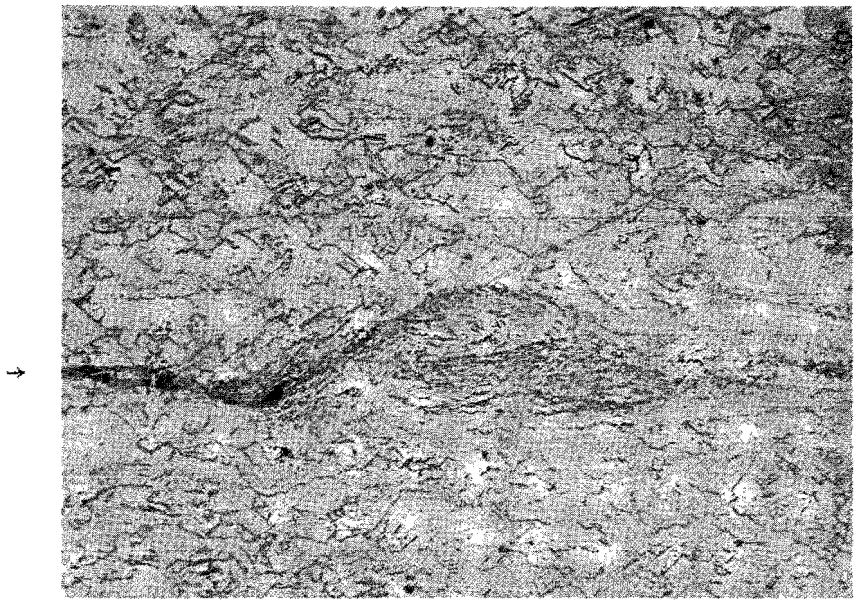

b. Detail from a.

Fig. 4.16. Microsections of ultrasonic welds. Material: Ni.
→← weld interface ——— = 50 μm

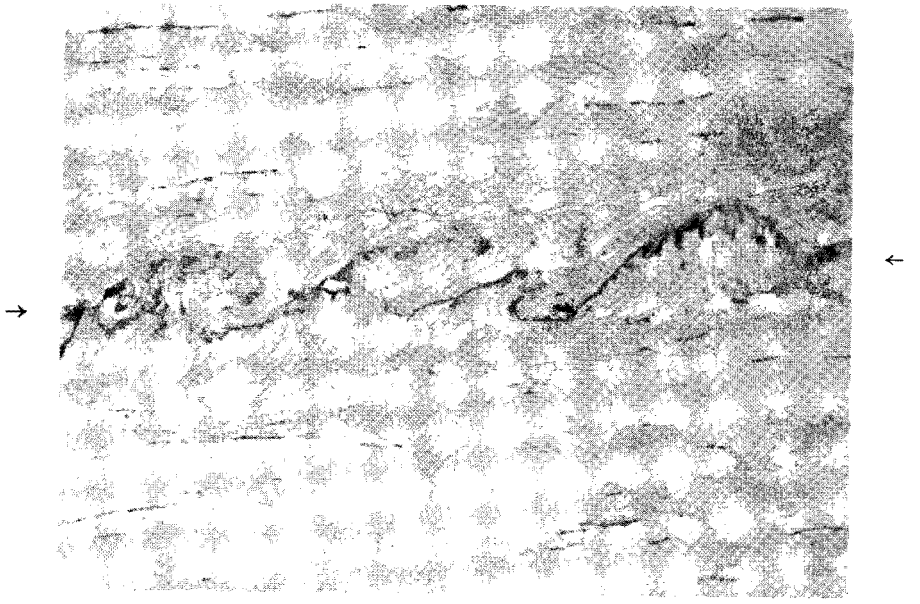

a. Periphery of the welding zone.

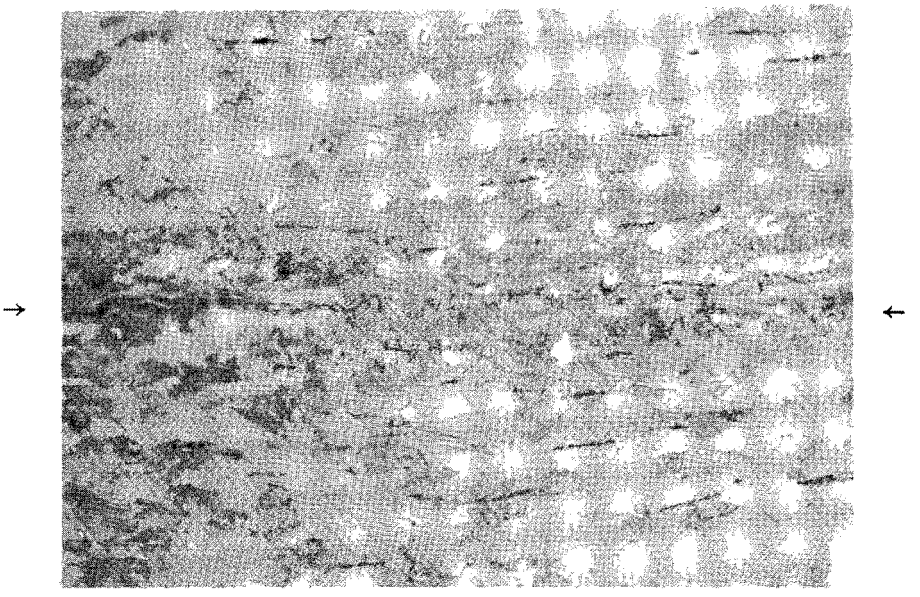

b. Center of the welding zone.

Fig. 4.17. Microsections of ultrasonic welds. Material: stainless steel.
→← weld interface ——— = 50 μm

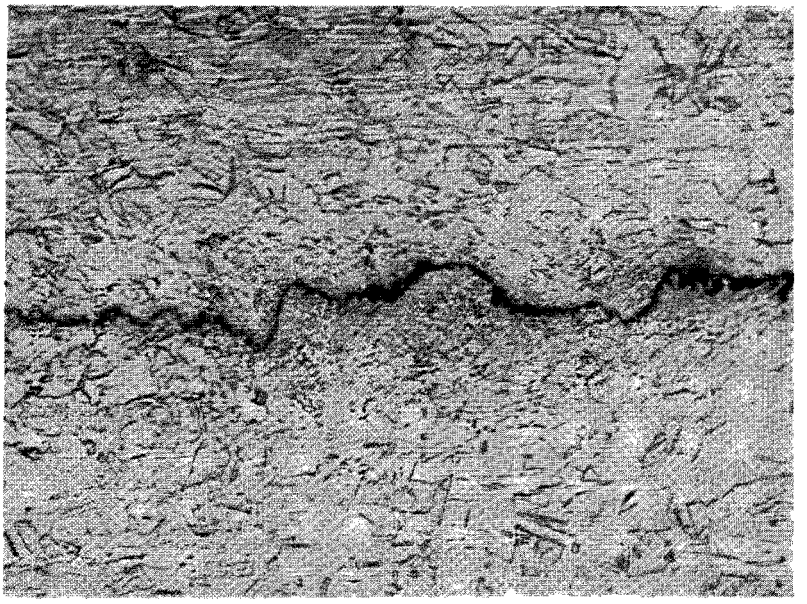

a. Periphery of the welding zone.

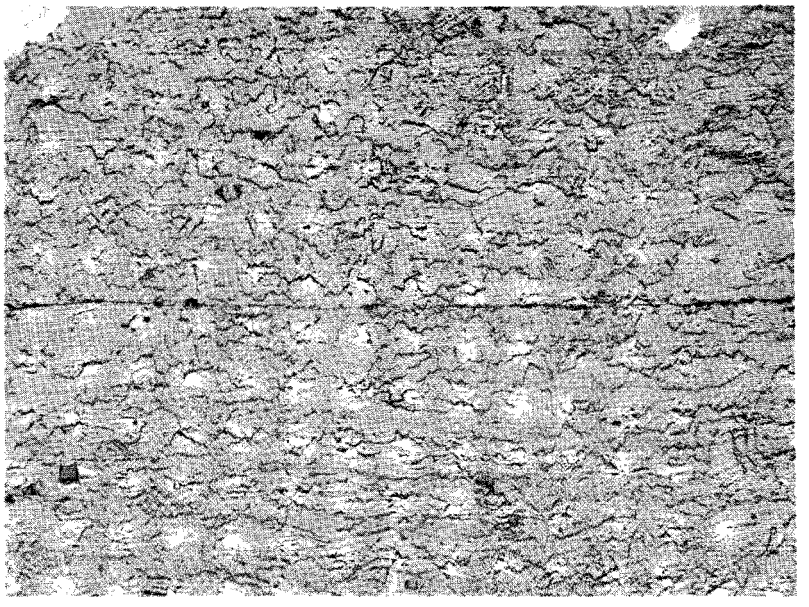

b. Center of the welding zone.

Fig. 4.18. Microsections of ultrasonic welds. Material: mild steel.
→← weld interface ——— = 100 μm

a. Periphery of the welding zone.

b. Center of the welding zone.

4.2.3. The microwelds

4.2.3.1. Length of the microwelds as a function of vibrational amplitude and welding time

Experiments were carried out to investigate the influence of vibrational amplitude and welding time on the length of the microwelds. Polished Al sheets (thickness 0.5 mm) were ultrasonically welded. The clamping force was 375 N; the welding time 40 and 100 ms. resp.;the values of the vibrational amplitude are given in table 4.4. With each setting three welds were made after which the welds were peeled off and the weld area was photographed. An area (0.4 x 0.6 mm^2) in the middle of the weld was chosen on each photograph. Within this area the microwelds were classified according to their length and the results are displayed in figs. 4.19, 20. From this distribution we can calculate the average length $\bar{l}$ of the microwelds (table 4.4). The average width of the microwelds was estimated to be 20 μm in all cases.

TABLE 4.4.
The average length of microwelds in Al (medium hard) at different levels of vibrational amplitude and welding time (compare figs. 4.19, 20).

welding time t (ms)	vibrational amplitude ξ (μm)	average length $\bar{l}$ of microwelds (x 10 μm)
40	13	7
40	21	8
40	30	9
100	13	6
100	17	6
100	20	6

Some limitations of these observations must be mentioned. First, it was difficult to distinguish between two adjacent microwelds. Hence in the classification some conjecture was inevitable. Next, it was only possible to measure the size of the microwelds in welds which were less than half completed. In a completed weld no individual microwelds could be distinguished.

From table 4.4 it can be seen that the average length of the microwelds slightly increases with increasing vibrational amplitude ξ when a welding time 40 ms is used. However, for a welding time of 100 ms no increase is observed.

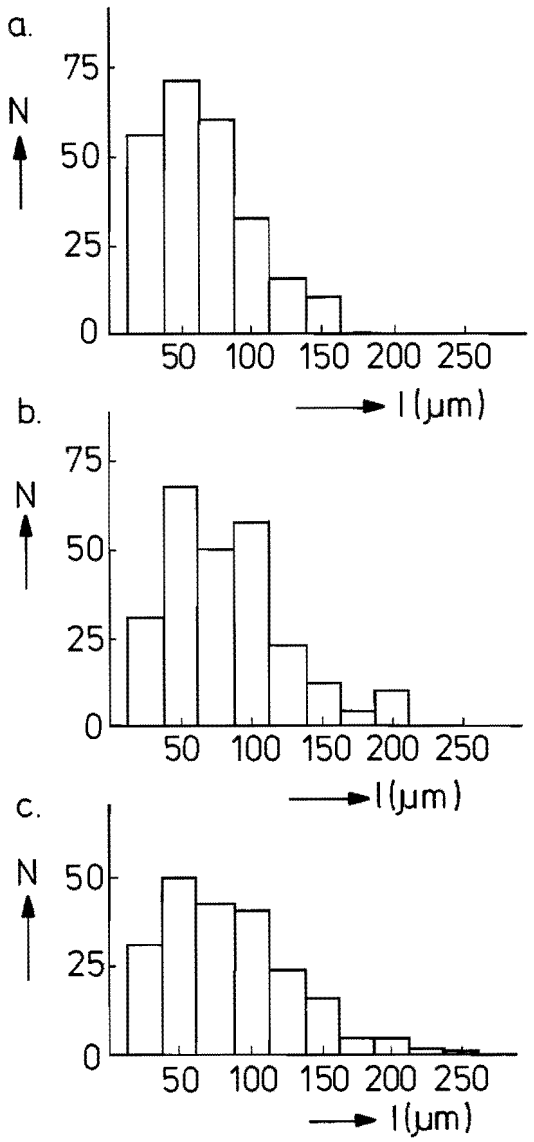

Fig. 4.19. Classification of the number of microwelds N in an ultrasonic weld as a function of the length l of the microwelds (see sec. 4.2.3.1). Material: Al (medium hard). Clamping force F_c = 375 N. Welding time t = 40 ms.

a. Vibrational amplitude ξ = 13 μm

b. Vibrational amplitude ξ = 21 μm.

c. Vibrational amplitude ξ = 30 μm.

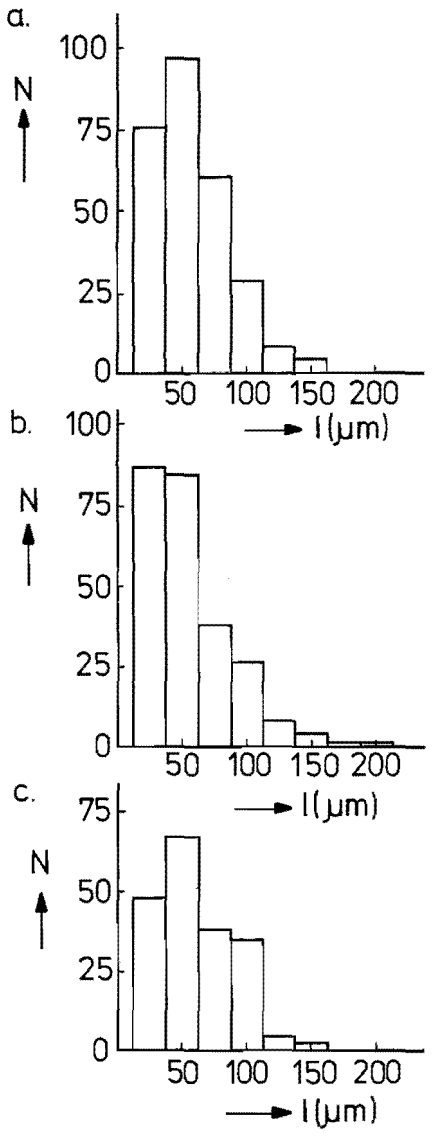

Fig. 4.20. Classification of the number of microwelds N in an ultrasonic weld as a function of the length l of the microwelds (see sec. 4.2.3.1). Material: Al (medium hard). Clamping force F_c = 375 N. Welding time t = 100 ms.

a. Vibrational amplitude ξ = 13 µm

b. Vibrational amplitude ξ = 17 µm.

c. Vibrational amplitude ξ = 20 µm.

From the preceding observations it appears that both the average length and width of the microwelds are independent of both vibrational amplitude (within the range 13 to 30 μm) and welding times considered. Hence in the present experiment the average area of a microweld A_m is independent of vibrational amplitude and welding time. Obviously the growth of the weld is brought about by an increase in the number of microwelds, rather than by continous growth of the dimensions of the microwelds.

4.2.3.2. Influence of surface conditions on weld formation

As mentioned in the literature (sec. 2.3.3) the specimens are usually degreased before welding. In this section the influence of a lubricant on the formation of the weld is studied and an attempt to study the influence of surface roughness is described.

Two batches of aluminium sheets (medium hard; thickness 0.5 mm) were welded (welding time 20 ms; clamping force 375 N). The first batch was degreased in acetone and before welding the second batch a droplet of light machine oil was spread over the spot to be welded. The setting of the equipment remained the same in both cases but the vibrational amplitude was 15 μm for the first batch and 20 μm for the second. All welds were peeled off by hand.

The welded surface of the degreased specimens looked the same as the specimens shown in fig. 4.8 i.e. a few hundreds of microwelds with lengths between 50 and 200 μm. The lubricated specimens showed much fewer microwelds with lengths ranging from 500 to 800 μm (see fig. 4.21). The large increase in the average length of the microwelds in the lubricated specimens cannot be explained by the slightly higher vibrational amplitude during welding. We can see from table 4.4 that increasing the vibrational amplitude by a factor 2.3 only results in a change of 30% in the average length of the microwelds.

The oil film obviously reduces the real contact between the specimens and hence the number of metal to metal contactpoints is reduced. This implies that the number of microwelds is smaller in the lubricated specimens than it is in the degreased samples. *)

From these observations it appears that the number and size of microwelds are strongly influenced by the presence of a lubricating layer. Therefore it is clear that

---

*) In the present experiments the lubricated specimens of aluminium could be welded completely by using a longer welding time of 60 ms. Copper specimens with an oil layer on them could not be welded at all.

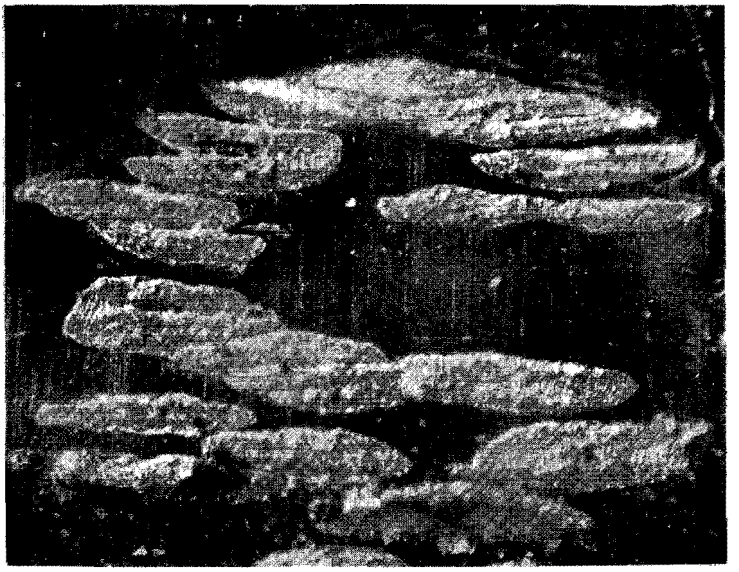

——— = 250 μm

Fig. 4.21. Surface of a peeled weld. Material: Al (medium hard). Before welding a droplet of oil was spread over the spot to be welded (see sec. 4.2.3.2)

the formation of an ultrasonic weld cannot be explained by considering merely material properties of the contacting metals.

A natural case of a lubricating layer is the surface oxide on Cu, which is considered to act as a lubricant (4.8). Removal of the oxide layer in a HCl-solution is necessary to produce a good weld (see sec. 4.1) and as long as the time interval between cleaning and welding is less than a few hours the new oxide layer is so thin that ultrasonic welding is not impaired.

Lightly abrading the surface of one of the (uncleaned) Cu weldmembers results in good welds. Probably the surface irregularities on one member pierce through the contaminants on the other, creating the initial metal to metal contact required for welding. Fig. 4.22 shows the surface of an unabraded Cu specimen after welding to an abraded specimen. The scratches from the abraded sheet are clearly discernible as lines where many microwelds are clustered.

An attempt to study the formation of microwelds in roughened Al and Cu specimens failed. The surfaces to be welded were roughened by bead and sand blasting. After peeling the welds, the welded areas could not be distinguished from the original rough surface. A number of tensile shear measurements, listed in tables 4.5, 6, show the influence of surface roughness. For sandblasted Al an increase of the welding time to 100 ms resulted in a breaking force of 350 ± 50 N. For bead and sandblasted Cu increasing the welding time to 10 s did not result in a perceptible increase of the breaking force.
From these measurements it appears that surface roughness over a certain limit makes welding more difficult or even impossible. Probably the reason for this is that mechanical interlocking of the rough contact areas hinders relative movement of the surfaces to be welded.

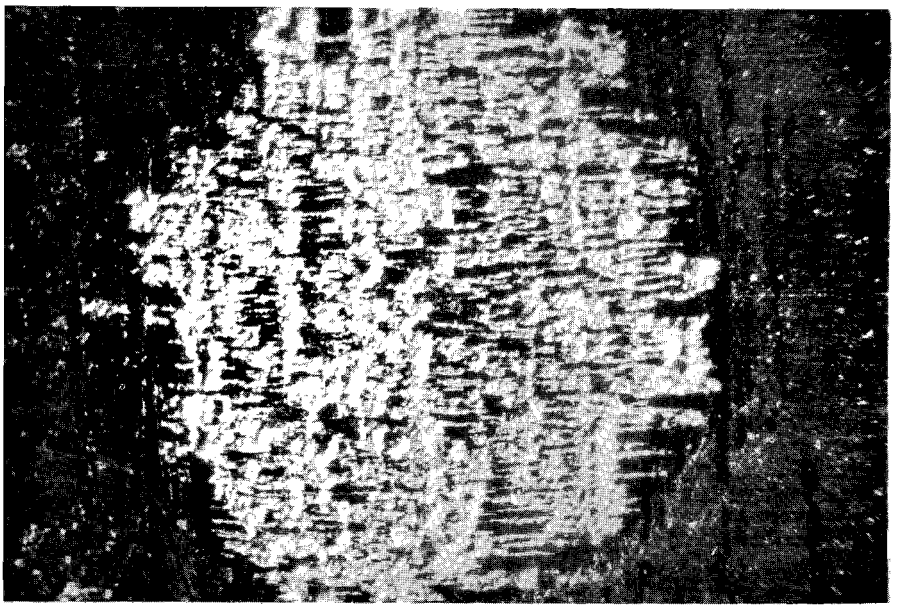

——— = 200 μm

Fig. 4.22. Surface of a peeled weld. Material: Cu. Before welding one of the weld members was not degreased but lightly abraded using emery paper. The photograph shows the unabraded weld member (see sec. 4.2.3.2). Clamping force F_c = 375 N. Welding time t = 40 ms. Vibrational amplitude ξ = 19 μm.

TABLE 4.5
Tensile shear force F_b as a function of specimen roughness R_a.

Material : Al (medium hard); thickness: 0.5 mm
Clamping force : 375 N
Welding time : 40 ms
Electrical power deliverd by the amplifier: 400 W.

Roughness R_a [1] (μm)	Roughened by:	Tensile shear force F_b [2] (N)
0.25	untreated	300 ± 40
0.55	etching	340 ± 40
1.8	bead blasting	160 ± 30
6.0	sand blasting	180 ± 50

[1]) CLA value
[2]) Mean value of 10 measurements (with standard deviation).

TABLE 4.6
Tensile shear force F_b as a function of specimen roughness R_a.

Material : Cu; thickness 0.5 mm
Clamping force : 375 N
Welding time : 1000 ms
Electrical power delivered by the amplifier: 500 W.

Roughness R_a [1] (μm)	Roughened by:	Tensile shear force F_b [2] (N)
0.04	untreated	850 ± 110
1.2	bead blasting	150 ± 80
3.2	sand blasting	90 ± 70

[1]) CLA-value
[2]) Mean value of 10 measurements (with standard deviation).

4.3. The alternating force exerted on the workpieces

4.3.1. Experiments

In the experiment described in this section the amplitude of the alternating force exerted by the welding tool on the specimens $|\bar{F}_l|$ was determined. Initially a relationship between welded area and alternating force was expected such that the force would provide a measure of the strength of the weld. This expectation was however not realised.

Specimens of 4 materials were welded (see table 4.7). During welding the current i through the transducer, the voltage V on the transducer and the frequency deviation $\Delta\nu_r$ (sec. 3.3.2) were recorded. The data for a representative weld are listed in table 4.7. From these data R_{ml} and X_{ml} can be calculated using eqs. (3.28) and (3.29). Numerical information required for this calculation is given in appendix A3. Using eq. (3.31) in combination with eqs. (3.30) and (3.1) $|\bar{F}_l|$ can be determined:

$$|\bar{F}_l| = |\bar{v}_l| \; |\bar{Z}_{ml}|$$

The values of $|\bar{F}_l|$ resulting from these calculations are listed in table 4.7. In this table the values of the breaking force $F_b(t)$ as taken from figs. 4.1 to 4.4 have also been noted for comparison. The value of $|\bar{F}_l|$ is also displayed as a function of time in figs. 4.23.
From this experiment it appears that the alternating force amplitude $|\bar{F}_l|$ slowly increases during the welding period. The intitial value is measured after 20 to 40 ms, during which time the transient phenomenon of switching the generator has decayed. This initial value amounts to 70 to 80% of the value ultimately achieved. However, after the transient phenomenon the tensile shear force $F_b(t)$ increases a factor 3 to 7 depending upon the material, as can be see from figs. 4.1 to 4.4.

The alternating force $\bar{F}_w$ exerted in the welding zone by the upper sheet upon the lower sheet, is approximately equal to $\bar{F}_l$. The difference between $\bar{F}_l$ and $\bar{F}_w$ can be neglected, because the thickness of the upper sheet (0.5 mm) is much smaller than the length of waves travelling in the materials (the wave length of transverse waves in different metals at 20 kHz ranges between 50 and 100 mm); hence $\bar{F}_l$ and $\bar{F}_w$ cannot be expected to differ for this reason. In other words: the force required to vibrate the part of the upper specimen lying under the welding tip is much smaller than $\bar{F}_l$. An estimate of this force is made in appendix A4.

As the alternating force amplitude $|\bar{F}_l|$ remains virtually constant during welding, while the tensile shear force $F_b(t)$ increases considerably, no relationship as mentioned above was found.

TABLE 4.7

Determination of the alternating force amplitude $|\bar{F}_1|$ as a function of welding time t, for different materials (see sec. 4.3.1).

Material Clamping force F_c Vibrational amplitude ξ	Welding time t (ms)	Current i [1])[3]) (A)	Voltage V [2])[3]) (V)	Frequency deviation $\Delta\nu_T$ (Hz)	Alternating force amplitude $\lvert\bar{F}_1\rvert$ (N)	Tensile shear force $F_b(t)$ [4]) (N)
Al	20	1.05	420	87	310	120 ± 50
(medium hard)	40	0.95	420	125	380	200 ± 30
F_c = 375 N	100	0.90	420	149	420	300 ± 50
ξ = 16 μm	200	0.90	420	148	420	380 ± 30
Al	20	1.10	420	83	320	120 ± 60
(hard)	40	1.10	420	110	390	180 ± 80
F_c = 675 N	100	1.10	420	119	410	320 ± 120
ξ = 17 μm	200	1.05	420	130	420	450 ± 70
	400	1.05	420	143	460	
	1000	0.90	420	171	470	590 ± 40
Cu	40	1.10	720	78	390	120 ± 40
	100	1.10	720	84	400	320 ± 50
F_c = 375 N	200	1.10	720	91	420	450 ± 90
ξ = 18 μm	400	1.10	720	109	460	560 ± 70
	1000	1.10	720	122	490	850 ± 110
Ni	40	1.35	580	175	720	560 ± 240
	100	1.35	580	200	810	840 ± 200
F_c = 1000 N	200	1.35	580	234	940	1090 ± 150
ξ = 22 μm	400	1.35	580	255	1020	1490 ± 100
	1000	1.35	580	255	1020	1840 ± 110

[1]) Current through the ultrasonic transducer: amplitude value
[2]) Voltage at the transducer terminals: amplitude value
[3]) Accuracy: 5%
[4]) With standard deviation.

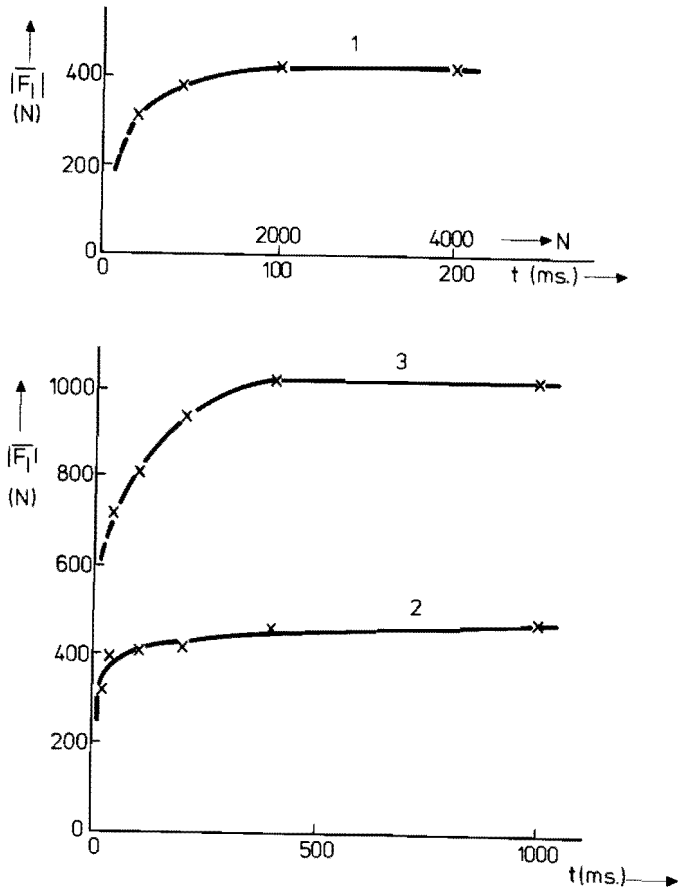

Fig. 4.23. The alternating force amplitude $|\bar{F}_l|$ exerted by the welding tip as a function of welding time t. Curve 1 for Al (medium hard); curve 2 for Cu and Al (hard); curve 3 for Ni. (Data from table 4.7). N is the number of oscillations; a welding time of 100 ms corresponds to 2000 oscillations.

These observations can be explained by assuming that the alternating force exerted in the welding zone $\bar{F}_W$ (= $\bar{F}_l$) is borne by the area of real (but initially unwelded) contact between the weld members. In the beginning of the welding period this area of real contact must be virtually equal to the ultimately welded area; at that moment the welded area is considerably smaller than the area of real contact. In this contact area a number of microwelds gradually develop. At the end of the welding interval the contact area is completely welded and the force $\bar{F}_W$ is borne by the weld. As the growth of the weld in the contact area has little influence on $\bar{F}_W$, the quantity $\bar{F}_W$ is not suitable as a measure of the welded area and the strength of the weld.

From a second experiment the mean alternating stress amplitude in the welding interface $\hat{\tau}_W$ was determined. In table 4.8 measurements of the alternating force amplitude $|\bar{F}_l|$ ($= |\bar{F}_W|$), the contact area A between the weld members and the tensile shear force of the welds F_b, are listed. Each value is an average of 5 observations. From these data the value of the mean alternating stress amplitude in the contact zone was calculated

$$\hat{\tau}_W = \frac{|\bar{F}_W|}{A}$$

In table 4.8 it can be seen that increasing the vibrational amplitude (at constant welding time) does not result in an increase of $\hat{\tau}_W$; this can only occur when the contact zone of the two weld members is in a plastic state.

4.3.2. The area of real contact

The next experiment shows the rapid growth of the area of real contact between the weld members during an ultrasonic vibration period of a few milliseconds. An aluminium sheet was roughened by bead blasting and the rought surface was pressed against a glass plate. This was done in the welding equipment (fig. 3.2); the metal sheet being in contact with the sonotrode and the glass plate supported by the anvil. The contacting asperities on the metal surface were flattened as can be observed through the glass plate and is shown in fig. 4.24a. Next an ultrasonic vibration of a few milliseconds duration was applied to the metal sheet, similar to ultrasonic metal welding. After this pulse the area of real contact increased considerably as shown in fig. 4.24b.

This experiment supports the view that after only a short period of ultrasonic vibration (a few milliseconds) the area of real contact between the weld members has grown to such an extent that it virtually equals the final nominal contact area.

4.4. The relative displacement between the welded surfaces

The experiments described in the next three sections are directed towards the following questions

1. What is the actual value of the relative displacement amplitude between the weld members during the formation of a weld?
2. Can the weld, once formed, be destroyed by increasing welding time or vibrational amplitude?

Slip or relative displacement between the weld members is defined as the displacement of point A relative to point B (in fig. 4.25) in a direction parallel to the interface. The points A and B are situated just outside the zone of severe plastic deformation as described in sec. 4.2.2. So the distance AB is about 100 μm in the present experiments. This definition implies that in a welded junction (microweld) a relative displacement still can exist; in such a case a (plastic) deformation of the layer between A and B occurs.

TABLE 4.8.

Values of a number of quantities (see sec. 4.3.1).

$|\bar{F}_w|$ is the amplitude of the alternating force in the welding zone

$F_b(t)$ is the breaking force of a weld

A is the contact area

$\hat{\tau}_w$ is the average alternating stress amplitude in the contact area.

Material	Vibrational amplitude (μm)	Welding time t = 20 msec				Welding time t = 40 msec				Welding time t = 200 msec				Welding time t = 1000 msec			
		$\lvert\bar{F}_w\rvert$ [1] (N)	$F_b(t)$ (N)	A [2] (mm^2)	$\hat{\tau}_w$ (N/mm^2)	$\lvert\bar{F}_w\rvert$ (N)	$F_b(t)$ (N)	A (mm^2)	$\hat{\tau}_w$ (N/mm^2)	$\lvert\bar{F}_w\rvert$ (N)	$\bar{F}_b(t)$ (N)	A (mm^2)	$\hat{\tau}_w$ (N/mm^2)	$\lvert\bar{F}_w\rvert$ (N)	$F_b(t)$ (N)	A (mm^2)	$\hat{\tau}_w$ (N/mm^2)
Al (medium hard)	14					320	130	5.1	63	410	420	7.1	58				
	26	370	190	5.8	64	370	390	7.2	51								
Al (hard)	17									660	270	4.6	143	710	460	6.1	116
	23					610	240	5.1	120	860	850	6.6	130				
Cu	15					210	28	1.8	117	280	260	2.6	108	380	570	4.1	93
	21					270	60	2.5	108	270	270	2.7	100	350	710	4.8	73
Ni	17					750	110	2.6	288	910	340	3.3	276	1010	990	4.8	210
	21					900	310	2.9	310	1020	970	4.4	232	1070	1600	5.1	210

[1]) $|\bar{F}_l| = |\bar{F}_w|$

[2]) The inaccuracy in A is estimated to be 10%.

Fig. 4.24. Rough aluminium sheet, pressed against a glass plate; photographed through the glass. The bright spots are contact areas between the metal and the glass. Clamping force F_C = 125 N. Roughness of the sheet R_a = 1.8 μm.

——— = 400 μm

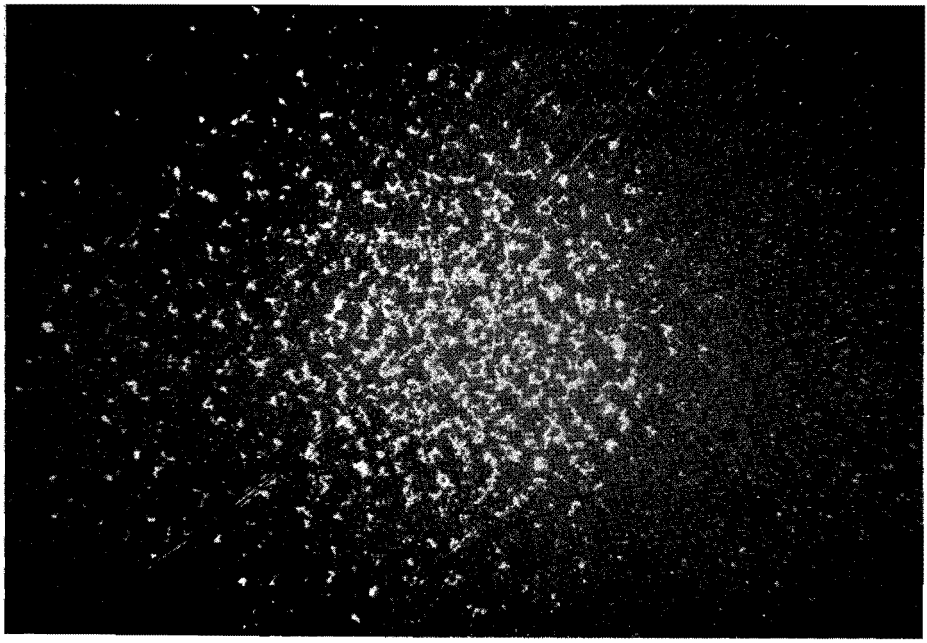

a. Situation after applying the clamping force only.

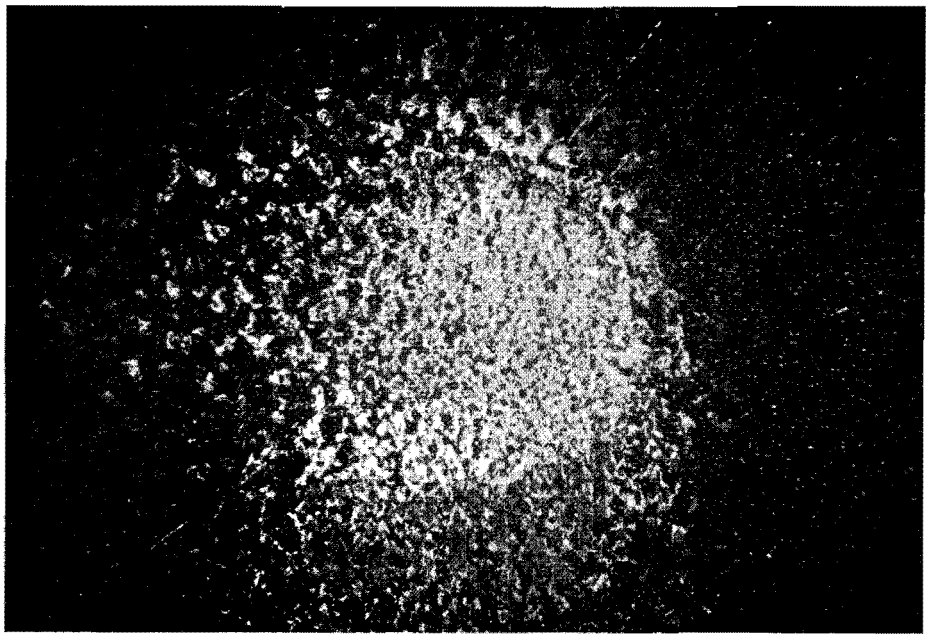

b. Situation after applying an ultrasonic vibration pulse during 2 ms. The direction of vibration was parallel to the contact plane. The average amplitude of vibration was 20 μm.

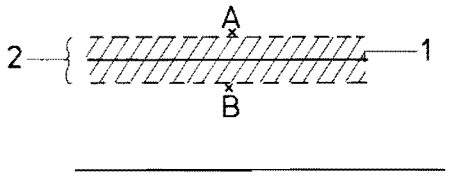

Fig 4.25. Schematic section of an ultrasonic weld. 1: interface; 2: plastic deformation zone.

4.4.1. Equipment and experiments

For the experiments the equipment as shown in fig. 3.2 was used, after some modifications. A hard aluminium (table 4.1) ring with a spherical outer surface was used as welding tip, as shown in fig. 4.26. The anvil was made out of hard aluminium. This equipment enabled us to weld the welding tip directly to the anvil. During welding no vibrational displacements of the anvil could be detected by means of the 'Fotonic sensor'. Thus the movement of the end face of the amplitude transformer is equal to the relative displacement of the contacting surfaces of tip and anvil. The vibrational amplitude at the end face was also measured by means of the 'Fotonic sensor'. In each specific position of welding tip and anvil only one weld could be made. To obtain a new surface to produce another weld the anvil was moved a few millimeters and the vibrating system was rotated approx. 10° about its axis. A number of welds were made in this way. The clamping force F_c was in all experiments 100 N. Three welding times were used, i.e. 200, 400 and 1000 ms and for each welding time a number of different vibrational amplitudes was used.

The welds were broken and classified into one of three classes: no weld, weak weld, strong weld. For some of the welds the alternating force amplitude $|\bar{F}_w|$ and the contact area A were measured in a way similar to the measurements described in sec. 4.3. The broken welds at the anvil were photographed as shown in figs. 4.27 to 4.29.

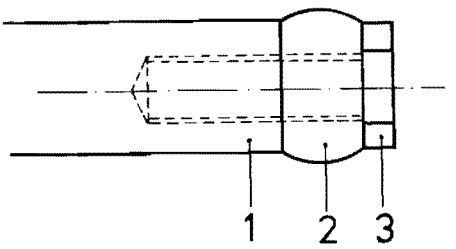

Fig. 4.26. Welding tip for welding directly to an aluminium anvil. 1. End of the amplitude transformer. 2. Hard Al ring; radius of the outer spherical surface is 12 mm. 3. Bolt to fasten the ring to the amplitude transformer.

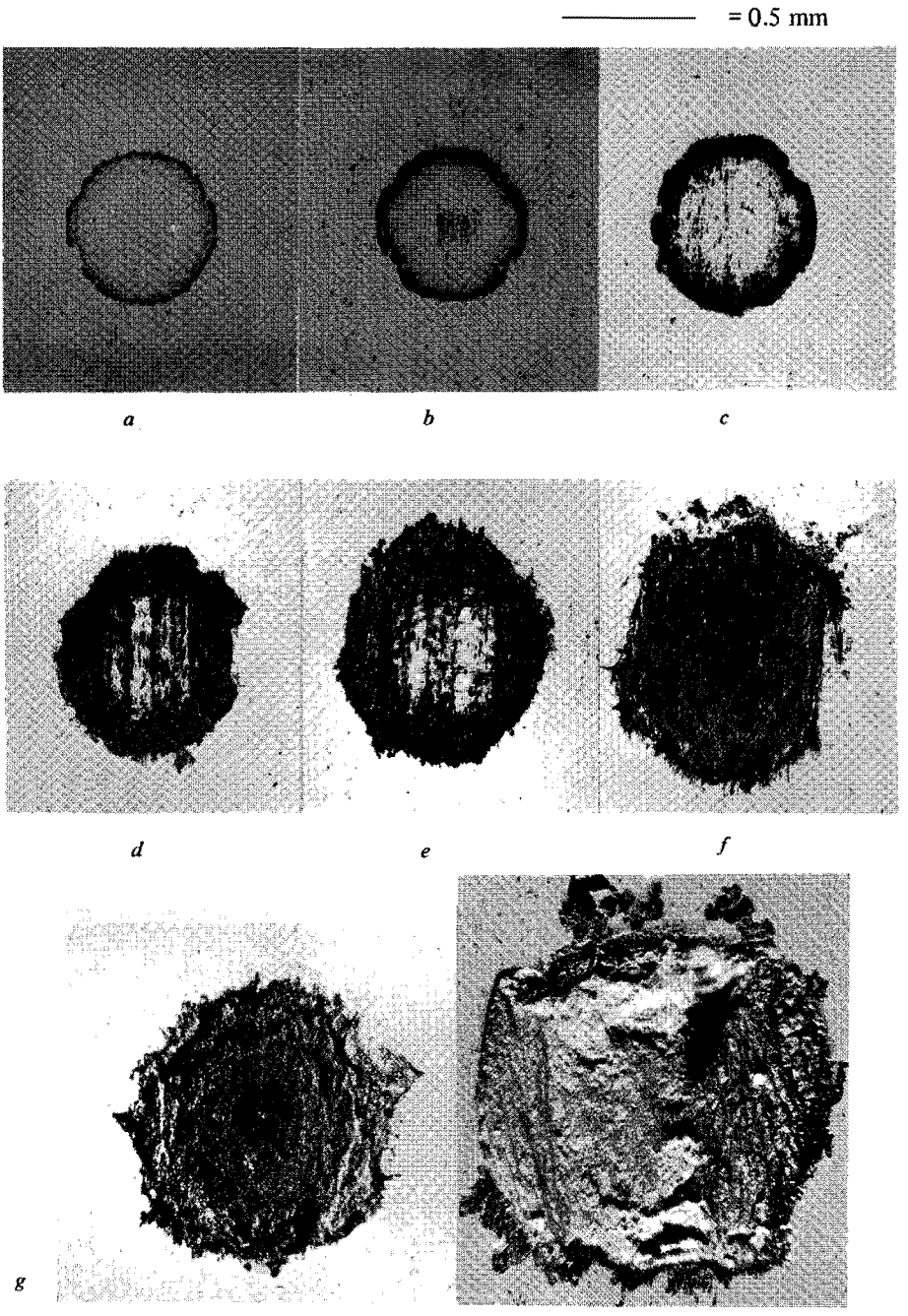

Fig. 4.27. Welds produced by welding the spherical welding tip directly to the anvil. Material of tip and anvil: Al (hard). Clamping force F_c = 100 N. Welding time t = 200 ms. Vibrational amplitude:

a ξ = 1.5 μm b ξ = 2.3 μm c ξ = 3.8 μm
d ξ = 5.0 μm e ξ = 6.4 μm f ξ = 8.0 μm
g ξ = 10.4 μm h ξ = 15.0 μm

———— = 0.5 mm

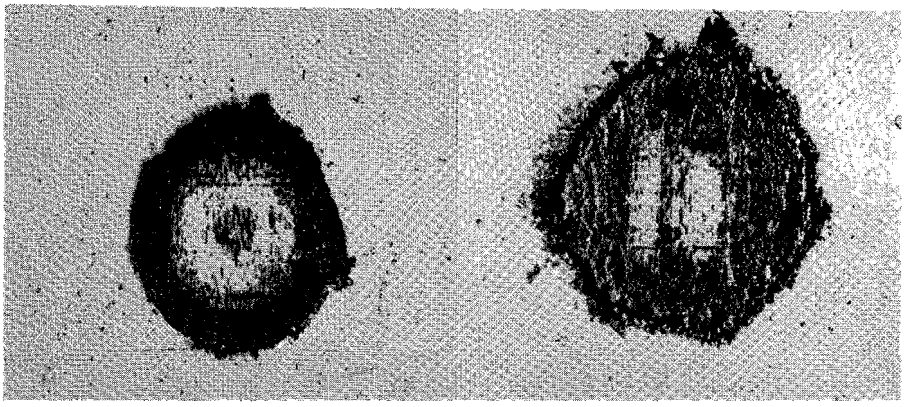

a *b*

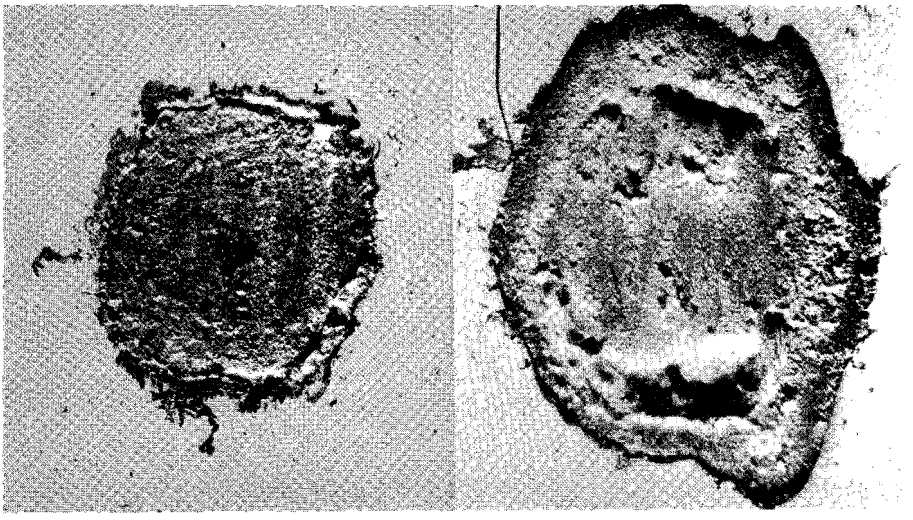

c *d*

Fig. 4.28. Welds produced by welding the tip directly to the anvil. Material: Al (hard). Clamping force F_C = 100 N. Welding time t = 400 ms.
Vibrational amplitude:

a. ξ = 4.4 μm b. ξ = 6.4 μm
c. ξ = 8.8 μm d. ξ = 12.0 μm

———— = 0.5 mm

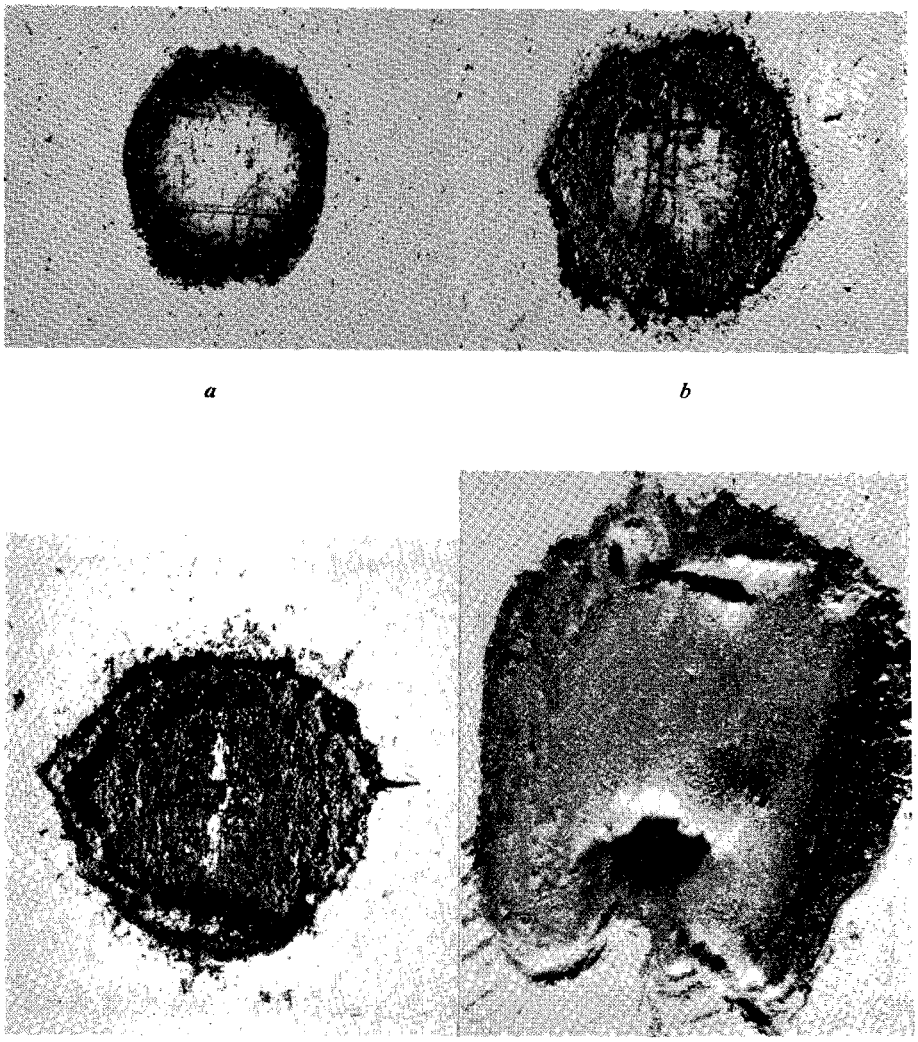

a *b*

c *d*

Fig. 4.29. Welds produced by welding the tip directly to the anvil. Material: Al (hard). Clamping force F_c = 100 N. Welding time t = 1000 ms.
Vibrational amplitude:

a. ξ = 3.7 μm b. ξ = 5.3 μm
c. ξ = 7.0 μm d. ξ = 9.6 μm

4.4.2. Results and discussion

The results of the experiments are

1. Using a vibrational amplitude of 2 μm no significant welding took place. Only a narrow ring at the periphery of the contact area shows signs of welding (fig. 4.27a).
2. At amplitudes ranging form 5 to 10 μm and a welding time of 200 ms, strong welds were formed between tip and anvil (figs. 4.27d, e, f, g). This was also the case for amplitudes ranging from 4 to 9 μm with a welding time of 400 ms and for 5 to 7 μm with a welding time of 1000 ms.
3. The larger vibrational amplitudes (15 μm at 1000 ms welding time; 12 μm at 400 ms welding time; 10 μm at 1000 ms welding time) resulted in complete destruction of the weld. The destruction of the weld area is clearly visible on the photographs (figs. 4.27h, 4.28d, 4.29d).

The results show that the higher the number of vibrations the smaller the amplitude of vibration to destroy the weld. This behaviour resembles fracture by fatigue. As in the welding experiments (sec. 4.2) such fracture did not occur, it proved that the relative displacement amplitudes in these experiments were considerably smaller than those given in paragraph 3 above.

From the photographs (figs. 4.27 to 4.29) and the data in paragraph 2 above we can estimate the relative displacement amplitude required for making a weld in hard Al in a specified welding time. This estimation is given in table 4.9. We can compare

TABLE 4.9

Estimated values of relative displacement amplitude for welding of Al (hard).

Welding time (ms)	Relative displacement amplitude (μm)
200	7–10
400	6– 9
1000	6– 7

these estimated values with the data from the welding experiments using hard Al sheets (sec. 4.2.1.2, fig. 4.2). The upper curve of fig. 4.2 represents welds produced applying a vibrational amplitude of the welding tip ξ = 25 μm. After a welding time of 200 ms no deterioration of the weld is observed. Therefore the relative displacement amplitude could not have exceeded 15 μm (compare paragraph 3 above). According to the estimation of table 4.9 this displacement amplitude ranged between 7 and 10 μm. Likewise the welds represented by the middle curve in fig. 4.2 (ξ = 15 μm) did not show deterioration after a welding time of 1000 ms.

Consequently the relative displacement did not exceed 10 μm and occurred in the range 6 – 7 μm.
In this way we have made an estimate of the relative displacement amplitude in the interface, during welding of hard aluminium. It may be concluded that the relative displacement amplitude occurred between 30% and 50% of the vibrational amplitude of the welding tip when welding aluminium sheets 0.5 mm thick.

From the measurements of the alternating force amplitude $|\bar{F}_W|$ and the contact area A, the mean alternating stress amplitude in the welded interface is calculated: $\hat{\tau}_W = |\bar{F}_W|/A$. The results, listed in table 4.10, show that the value of $\hat{\tau}_W$ is independent of the vibrational amplitude (in the range 5 to 8 μm). The average value of $\hat{\tau}_W$ is 120 N/mm^2; this is very close to the tensile shear stress (breaking stress) determined in sec. 4.2 table 4.2. (τ_b = 130 N/mm^2). These two facts support the assumption that the material in the welding interface is in a plastic state.

TABLE 4.10
The alternating force amplitude $|\bar{F}_W|$ and the welded area A during welding of the tip directly to the anvil.

Material : Al (hard)
Welding time : 200 ms
Clamping force : 100 N

Vibrational amplitude ξ (μm)	Weld area A (mm^2)	Alternating force amplitude $|\bar{F}_W|$ (N)	Average stress amplitude $\hat{\tau}_W$ (N/mm^2)
5.0	0.50	57	114
6.4	0.62	77	124
8.0	0.72	85	121

4.4.3. *Further experiments, results and conclusions*

The relative displacement amplitude (slip) between the weld members was also estimated from sheet welding experiments *). Ultrasonic welds in medium hard aluminium sheets were made. In the first series of welds the lower sheet (on the anvil) was 0.5 mm thick; the upper sheet (contacting the welding tip) had a thickness of 0.25, 0.5, 0.8 and 1.0 mm. In the second series the upper sheet was

*) These experiments are described in more detail in ref. 4.9.

0.5 mm and the lower sheet had a thickness of 0.25, 0.5, 0.8 and 1.0 mm. For each possible combination of thicknesses, the vibrational amplitude of the welding tip was adjusted in such a way that – using a welding time of 200 ms and a clamping force of 375 N – the average tensile shear force of a series of 8 welds was 250 ± 10 N *). Having produced welds of the same strength, using a constant welding time and clamping force, we assume the relative vibrational displacement amplitude (slip) between the weld members to be the same for all the different combinations of thicknesses. In figs. 4.30, a and b, the required vibrational amplitudes of the

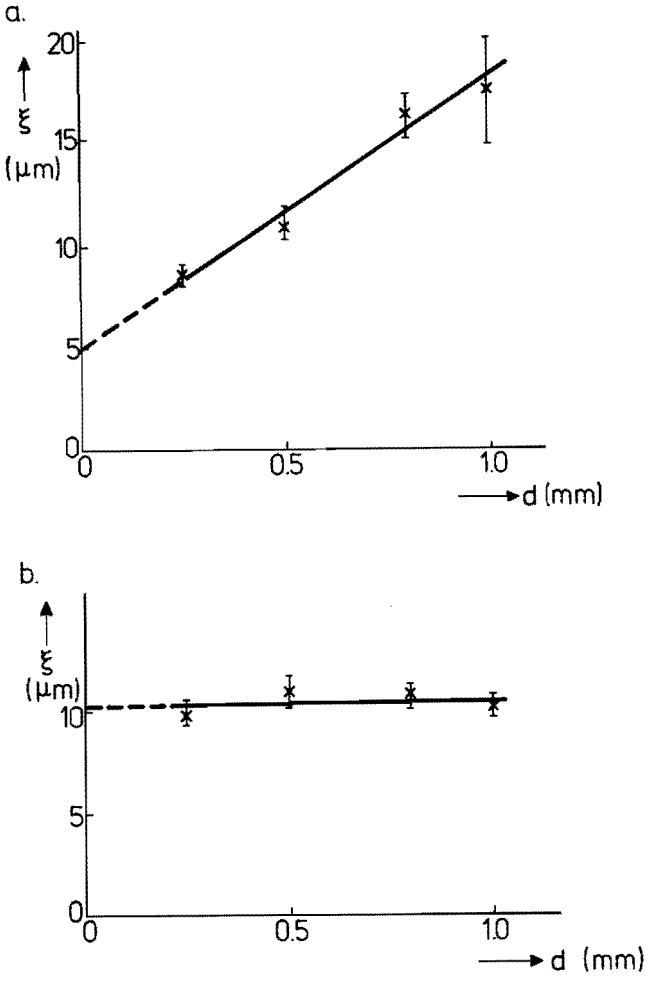

Fig. 4.30. Vibrational amplitude ξ of the welding tip, required to produce welds with constant strength (F_b = 250 N) in specimens of various thicknesses. Welding time t = 200 ms. Clamping force F_c = 375 N. Material: Al (medium hard).
a. ξ as a function of the thickness d of the upper sheet; thickness of the lower sheet 0.5 mm.
b. ξ as a function of the thickness d of the lower sheet; thickness of the upper sheet 0.5 mm.

*) The adjustment was obtained by trial and error; an amplitude setting was chosen, 8 welds were made, the average tensile shear force was measured and compared to the desired 250 N. Then the amplitude setting was adjusted and the process repeated untill the desired strength was obtained.

welding tip are plotted as a function of the thickness of the upper and lower sheet. Measurements of the vibrational amplitude in a small cavity in the anvil right under the welding tip shows that the average amplitude of the anvil does not exceed 1 μm (4.9). (The vibration at the anvil is in phase with the vibrational movement of the welding tip).

Extrapolation of fig. 4.30a to zero thickness of the upper sheet shows that the vibrational amplitude just above the interfacial plastic deformation zone is about 5 μm (i.e. the amplitude at point A in fig. 4.25). From fig. 4.30b we see that the thickness of the lower sheet hardly influences the formation of a weld. It appears therefore that the lower specimen simply follows the movement of the anvil. This is affirmed by some measurements of the vibrational amplitude on the front side of the lower specimen. As the amplitude of the anvil is about 1 μm, the relative displacement amplitude between the weld members is estimated to be about 4 μm, in the present experiments. The vibrational amplitude of the welding tip was 11 μm for welding sheets of 0.5 mm. In this case the ratio between the relative displacement amplitude (slip) and the amplitude of the welding tip is 0.4; this agrees well with the estimation given in sec. 4.4.2.

From the experiments mentioned above we see

1. The lower specimen and the anvil are virtually at rest during welding.
2. The difference between vibrational amplitude of the welding tip and relative displacement between the specimen is approximately proportional to the thickness of the upper specimen. Thus the upper specimen undergoes a shear deformation in the area between welding tip and welding zone. The average shear angle is about 10^{-2} radians in the present experiments *). Hence this deformation is much less than the deformation in interfacial welding zone.

---

*) From fig. 4.30a we see that the shear deformation in a sheet of 1 mm thickness is 13 μm; thus the average shear angle amounts to 1.3×10^{-2} radians.

5. SUBSONIC WELDING, EXPERIMENTS AND RESULTS *)

During the ultrasonic welding experiments two points emerged. First the welding period was so short that observation of the welding process cycle by cycle was very difficult. A number of experiments designed to observe the ultrasonic alternating tangential force exerted by the welding tip directly (by the use of strain gauges or piezo electric transducers) were unsuccessfull. Secondly, the power density in the welded area was high enough to cause a temperature rise of several hundreds of degrees centigrade; thus a contribution of temperature dependent phenomena to the welding mechanism can not be excluded on the basis of ultrasonic welding experiments only.

Because of these two facts a mechanical 'slow-motion' model of ultrasonic welding was sought. A study of the phenomena occurring during fretting showed a possible relationship between ultrasonic welding and fretting. Fretting occurs when two metallic surfaces are in contact and perform a relative (vibrational) sliding movement. Hurricks (1.15) describes that initially in this process adhesion junctions (microwelds) are formed which are then broken producing wear debris. It was anticipated that the formation of joints in the first stage of fretting would be similar to ultrasonic welding. Therefore experiments using a vibrational frequency of 30 Hz were carried out. Two sheets of Al (medium hard) were brought into contact by a clamping force. One of the specimens was fixed to an anvil, the other one was allowed to vibrate parallel to the plane of contact. The apparatus is described in sec. 3.5. Between the two sheets welded junctions were formed which proved to be very similar to ultrasonic welds; therefore we named this method subsonic welding.
In the following sections we will compare the joints produced by subsonic and ultrasonic welding, with respect to strength, appearance, alternating tangential forces in the interface during the vibrational process and energy dissipated during welding.

5.1. Parameters in subsonic welding

A number of preliminary experiments were carried out to show that subsonic vibrational motion of one metal surface relative to another results in welded joints in the contact area. In further experiments we selected similar parameters for the subsonic welding process to those used in ultrasonic welding of Al.

1. The clamping pressure in subsonic welding was 46 ± 8 N/mm^2, and in ultrasonic welding ~ 50 N/mm^2).

---

*) Results mentioned in this chapter were partly published separately (5.1).

2. A number of 5000 oscillations was used which corresponds to an ultrasonic welding time of 250 ms at a vibrational frequency of 20 kHz.
3. The vibrational amplitude required to obtain a subsonic weld was determined empirically. At a vibrational amplitude of 2 μm no welding was observed. An amplitude of 10 μm resulted in a severely worn contact area with the joints broken due to relative movement. A completely welded contact area could be obtained using a vibrational amplitude of 5 μm, consequently this value was chosen in the subsonic welding experiments. From the ultrasonic welding experiments described in sec. 4.4 we know that the relative displacement (slip) amplitude is about 4 μm when using a vibrational amplitude of about 11 μm at the welding tip.

Hence the parameters used in the subsonic welding experiments are comparable to the conditions in ultrasonic welding represented by point A in fig. 4.1.

5.2. Properties of subsonic welds

We will review some properties of the subsonic welds produced under the conditions as defined in the previous section. A comparison with the properties of ultrasonic welds will also be made.

1. *The tensile shear strength*
   The tensile shear force was determined, as described in sec. 3.4. The welded area was measured by means of a microscope equipped with a measuring eye piece. From these measurements the average tensile shear stress of the subsonic weld in Al was calculated to be 50 ± 4 N/mm^2 from a sample of 10 welds.
   This value is comparable to the tensile shear stress of an ultrasonic weld: $\tau_b = 55 \pm 5$ N/mm^2 (see table 4-2).

2. *Metallographic sections*
   Figure 5.1 shows sections of subsonic welds which are similar to sections of ultrasonic welds shown in fig. 4.14a. Near the interface of the weld members severe deformation is observable. The thickness of the deformed layer varies between 15 and 30 μm in both cases. Outside this interfacial zone the material has its original texture of elongated grains, caused by rolling.

3. *Development of a subsonic weld*
   Successive stages in the development of a subsonic weld are shown in fig. 5.2, i.e. after 100, 1000 and 5000 oscillations. The specimens were peeled. The direction of vibration during subsonic welding is indicated in the photographs. From these photographs it can be seen that

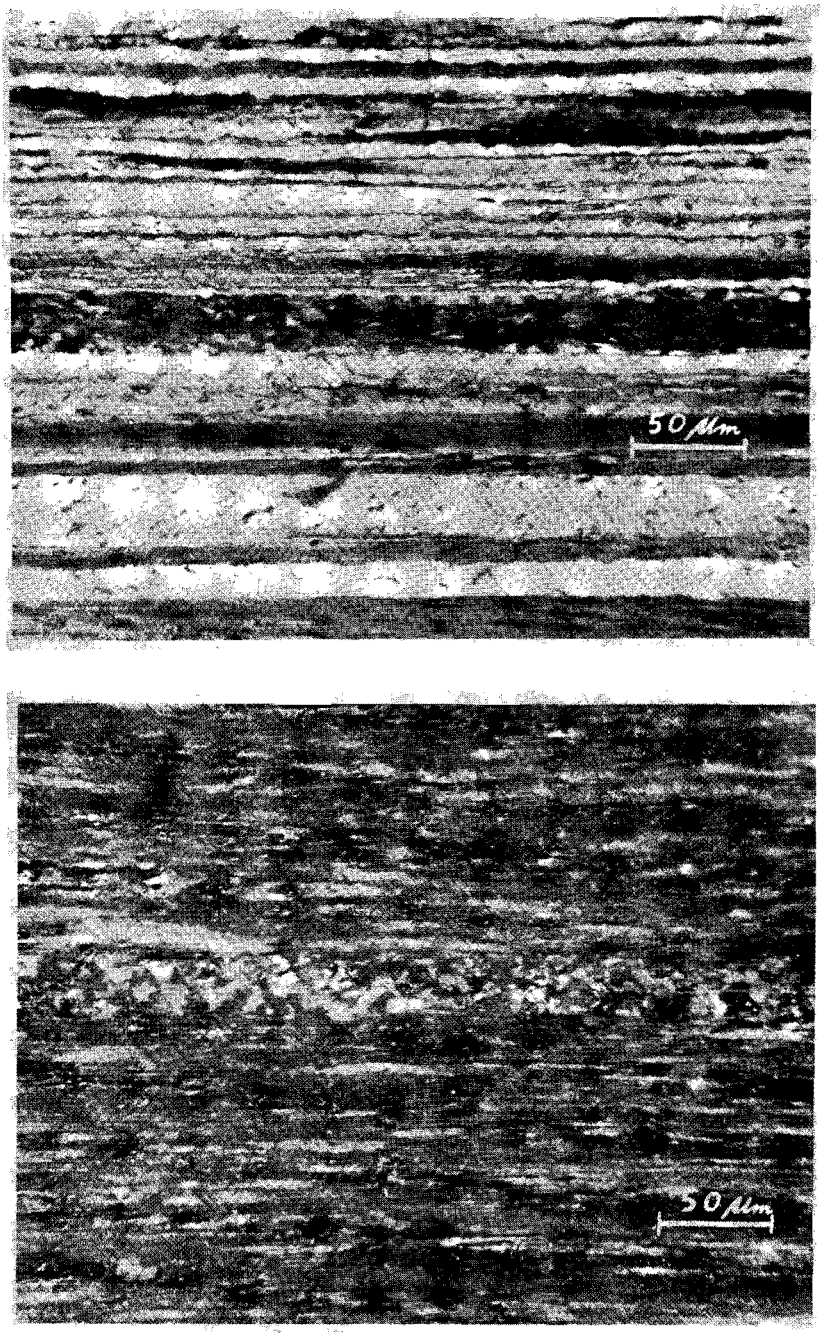

Fig. 5.1. Microsections of subsonic welds of Al (medium hard). →← weld interface

a. A subsonic weld consists of a number of welded spots (microwelds).
b. The microwelds are oblong and their longest axis is parallel to the direction of vibration.
c. The number of microwelds increases as the number of oscillations increases.

Comparing these facts with the observations of ultrasonic welding in sec. 4.2.2, it can be seen that the development of a subsonic weld and an ultrasonic weld are very similar. *)

Fig. 5.2. Photographs of peeled subsonic welds in Al.

a. ——— = 200 μm

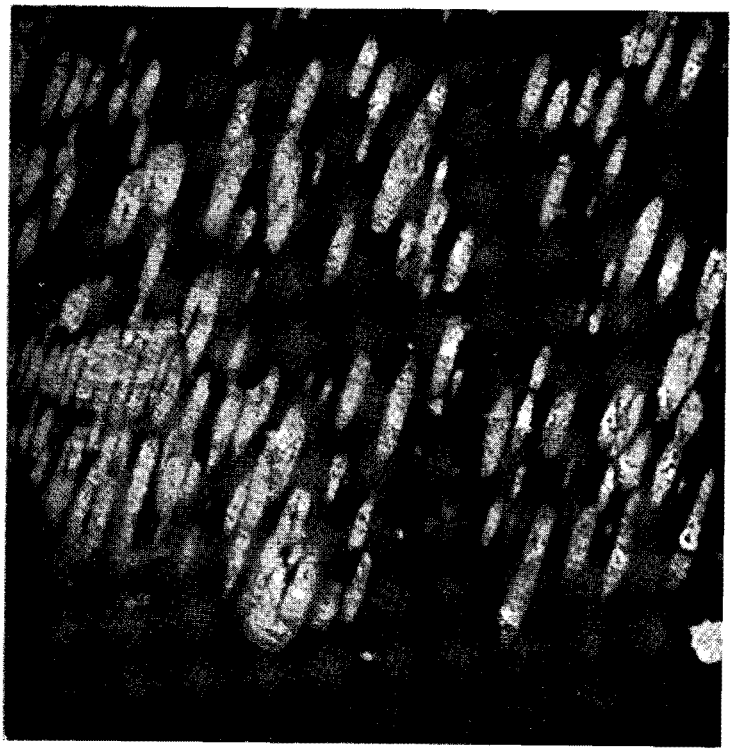

a. after 100 oscillations.

*) Subsonic and ultrasonic welding of Cu showed the same similarity as Al.

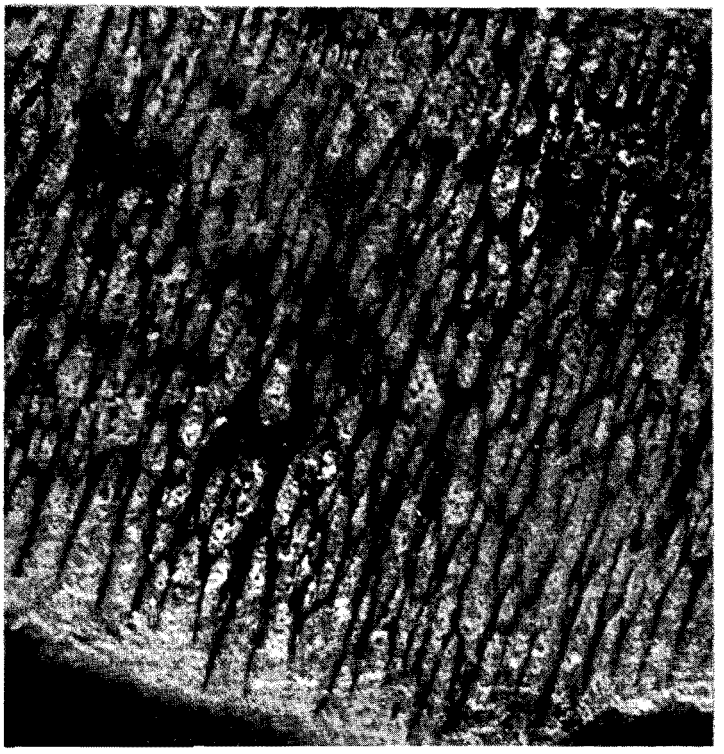

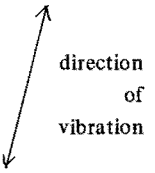

b. after 1000 oscillactions;

c. after 5000 oscillations.

5.3. The alternating tangential force during subsonic welding and the energy dissipation

A subsonic welding experiment was carried out, using the conditions mentioned in sec. 5.1. During the process the relative displacement of the weld members s and the total alternating force F_a acting on the contact area were measured using the driving lever as a dynamometer, as mentioned in sec. 3.5. The relative displacement of the specimens was measured by a 'Fotonic sensor' as indicated in fig. 3.6. Elastic deformations in the lever and in the specimens, a few millimeters beyond the welding zone, were negligible compared to the relative displacement. F_a is the force exerted by the upper specimen, driven by the lever, on the lower specimen. The direction of F_a is parallel to the relative displacement.
The signals from the 'Fotonic sensor' and the dynamometer strain gauge were recorded on magnetic tape and subsequently displayed on the y and x axes resp. of a storage oscilloscope. Thus we could obtain a force-path diagram for any particular vibration cycle. Photographs of those diagrams are shown in fig. 5.3. The centre of symmetry of the force-path diagrams is the origin. The movement is represented by following the loop clockwise. In fig. 5.3 the points A and C represent the turning points of the movement.
As the vibrational amplitude is kept constant the dimension of the loop measured along the s-axis remains constant. The line AB corresponds to the elastic deformation of the material surrounding the welding zone. In B the tangential force F_a is so large that relative slip in the contact plane between the specimens occurs. This sliding continues to C when the movement reverses and the elastic part CD is followed by slip from D back to A. The character of the loop remains the same for an increasing number of oscillations. The area of each diagram represents the energy dissipated during a single vibration cycle.

TABLE 5.1.
Dissipated energy E per oscillation and alternating tangential force amplitude F_a as a function of the number of oscillations in subsonic welding.

Clamping force : 50 N
Material : Al (medium hard)
Welded area : 0.9 ± 0.1 mm²

Number of oscillations	Dissipated energy per oscillation E (10^{-3} J)	Alternating tangential force amplitude F_a (N)
100	0.13	7
200	0.19	12
300	0.25	21
500	0.29	29
1000	0.30	36
2000	0.32	41
5000	0.32	47

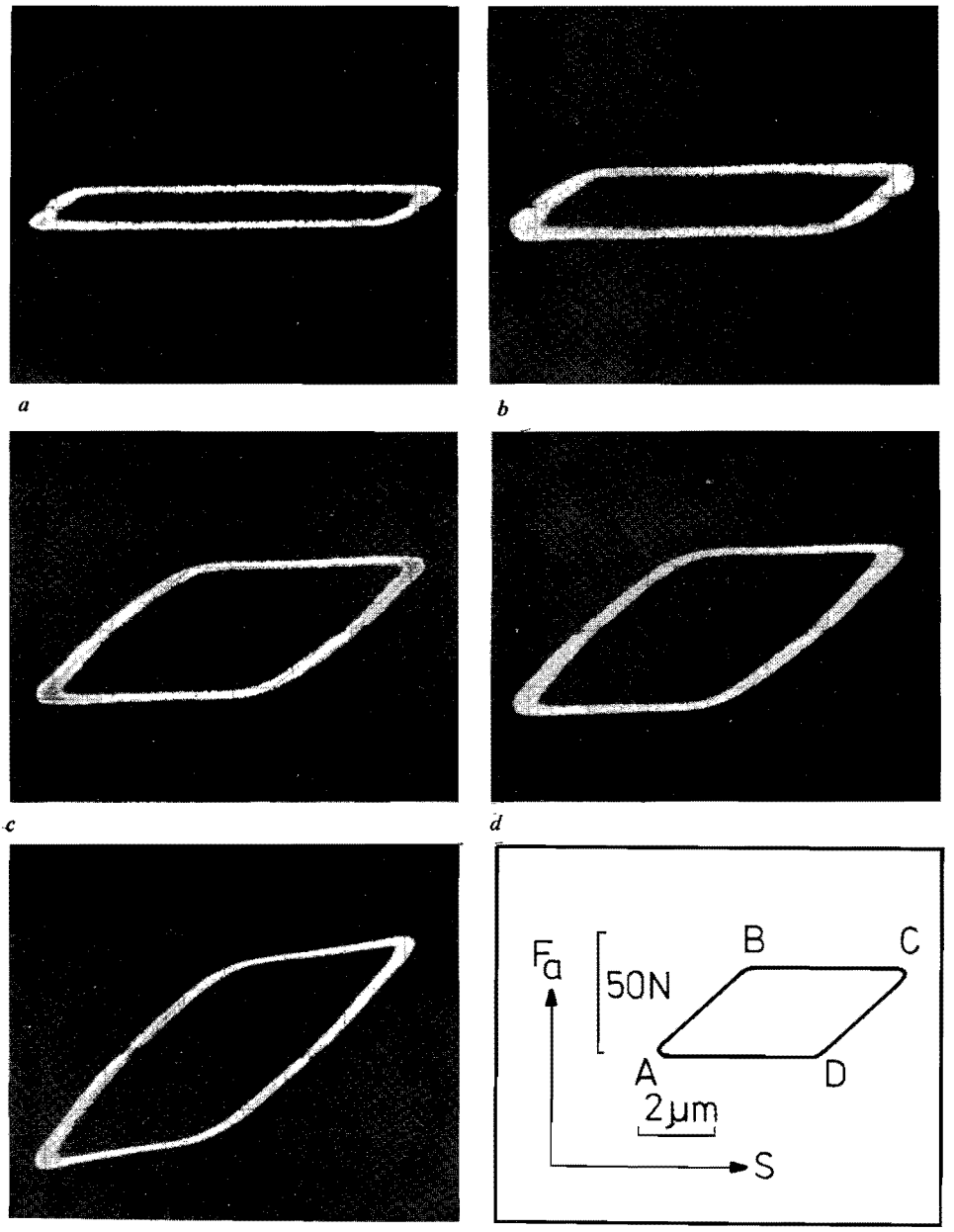

Fig. 5.3. Force-path diagrams for a single oscillation in subsonic welding of Al. F_a is the alternating tangential force; s is the relative displacement.
a. after 100 oscillations; b. after 200 oscillations; c. after 500 oscillations;
d. after 1000 oscillations; e. after 5000 oscillations.

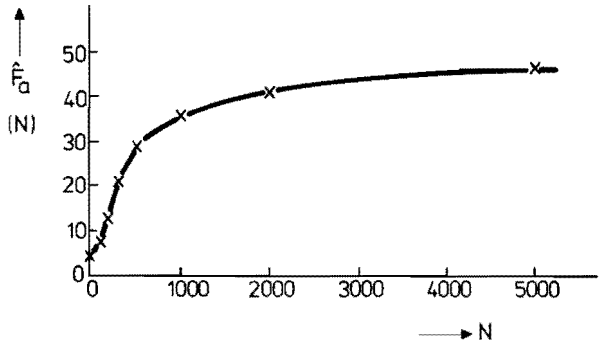

Fig. 5.4. The alternating tangential force amplitude $\hat{F}_a$ as a function of the number of oscillations N in subsonic welding of Al.

Measurements of this area yield the values of table 5.1.
In fig. 5.4 the maximum value of the alternating force $\hat{F}_a$ is plotted as a function of the number of oscillations. From these measurements it follows that

1. The maximum value of $\hat{F}_a$ grows rapidly during the first 500 oscillations.
2. The alternating tangential stress amplitude $\hat{\tau}_a = \hat{F}_a/A$ after 5000 oscillations equals 52 ± 7 N/mm^2 as calculated from $\hat{F}_a = 47 \pm 3$ N (table 5.1) and the contact area $A = 0.9 \pm 0.1$ mm^2.
3. The energy dissipation per cycle is virtually constant after 500 cycles.

We will compare these observations to the facts observed in ultrasonic welding.

The alternating force amplitude $\hat{F}_a$ is comparable to the force amplitude $|\bar{F}_l| = |\bar{F}_w|$ in ultrasonic welding (see sec. 4.2). In fig. 4.23 $|\bar{F}_l|$ is plotted as a function of welding time. Compare fig. 5.4 and fig. 4.23, bearing in mind that in 100 ms welding time in ultrasonic welding 2000 oscillations occur. The rapid growth of $\hat{F}_a$ during the initial 500 oscillations is similar to the increase of $|F_l|$ in ultrasonic welding during the first tens of milliseconds, as described in sec. 4.3.1. During the remainder of the welding period the forces show a moderate increase, both in the subsonic and ultrasonic case. The behaviour of the alternating tangential forces in both ultrasonic and subsonic welding supports the assumption that during the first few hundreds of oscillations the area of real contact grows and reaches the value of the finally welded area; in this area of real contact microwelds are formed and at the end of the welding period the area of real contact is completely welded.

The alternating tangential stress amplitudes are of the same magnitude both in subsonic and ultrasonic welding of Al; subsonic welding: $\hat{\tau}_a \sim 50$ N/mm^2; ultrasonic welding: $\hat{\tau}_w \sim 50$-60 N/mm^2 (see table 4.8). These values exceed the elasticity limit considerably, hence the contacting interface is in a plastic state, in both cases.

At the end of the welding period the energy dissipation per oscillation per mm^2 welded interface is 0.36×10^{-3} J/mm^2 (see table 5.1). The energy dissipation per oscillation in ultrasonic welding (under conditions comparable to the subsonic welding experiments, as mentioned in sec. 5.1) is 0.55×10^{-3} J/mm^2 (see Appendix A5).

The calculation of the energy dissipation per oscillation in the interface, assuming that the contact between the weld members is (after the initial few hundreds of oscillations) complete and that the interfacial layer is in a plastic state is performed in Appendix A5. The calculated value of 0.45×10^{-3} J/mm^2 energy dissipated per oscillation is in agreement with the experimental values from ultrasonic and subsonic welding.

The similarity between ultrasonic and subsonic welding, mentioned in the previous section, is supported by the comparisons made above.

5.4. Conclusion

The similarity of ultrasonic and subsonic welds with respect to strength and appearance (sec. 5.2) and the similarity of the welding processes with respect to alternating tangential stresses and energy dissipation per oscillation per unit area (sec. 5.3) leads to the assumption that the physical process of weld formation is the same in both ultrasonic and subsonic welding.
This has the following important consequences.
Weld formation in ultrasonic welding is independent of the frequency of vibration. The number of oscillations and the vibrational amplitude determine rate of growth of the weld.
During the formation of a subsonic weld temperature rise is negligible, as the power input is of the order of 10 mW/mm^2. This indicates that for the formation of an ultrasonic weld a temperature rise is not essential.
Temperature effects being ruled out, the formation of a weld in subsonic welding can only be caused by metallic adhesion in clean contact areas. The relative motion of the parts causes growth of the real contact area (sec. 2.5.3.1) and rupture or dispersion of the surface contaminant layer (sec. 2.5.3.2). Thus clean metal is brought into contact and metallic adhesion junctions are formed. We propose that this mechanism also causes weld formation in ultrasonic welding.

6. THE ULTRASONIC METAL WELDING PROCESS – A MODEL, DISCUSSIONS AND CONCLUSIONS

Based on the present experiments and data from literature an elementary model for the ultrasonic metal welding process is proposed. In section 6.1 this model will be outlined and in section 6.2 a more detailed description is given. In section 6.3 findings from the model will be compared with the experimental results followed by a discussion of the results and some possible improvements of the model.

6.1. Outline of the model

The surfaces to be welded are pressed together by the clamping force. The area of real contact is then about 10% of the total area to be welded. At the contact spots a contaminating surface layer (oxide, adsorbed gas, grease, moisture) prevents metallic adhesion.

Next the vibration of the welding tip starts. The action of the alternating force, parallel to the contact plane, exerted by the vibrating welding tip, causes the area of real contact to increase in a short time compared to the total welding period, to the size of the total area to be welded. The contact surfaces perform a relative sliding motion resulting in local rupture or removal of the contaminant layer. Hence in small areas, approx. 10 μm in size, clean metal of the two surfaces is brought into contact. At these clean contacts metallic adhesion (cold welding) takes place. Further relative vibrational movement of the surfaces causes these initially welded contacts to grow outwards from their periphery by continual rupture or dispersion of the contaminant layer and adhesion. As growth of the welded contacts mainly occurs at the sides, perpendicular to the direction of relative movement, elongated welded areas (microwelds) are generated. The longest axis of these microwelds is parallel to the direction of the relative movement of the surfaces. Once a microweld is formed it is not ruptured by the relative vibrational movement. During the continuing vibration it is subjected to a (vibrational) shear deformation. The welded interfacial layer is then in a plastic state. The average area of a microweld is independent of vibrational amplitude and welding time but appears to depend upon surface conditions.
The growth of a single microweld to its final size occurs in a period which is short compared to the total welding time. The growth of the entire weld can be described as follows: the number of microwelds generated per unit unwelded contact area is proportional to the total distance of relative displacement (slip) of the contacting surfaces. The total distance of displacement increases with the welding time and hence, as the welding time proceeds, the number of microwelds increases. This process is continued untill the whole contact area is welded.

These basic facts and assumptions form a model to describe how the welded area depends upon the vibrational amplitude and the welding time. The breaking shear

force of the weld is proportional to the welded area. In the model, outlined above, introduction of temperature effects is not necessary for the understanding of the formation of a weld.

6.2. The model

6.2.1. The area of real contact

The area of real contact equals the ratio of the clamping force F_C and the hardness H_V. Using the data from table 4.2 the area of real contact varies between 0.5 and 1 mm^2. Using the breaking stress from table 4.2 and the maximum breaking forces from figs. 4.1 to 4.6, the final welded area occurs in the range 6 to 7 mm^2. Hence by the action of the clamping force alone only about one tenth of the area to be welded is brought into real contact. However, metallic contact and adhesion is prevented in this real contact area by surface contaminants.

When the vibration of the welding tip starts an alternating tangential force is exerted on the weld members, resulting in a relative displacement (compare sec. 4.4). By this action the area of real contact grows, as shown in sec. 2.5.3.1. The experiment in sec. 4.3.2. clearly demonstrates that this growth proceeds in a few milliseconds to a multiple of the initial contact area. Measurements of the alternating force amplitude $|\bar{F}_1|$ (sec. 4.3.1) show a saturation after a few tens of milliseconds. This indicates that the area of real contact is close to the final weld area after the initial 10 – 20 ms of the welding period (100 – 1000 ms).

The first assumption of our model is that the area of real contact between the specimens grows, by the action of the alternating tangential force, to the value of the final welded area A (∞), during a time interval which is very short compared to the welding period. Surface contaminants prevent welding in this initial stage.

6.2.2. The microwelds

During the relative displacement of the contacting surfaces, local stresses are sufficiently large to cause plastic deformation of an interfacial layer (see sec. 4.2.2). This deformation can bring about local rupture of the surface contaminant layer. Another possibility is that this layer is ruptured by the ploughing action of the surface asperities. Rupture of the contaminant film makes metallic adhesion (welding) possible (see sec. 2.5.3). The first adhesion spots are much smaller than the microwelds. Rabinowicz (6.1) estimates the average diameter of spots of real contact (junctions) in sliding friction to be of the order of 10 μm. The first adhesion spots in ultrasonic welding probably are of that size.

An adhesion spot grows by plastic deformation of the surrounding material. We will outline the proceeding of this process. Suppose an adhesion spot exists between

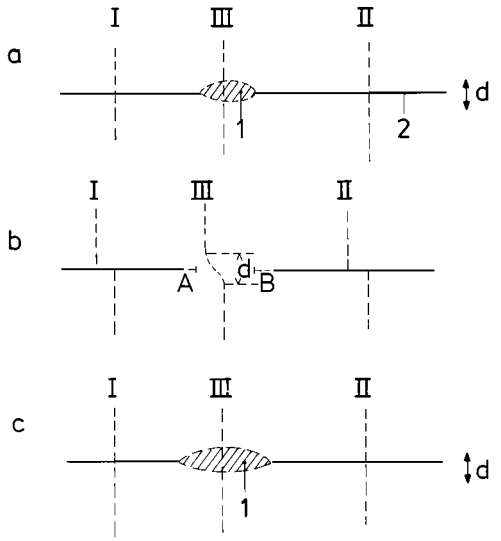

Fig. 6.1. Diagram of the growth of a microweld (cross section).

a. A welded spot with a plastic deformation zone (1) exists between two contacting surfaces (2). The surfaces are covered with a contamination layer; d is the thickness of the deformed layer.

b. The upper specimen moved to the left. The relative displacement is indicated by the deformation of the lines I, II and III. Rupture of the surface layer occurred in the dotted regions A and B.

c. The upper specimen moved back to its original position. The welded spot has grown in the direction of the relative displacement.

two contacting surfaces. A cross-section of this situation looks like fig. 6.1a. The full drawn line represents the unwelded contacting surface. The dotted lines I, II and II indicate the relative position of the surfaces. As the upper specimen in fig. 6.1a moves to the left, the material must be sufficiently ductile not to fracture the adhesion spot. The material close to the adhesion spot will deform plastically *) whilst the unwelded surface will slide, as indicated in fig. 6.1b by the positions of the lines I, II and III. At the edges of the adhesion spot (the dotted parts of the interface, indicated by A and B in fig. 6.1b) the surfaces are stretched and compressed respectively. By this action the surface contaminant layer is ruptured at the edges of the adhesion spot where contact between clean metal is again made possible and adhesion takes place. This process proceeds and the relative vibrational

*) A large scale model of this process is described by Greenwood and Tabor (6.2, 3).

movement thus causes the adhesion spot to grow to an oblong microweld (fig. 6.1c); the longest axis of this microweld being parallel to the direction of vibration. The physical reality of the microwelds is demonstrated by the observations (see sec. 4.2.2 and 5.2). The growth of a microweld to its final value proceeds in a time interval which is short compared to the welding interval. This assumption is based on the following observations

1. The average length of the microwelds is independent of welding time (sec. 4.2.3.1).
2. In subsonic welding long microwelds were formed after the first 100 oscillations (see fig. 5.2a).

One might expect the growth of a microweld to go on as long as the vibration is maintained. In reality, however, growth stops and the microwelds reach an average length and width which appears from the present experiments to be independent of welding time and vibrational amplitude (see sec. 4.2.3.1). The average length is strongly influenced by surface contaminants as well as by surface geometry (roughness), as demonstrated in sec. 4.2.3.2.
The limited growth of the microweld can be partly understood on the assumption that the contact between the surfaces is never perfect. Small gaps may exist locally preventing the growth of the microwelds. The occurrence of these gaps will be greater the rougher the original surface (also after the growth of the contact area). Hence the roughter the surface the shorter the microwelds. This is in agreement with the observation in sec. 4.2.3.2: the abraded copper surface of fig. 4.22 contains much shorter microwelds than the original copper surfaces of fig. 4.10 a, b.

The next assumption of the model is that an ultrasonic metal weld consists of a number of oblong microwelds which grow in the area of real contact by the vibrational relative displacement of the mating surfaces. The average area (size) of a microweld is constant in a welding operation, but depends upon the surface conditions of the weld members.

6.2.3. The number of microwelds

In the theory of wear a hypothesis states that the worn volume per unit area of real contact is proportional to the sliding distance (5.4, 5, 6). Analoguous to this, we assume for ultrasonic metal welding that the number of adhesion spots and consequently the number of microwelds generated per unit area of real contact is proportional to the distance of relative displacement of the contacting surfaces. Relative displacement is used in the same meaning as in sec. 4.4.

Assume the number of newly formed microwelds in time interval dt of a welding period amounts to dn per unit contact area. Let the amplitude of the relative vibrational displacement be ξ_s, henceforth to be called the slip amplitude. The total distance of relative displacement in time interval dt equals $4\,\xi_s\,\nu\,dt$, where ν is the frequency of vibration.

According to the above assumption

$$dn = C \times 4 \xi_s \nu \, dt \tag{6.1}$$

where C is a constant.

The area of real contact in a weld equals A (∞) (see sec. 6.2.1). At time t this area is partly covered with microwelds. The total welded area then is A(t) and hence the unwelded area of real contact equals A (∞) – A(t). The number of newly formed microwelds in this unwelded area during the interval dt is.

$$dN = \{A(\infty) - A(t)\} dn =$$

$$= 4C \xi_s \nu \{A(\infty) - A(t)\} dt \tag{6.2}$$

6.2.4. The growth of the welded area

The average area of a microweld is A_m (see sec. 4.2.3.1). Then the increase of the welded area A(t) in time interval dt is

$$d A(t) = A_m dN \tag{6.3}$$

$$d A(t) = 4 A_m C \xi_s \nu \{A(\infty) - A(t)\} dt \tag{6.4}$$

The slip amplitude ξ_s in the welded interface cannot be measured directly. However, the estimates given in secs. 4.4.2 – 3 suggest a proportionality between the slip amplitude ξ_s and the welding tip amplitude ξ. Although this proportionality has not been proven in general, it will be assumed for the purpose of the model

$$\xi_s = a \xi \tag{6.5}$$

where a is constant (according to sec. 4.4.2 the value of a varies from 0.3 to 0.5 for the geometry of specimens used in our experiments).

From the observations in sec. 4.2.1.2 it appears that the vibrational amplitude varies by a maximum of 20% during the welding period. In this model, however, we will assume that ξ does not depend on the welding time t. Integration of eq. (6.4) then renders

$$\ln \{A(\infty) - A(t)\} = - K \xi t + B \tag{6.6}$$

with

$$K = 4 A_m a \nu C \tag{6.7}$$

The integration constant B is found from the boundary condition that at time t = o the welded area A(o) = o. Hence B = ln A (∞). Equation (6.6) now becomes

$$A(t) = A(\infty)\left\{1 - \exp(-K\xi t)\right\} \tag{6.8}$$

Section 4.2.1.3 shows that the breaking force is proportional to the welded area. Thus eq. (6.8) can be written

$$F_b(t) = F_b(\infty)\left\{1 - \exp(-K\xi t)\right\} \tag{6.9}$$

This equation describes the dependence of F_b (t) (= breaking force at time t) on the amplitude of vibration of the welding tip ξ and the welding time t. This relation can be verified experimentally, if the final value of the breaking force F_b (∞) and the constant K of the model are known.

6.2.5. Determination of the final value of the tensile shear force F_b (∞)

In this section the method to evaluate F_b (∞) is described. The alternating force amplitude $|\bar{F}_w|$ can be determined, as described in sec. 4.3.1. When the contact area is completely welded, the welded area equals $|\bar{F}_w| / \hat{\tau}_w$, where $\hat{\tau}_w$ is the average alternating stress amplitude in the contact zone. According to eq. (4.1) the total welded area also equals F_b (∞) / τ_b.

Hence

$$\frac{F_b(\infty)}{\tau_b} = \frac{|\bar{F}_w|}{\hat{\tau}_w} \tag{6.10}$$

Using eqs. (3.31) and (3.7) we obtain

$$|\bar{F}_w| = |\bar{F}_l| = |\bar{v}_l| \, |\bar{Z}_{ml}| = \omega\xi \, |\bar{Z}_{ml}|$$

Equation (6.10) then becomes:

$$F_b(\infty) = \frac{\tau_b}{\hat{\tau}_w} \omega\xi \, |\bar{Z}_{ml}| \tag{6.11}$$

By this formula F_b (∞) is expressed in terms of

1. Constants to be determined experimentally for a particular material. These are τ_b and $\hat{\tau}_w$.
2. Quantities depending on the welding parameters which can be measured (indirectly) at the electrical terminals of the transducer. These are ξ and $|\bar{Z}_{ml}|$.

6.2.6. Evaluation of the constant of the model K

From eq. (6.7) $K = 4\ A_m\ a\ \nu\ C$, we see that K consists of a number of different factors.
The vibrational frequency is $\nu = 2 \times 10^4$ Hz. As to the average area of a microweld A_m we can make an estimation using data as given in sec. 4.2.3.1. (average length and width). An estimate of the quantity a is given in sec. 4.4.3.
The quantity C represents the number of adhesion spots per unit area of real contact, formed after a relative sliding distance of one unit length of the contacting surfaces. A theoretical evaluation of C is subject to many uncertainties. In order to be able to make an estimation of C we have assumed that the number of adhesion spots formed in sliding contact, equals the number of unit events of wear. According to Archard (6.5) a unit event in wear is the encounter of two surface asperities in sliding contact, resulting in mutual deformation and formation of wear particle. Archard supposes that only a fraction of the encounters gives rise to the production of a wear particle. This fraction varies from 10^{-2} for materials with a low wear resistance to 10^{-7} for materials with a high wear resistance. We can estimate the number of asperities per m^2 on the surface of the middle hard aluminium sheets used in our experiments. A surface profile showed about 100 asperities on a 3 mm trace *). Hence the number per m^2 is 10^9. When 1 m^2 of such a surface slides 1 m distance over a much larger similar surface the number of asperity encounters is about 3×10^{13} **). Aluminium has a low wear resistance, hence the fraction of encounters giving rise to production of a wear particle is large. Choosing this fraction from 10^{-3} to 10^{-2}, the number of unit events per m^2 real contact amounts to 3×10^{10} to 3×10^{11}. Consequently we estimate C to be equal to this value, as this is the number of adhesion spots formed per m^2 real contact area per meter sliding distance.

This estimation of C indicates the order of magnitude only. As it is based on the encounter and mutual deformation of asperities in sliding friction, resulting in the local rupture of the contaminating surface layer followed by adhesion of clean metal, its validity for ultrasonic welding is open to discussion. In ultrasonic welding, the mating surfaces are in real contact over the whole nominal contact area (after a short period, see sec. 6.2.1). As to the mechanism causing rupture of the contaminant layer the following possibility was considered. The interface making real contact is a plane of a wavy nature; its average 'amplitude' being about the roughness of the original surfaces and its average 'wavelength' being a few tens of micrometers. A relative displacement of the contacting weld members may result

---

*) Only asperities having a height of at least half the RMS roughness value of the surface profile were taken into account.

**) One asperity on the sliding surface will encounter $(10^9)^{0.5}$ other asperities. Thus 10^9 asperities will encounter $10^9 \times (10^9)^{0.5} \sim 3 \times 10^{13}$ asperities.

in interfacial slipping or sticking of the surfaces and consequently deformation of the layer of material in which the (wavy) contact plane is situated. Both possibilities might give rise to rupture of the contaminating layer. When interfacial slip occurs the mechanism of rupture is supposed to be similar to the asperity encounter mechanism. In the deformation of an interfacial layer the rupture can be caused by local stretching and shrinking of the surfaces. Whether these mechanisms will yield similar values of C is not known.

We estimate the order of magnitude of K for medium hard aluminium as follows. The average area of a microweld is about 2×10^{-9} m^2 (sec. 4.2.3.1). The quantity a equals 0.4, which is a reasonable value according to sec. 4.4.3, the vibrational frequency is 2×10^4 Hz and C is estimated above. Using (6.7) we can find K to be of the order of 10^6 to 10^7 m^{-1}s^{-1}. From the following section it will appear that the experimental value of K is of the same order of magnitude.

6.3. Verification of the model and discussion

Equation (6.9) describes the breaking force of a weld as a function of vibrational amplitude ξ and welding time t. In order to check its validity the quantities $F_b(\infty)$ and K are evaluated. Using the obtained values $F_b(t)$ is calculated from eq. (6.9) for the values of ξ and t from the experiments. It appears that these calculated values fit well to the experimental results.

6.3.1. The values of $F_b(\infty)$ and K

In order to determine the final value of the breaking force $F_b(\infty)$ (sec. 6.2.5) and the constant K of the model (sec. 6.2.6) experimental data are used.

The simplest way to determine $F_b(\infty)$ would be to take the reading of the final value direct from the experiments (fig. 4.1 to 4.4). By doing so, we would get no insight into the connection between the values of $F_b(\infty)$ for different values of the vibrational amplitude and for different materials. For this reason we have chosen a less direct method. Equation (6.11)

$$F_b(\infty) = \frac{\tau_b}{\hat{\tau}_w}\,\omega\xi\,|\bar{Z}_{ml}|$$

expresses $F_b(\infty)$ as a function of a number of quantities. The value of the average tensile shear stress τ_b is given in table 4.2. The average alternating stress amplitude $\hat{\tau}_w$ can be found from measurements of the alternating force and contact area as listed in table 4.8. The quantity $\hat{\tau}_w$ is determined in the case of the highest power and longest welding time used in this series of welding experiments. This situation was chosen because the weld was then fully grown, i.e. the contact area is completely welded. Hence this value of $\hat{\tau}_w$ refers to a welded area. The angular

frequency ω equals 12.57×10^4 rad s^{-1}. The modulus of the mechanical load impedance $|\bar{Z}_{ml}|$ is calculated from measurements using the method as described in sec. 3.2.3.

All quantities required for the calculation $F_b(\infty)$ from eq. (6.11) are listed in table 6.1. $F_b(\infty)$ is calculated for the different materials and vibrational amplitudes used in the experiments. The result is given in the last column of table 6.1.

TABLE 6.1
Determination of the final breaking force $F_b(\infty)$

Material Clamping force F_c	Vibrational amplitude ξ (μm)	Alternating stress amplitude $\hat{\tau}_w$ (N/mm^2)	Breaking stress τ_b (N/mm^2)	Mechanical load impedance $\lvert\bar{Z}_{ml}\rvert$ (kg/s)	Final breaking force $F_b(\infty)$ (N)
Al (medium hard)	10	51	55	310	400
F_c = 375 N	16	51	55	250	540
	23	51	55	190	580
Al (hard)	12	130	130	290	420
F_c = 675 N	15	130	130	290	530
	25	130	130	290	920
Cu	10	73	150	200	530
F_c = 375 N	15	73	150	200	780
	21	73	150	200	1060
Ni	15	210	310	360	1000
F_c = 1000 N	17	210	310	360	1170
	22	210	310	360	1500

The accuracy of the calculated value of $F_b(\infty)$ can be assigned by a standard deviation of 20%. Each value of $|\bar{Z}_{ml}|$ is the average of a series of 5 independent measurements; the standard deviation of $|\bar{Z}_{ml}|$ is 10%. The inaccuracy in both τ_b and $\hat{\tau}_w$ are estimated to be 10%.
In sec. 4.2.1.2 we reported that the actual average vibrational amplitude for a single weld could deviate by up to 10% from the general average. These values give rise to the above mentioned estimate for the inaccuracy of $F_b(\infty)$.

Next the value of K has to be found. Equation (6.9) can be written as:

$$K = \frac{1}{\xi t} \ln \frac{F_b(\infty)}{F_b(\infty) - F_b(t)} \qquad (6.12)$$

For a particular value of ξ and t, the appropriate value of F_b (t) is determined in the welding experiments (sec. 4.2.1.2). In the tables 6.2 to 6.5 these data (ξ, t, F_b (t) and F_b (∞) are listed for the materials welded in the present experiments. From each set of data a value for K can be calculated using eq. (6.12). This calculation has been performed for the cases where F_b (t) $\leqslant$ ½ F_b (∞). The reason for this is that the inaccuracy in both quantities amounts to 20% and hence their difference will be very inaccurate as F_b (t) approaches F_b (∞). The results of the calculations of K are given in the tables 6.2 to 6.5, together with the average value and the standard deviation of the series of K-values for different materials.

In sec. 6.2.6 a speculative estimation of the value of K for medium hard aluminium was given as varying from 10^6 to 10^7 $m^{-1}s^{-1}$. Nevertheless the experimental value was determined as 0.8×10^6 $m^{-1}s^{-1}$.

The values of K were obtained by averaging the results from a number of measured values. It can be seen from the tables 6.2 to 6.5, that for a specified material the values determined from each measuring point show a scatter. There is no systematic relation between the value of K as determined from a measuring point and either the vibrational amplitude or the welding time at that measuring point. Hence we cannot separate the influence of different factors constituting K according to eq. (6.7). The quantities a and ν are fixed; the quantity A_m denoting the average area of a microweld has the character of an average of a statistical distribution; the quantity C is the average number of microwelds, developing after a unit distance of relative sliding, per unit area. The nature of the quantities A_m and C causes the scatter in the values of K as determined from the measurements *).

From eq. (6.9) it appears that the larger the value of K, the faster a weld will be formed with a specified combination of ξ and t. Consequently K is a measure of the velocity of weld formation.

---

*) Measurements of the number and size of microwelds in ultrasonic welds can be performed only for very limited parts of the welded area and for welds only partly covered with microwelds, as explained in sec. 4.2.3.1. Hence it is difficult to obtain reliable data concerning the number of microwelds and the value of the quantity C directly from experiments.

TABLE 6.2
Calculation of K for Al (medium hard)

Vibrational amplitude ξ (μm)	Final breaking force $F_b(\infty)$ (N)	Welding time t (ms)	Breaking force $F_b(t)$ (N)	K ($m^{-1} s^{-1}$)
10	400	10	26	6.8×10^5
		20	57	7.8×10^5
		40	103	7.6×10^5
		100	177	5.9×10^5
16	540	10	62	7.4×10^5
		20	118	7.5×10^5
		40	204	7.2×10^5
23	580	10	116	9.6×10^5
		20	211	9.7×10^5
		40	308	8.1×10^5
Average value of K (with standard deviation)				$(7.8 \pm 1) \times 10^5$

TABLE 6.3
Calculation of K for Al (hard)

Vibrational amplitude ξ (μm)	Final breaking force $F_b(\frac{1}{2})$ (N)	Welding time t (ms)	Breaking force $F_b(t)$ (N)	K ($m^{-1} s^{-1}$)
12	420	40	57	3.1×10^5
		100	147	4.6×10^5
		200	265	4.0×10^5
15	530	20	121	8.8×10^5
		40	178	7.0×10^5
		100	318	6.3×10^5
25	920	10	156	7.3×10^5
		20	233	5.8×10^5
		40	355	4.5×10^5
Average value of K (with standard deviation)				$(5.7 \pm 2) \times 10^5$

TABLE 6.4
Calculation of K for Cu.

Vibrational amplitude ξ (μm)	Final breaking force $F_b(\infty)$ (N)	Welding time t (ms)	Breaking force $F_b(t)$ (N)	K ($m^{-1}s^{-1}$)
10	530	100	107	2.2×10^5
		200	170	1.8×10^5
		400	215	1.2×10^5
15	780	40	58	1.3×10^5
		100	147	1.4×10^5
		200	254	1.3×10^5
		400	441	1.3×10^5
21	1060	20	66	1.5×10^5
		40	120	1.4×10^5
		100	316	1.7×10^5
		200	450	1.3×10^5
Average value of K (with standard deviation)				$(1.5 \pm 0.2) \times 10^5$

TABLE 6.5
Calculation of K for Ni

Vibrational amplitude ξ (μm)	Final breaking force $F_b(\infty)$ (N)	Welding time t (ms)	Breaking force $F_b(t)$ (N)	K ($m^{-1}s^{-1}$)
15	1000	40	64	1.1×10^5
		100	127	0.9×10^5
		200	248	1.0×10^5
		400	588	1.5×10^5
17	1170	20	97	2.5×10^5
		40	302	4.3×10^5
		100	463	2.9×10^5
22	1500	20	237	3.9×10^5
		40	561	5.3×10^5
		100	844	3.8×10^5
Average value of K (with standard deviation)				$(2.7 \pm 1.5 \times 10^5$

6.3.2. Agreement between the model and the experiments

According to the model, the tensile shear force F_b (t) of a weld can be found from

$$F_b(t) = F_b(\infty)\left\{1 - \exp(-K\,\xi\,t)\right\} \qquad (6.9)$$

where the vibrational amplitude ξ and the welding time t are known as welding parameters. The values of F_b (∞) and K are evaluated as shown in sec. 6.3.1. Hence F_b (t) remains to be computed. The calculated values of F_b (t) as a function of t with ξ as a parameter are plotted in figs. 6.2 to 6.5 for Al (medium hard and hard), Cu and Ni. In these graphs the experimental values of F_b (t) are also plotted, the error bars indicating the standard deviation (compare sec. 4.2.1.2).

For Al (medium hard and hard) and Cu, the calculated curves differ less than 25% from curves obtained from the experimental values. This difference is of the same order as the scatter of the measurements. Hence we conclude that the agreement between the model and the experiments is acceptable both for Al and Cu.

For Ni the calculated curve corresponding to the lowest vibrational amplitude (fig. 6.5; ξ = 15 μm) differs systematically from the observed values. From table 6.5 we see that the K-values for ξ = 15 μm are about 1 x 10^5 $m^{-1}s^{-1}$, whereas the K-values for ξ = 17 μm and ξ = 22 μm amount to 3 to 4 x 10^5 $m^{-1}s^{-1}$. Averaging

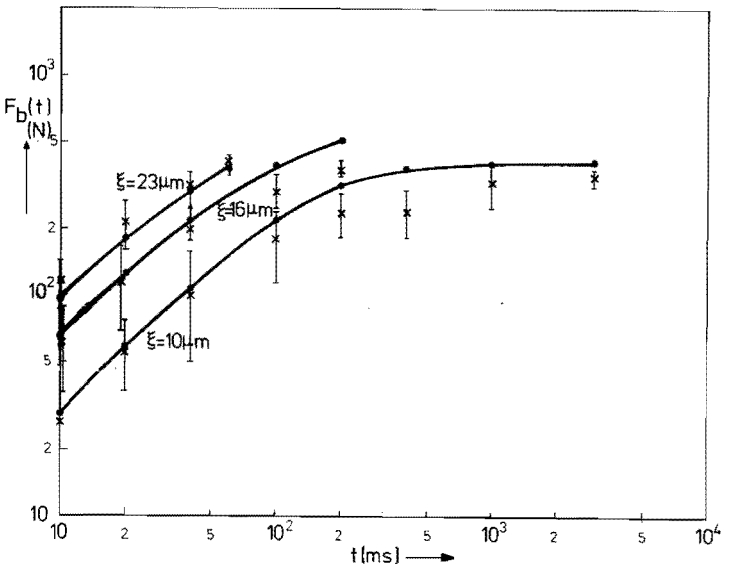

Fig. 6.2. Calculated values of the breaking force F_b (t) as a function of welding time t, at different levels of the average vibrational amplitude ξ. Material: Al (medium hard). The experimental results are also indicated (from fig. 4.1).

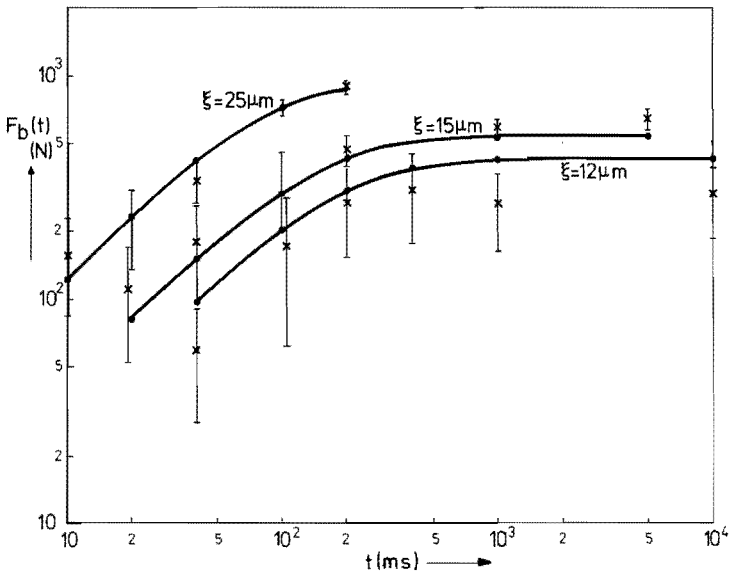

Fig. 6.3. Calculated values of the breaking force F_b (t) as a function of welding time t, at different levels of the average vibrational amplitude ξ. Material: Al (hard). The experimental results are also indicated (form Fig. 4.2).

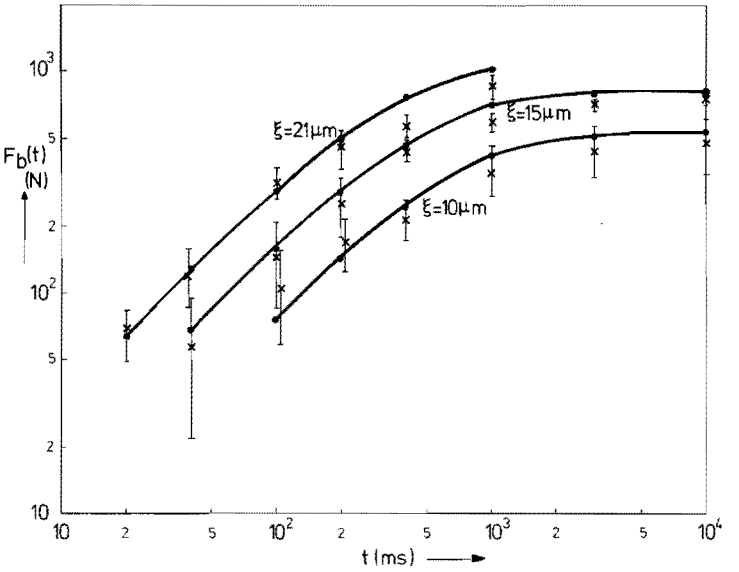

Fig. 6.4. Calculated values of the breaking force F_b (t) as a function of welding time t, at different levels of the average vibrational amplitude ξ. Material: Cu. The experimental results are also indicated (from Fig. 4.3).

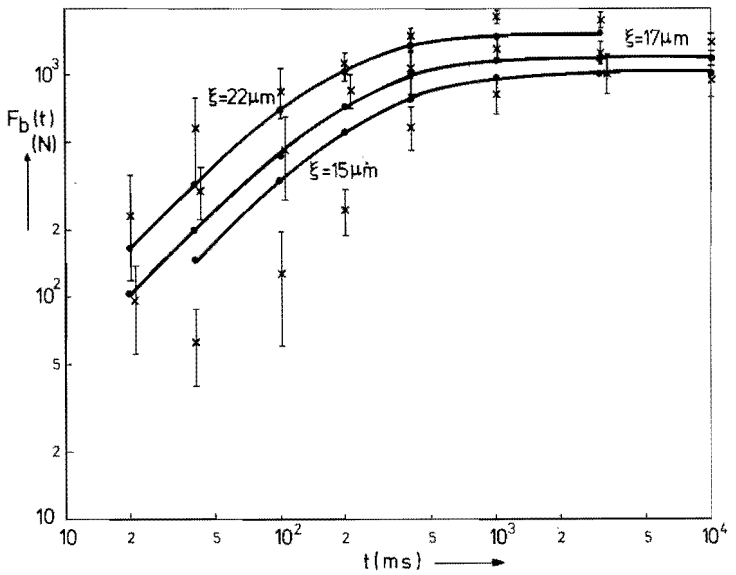

Fig. 6.5. Calculated values of the breaking force F_b (t) as a function of welding time t, at different levels of the average vibrational amplitude ξ. Material: Ni. The experimental results are also indicated (from Fig. 4.4).

these groups of values yields of course an average differing from both groups. Consequently the calculated curve for $\xi = 22\ \mu m$ is systematically too low and the curve for $\xi = 15\ \mu m$ is too high. The welds of Ni made with a vibrational amplitude $\xi = 15\ \mu m$ have a large unwelded central area. In this case the slip in the central area must have been zero. From the difference between the experimental data and the model for Ni we conclude that this model is not applicable in the case where no slip in the central region occurs. Thus we determined the average value of K using only the data from the series with $\xi = 17\ \mu m$ and $\xi = 22\ \mu m$ (table 6.5) as $K = (3.8 \pm 1) \times 10^5\ m^{-1}s^{-1}$. Calculation of F_b (t) using this value yields the curves displayed in fig. 6.6. These curves fit to the experimental data in the same way as the curves for Al and Cu. It is therefore considered that there is sufficient agreement between the model and the experimental data.
The model accounts for the shape of the breaking force vs. welding time curve and for the differences in weld strength when using different amplitude settings.

6.3.3. Discussion

The model of the ultrasonic welding proposed in this chapter contains simplifications in order to obtain a mathematical formulation

1. Immediately after the commencement of the ultrasonic vibration the area of real contact grows to its ultimate value.

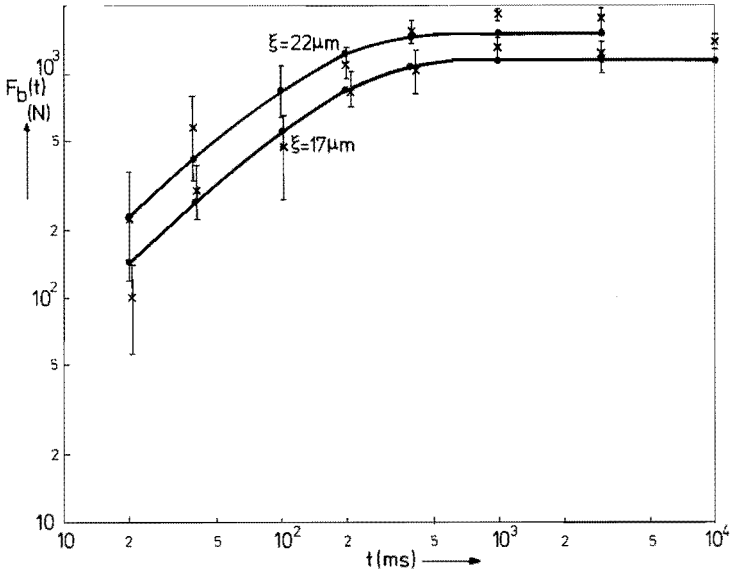

Fig. 6.6. Reinterpretation of the calculated values of F_b (t) of Ni.

2. The vibrational amplitude is assumed to be constant during the welding period.
3. It is assumed that in the contact area no difference in slip amplitude exists between the periphery and the centre of the weld zone.

The first assumption is implicit in eq. (6.2) in that the area of real contact is A (∞). It is the consequence of the physical fact that the area of real contact grows to the value of the finally welded area, during a time interval, which is short compared to the welding period (see sec. 6.2.1).
The second assumption is mentioned in sec. 6.2.4. No systematic relationship for the vibrational amplitude as a function of welding time could be observed but from the experiments it appeared that the value of the vibrational amplitude at any time (excluding the transient phenomenon) deviated less than ±10% from the average value, as mentioned in sec. 4.2.1.2. For this reason the vibrational amplitude is considered to be independent of the welding time.

The third assumption is implicit in the description of the growth of the welded area (secs. 6.2.3 and 6.2.4). From the present experiments we see that in most cases and normal welding conditions the microwelds are distributed at random over the welding area (see fig. 4.8 to fig. 4.13). So the same tendency for welding occurs over the entire welding area (except for the lowest vibrational amplitude setting of Ni and for stainless steel). Hence we assume that the slip amplitude can be considered to be constant over the entire contact area.

The possibility of differences in slip amplitude between centre and periphery of the welding area is discussed in the literature (6.7, 8). These discussions are based on an analysis by Mindlin and Johnson (6.9, 10, 11, 12) of the effect of an oscillating tangential force on the contact surface between a sphere and a plane. The result of this analysis is that in a contact surface two zones can be distinguished, the central zone in which no relative movement of the surfaces occurs and the periphery where relative slip of the surfaces is found. The dimensions of these two zones depend upon the normal clamping force applied to the contact area and the tangential force. The larger the tangential force, the smaller the central zone. For ultrasonic metal welding this means that the central part of the contact area is not being welded if the tangential force is below a certain value. A demonstration of this effect is given in figs. 4.27 a, b, c. A proper setting of the ultrasonic welding parameters prevents this effect.

In sec. 2.5.1 three different types of welding operations were mentioned
1. Welding by fusion of an internfacial zone
2. Solid state welding
   a. by heating without fusion
   b. by applying mechanical force alone (cold welding).

The aim of the experimental investigations was to determine which might be the physical background for the formation of a joint in ultrasonic metal welding.

Temperature measurements and metallographic examination as reported in the literature (see sec. 2.4.1 and 2.3.1) show that melting does not occur in ultrasonic welding. Hence the first welding operation mentioned above can be excluded.

In sec. 2.5.1 we saw that solid state welding by heating implies diffusion. In the literature on ultrasonic welding some investigators report bulk diffusion in dissimilar metal couples (2.19, 2.22); others did not find any diffusion (2.13, 14, 17) stimulation or enhancement if diffusion by ultrasound is not proved (see Appendix A1). Bulk diffusion of atoms of one weld member into the bulk of the second weld member is not required for weld formation. Only clean metallic contact is needed for welding. Surface diffusion and bulk diffusion in the separate weld members can bring about the contacting of the surface and consequently welding. These types of diffusion are not observed in the heavily deformed bonding zone of an ultrasonic weld; their effects, however, cannot be excluded. Hence, as far as reports in the literature are concerned, the role of diffusion and consequently the effect of temperature remains undecided and a choice between the two possible solid state welding operations mentioned above cannot be made.

The experiments on subsonic welding, described in chapter 5, show that a relative vibrational motion (under a normal pressure) of the contacting weld members is sufficient ot produce a weld, which is similar to an ultrasonic weld, regarding strength,

appearance of the welded interface, alternating tangential force during the process and energy dissipation per oscillation and per unit area. It was concluded that the process causing weld formation is the same in both ultrasonic and subsonic welding. The power input in subsonic welding is so small that no significant temperature rise can be expected. Consequently cold welding (metallic adhesion) is considered to be the operative mechanism in joint formation in both subsonic and ultrasonic welding. A quantative relationship between the adhesion of metals and the material properties cannot be given (see appendix A2).

During the growth of the area of real contact (in the initial 10-20 ms of the welding period) temperature "flashes" may occur. This happens when, in sliding contact, two asperities meet and undergo a highly localized and fast plastic deformation. In appendix A6 the temperature rise of these "flashes" is calculated which appears to be a few degrees centigrade. Therefore this effect may be neglected in the discussion of joint formation in ultrasonic welding.

The largest part of weld is formed in a period when the surfaces are in (almost) complete contact. Energy dissipation is then distributed uniformly over the contact area. In this case we can estimate the maximum surface temperature, which proves to be lower than the recrystallization temperature in two of the four calculated situations (appendix A6).
The present model is based on the physical mechanism of metallic adhesion in clean metallic contact between the weld members brought about by mechanical action only. The model accounts for the observed phenomena: the existence and the shape of microwelds, the growth of the weld as a function of welding time and vibrational amplitude. In particular the oblong shape of the microwelds can only be explained by the present model and not by thermal or diffusion processes.

7. SUMMARY

The aim of the present study was to determine which might be the physical background for the formation of a joint in ultrasonic metal welding.

A survey of the literature on ultrasonic metal welding and related subjects, such as metallic adhesion, was made.

In the experimental part of the study specimens of Al, Cu. Ni and steel were ultrasonically welded.
Observations concerning the formation and growth of ultrasonic welds were made and may be summarized as follows

1. The breaking force of a weld increases monotonously as a function of the welding time until a saturation value is reached. Extension of the welding time, after having reached the final weld strength, causes neither an increase or a deterioration in weld strength.
2. The breaking force (measured in a tensile shear test) of a weld is proportional to the welded area.
3. In ultrasonic metal welds an interfacial layer is plastically deformed. In the present experiments, using sheets of 0.5 mm thickness, the thickness of the deformed layer varies from 30 to 100 μm (determined from microsections).
4. An ultrasonic weld consists of a number of microwelds. These are welded areas, oblong in shape, with the longest axis parallel to the direction of vibration during welding.
5. During the welding period an increasing number of microwelds develops.
6. The dimensions of the microwelds are influenced by the surface conditions of the welded areas, such as roughness or the presence of oil films.

The breaking stress of the welds τ_b was compared to a characteristic breaking stress τ_n of the parent material. The ration τ_b/τ_n is a measure of the weld quality and is accepted to define the weldability of a material. Aluminium, copper and nickel specimens appeared to have good weldability; the values τ_b/τ_n varied between 0.7 and 0.9. Two different steels showed a τ_b/τ_n value of 0.4, hence their weldability was poor. The difference in weldability might be explained by the difference in "removability" of the surface contaminant layers (oxides, adhered gas, moisture and lubricants), a univocal relation between weldability and material properties, e.g. hardness and ductility, as suggested in the literature, is not supported by the present results.
A method to determine the amplitude of the alternating force exerted by the welding tip on the workpieces was developed. The basis of this method was found from an analysis of the ultrasonic vibrating system. It was observed that the alternating force amplitude increased during the initial tens of milliseconds of the ultrasonic welding period to a value of at least 70% of its final value at the end of the welding period. The resulting tangential stress amplitudes in the welded

interface are so large that plastic deformation occurs. From these experiments we conclude that the area of real contact after a few tens of milliseconds welding time is virtually equal to the final welded area. This is confirmed by separate experiments using roughened metal sheets in contact with a glass surface; a few milliseconds of ultrasonic vibration of the metal sheet was sufficient to cause a considerable growth of the area of real contact.

Welding of an aluminium welding tip directly to an aluminium anvil block enabled us to determine the relative vibrational displacement of the weld members during ultrasonic welding. Further welding experiments showed that the weld member contacting the anvil (lower sheet) was virtually at rest during welding. It also appeared that the difference between the vibrational amplitude of the welding tip and the relative vibrational displacement in the welding interface was proportional to the thickness of the sheet contacting the welding tip (upper sheet).

Subsonic welding of aluminium sheets was demonstrated by applying normal pressure (clamping force), relative vibrational displacement and the number of oscillations equal to the corresponing parameters in ultrasonic welding. The only difference being the vibrational frequency, 30 Hz in subsonic welding and 20.000 Hz in ultrasonic welding experiments.

A comparison was made of the characteristics of the subsonic and ultrasonic welding processes and of the welds, produced by these processes

1. Strength of the welds
2. Appearance of the welded interface; the existence of microwelds
3. Microsections of the welded interfaces, showing a plastically deformed layer
4. The behaviour of the alternating force during the two welding processes. The average tangential stresses in the welded interface during welding
5. The energy dissipation per oscillation.

The ultrasonic and subsonic welding processes proved to be very similar with respect to all these characteristics. It is therefore concluded that the mechanism of joint formation is the same for both ultrasonic and subsonic welding. As thermal effects are excluded in subsonic welding, weld formation in ultrasonic welding must be caused by mechanical action resulting in metallic adhesion of clean contacts (cold welding); the mechanical action is the application of an alternating tangential force, causing plastic deformation of the contacting interface. It is demonstrated that the temperature rise due to temperature "flashes" during this deformation is a few degrees.

The present observations enabled a model of the ultrasonic metal welding process to be constructed. The basic assumptions of the model are

1. By the action of the alternating tangential force the area of real contact between the weld members increases to the size of the total area to be welded during an initial period, which is short compared to the total welding period.

2. Local rupture or dispersion of the contaminant surface layer brings clean metal into contact at small spots (dimensions ~ 10 μm). These spots are welded by metallic adhesion (cold welding) and grow to oblong microwelds, a few hundreds μm long, by mutual deformation of the surfaces. This plastic deformation causes a further rupture of the surface layer and growth of the metallic adhesion area.
3. The number of microwelds developed per unit unwelded contact area is proportional to the total relative displacement of the contacting surfaces. The average area of the microwelds is independent of welding time and vibrational amplitude. The growth of a single microweld proceeds in a time interval, which is very short compared to the welding time.

From this model the strength of a weld, as a function of welding time and vibrational amplitude, can be derived. Agreement with the experimental results justifies the assumptions. The model also explains the oblong shape of microwelds.
The final conclusion is that thermal effects are not required to explain weld formation in ultrasonic metal welding. The weld is formed by metallic adhesion (cold welding) of clean metallic contacts.

SAMENVATTING

Het doel van het in dit proefschrift beschreven werk was te bepalen wat de fysische achtergrond voor de vorming van een verbinding in ultrasoon metaal lassen kon zijn.

Er werd een literatuuronderzoek gedaan, betreffende ultrasoon metaal lassen en verwante onderwerpen, zoals adhesie van metalen.

In het experimentele deel van het onderzoek werden proefstukken van Al, Cu, Ni en staal ultrasoon gelast.
De waarnemingen van de vorming en de groei van een ultrasone las kunnen als volgt worden samengevat:

1. De breekkracht van een las neemt als functie van de lastijd monotoon toe, tot verzadiging is bereikt.
2. De breekkracht van een las (gemeten met een schuif-trekproef) is evenredig met het gelaste oppervlak.
3. In ultrasone lassen wordt een tussenlaag plastisch vervormd. In de experimenten met plaatjes van 0.5 mm dik, varieert de dikte van deze tussenlaag tussen 30 en 100 μm (dit werd bepaald uit metallografische doorsneden).
4. Een ultrasone las bestaat uit een aantal microlassen. Dit zijn langwerpige lasgebieden, waarvan de lange as evenwijdig is met de trillingsrichting tijdens het lassen.
5. Gedurende de lastijd ontwikkelt zich een toenemend aantal microlassen.
6. De afmetingen van de microlassen zijn afhankelijk van de gesteldheid van het gelaste oppervlak, zoals ruwheid of de aanwezigheid van oliefilms.

De breeksterkte van de lassen τ_b werd vergeleken met een karakteristieke sterkte τ_n van het oorspronkelijke materiaal. De verhouding τ_b/τ_n is een maat voor de laskwaliteit en wordt gebruikt om de lasbaarheid van een materiaal te definieren. Proefstukken van aluminium, koper en nikkel bleken goed lasbaar te zijn; de τ_b/τ_n-waarden varieerden tussen de 0.7 en 0.9. Twee staalsoorten waren slecht lasbaar, hun τ_b/τ_n-waarde was 0.4. Het verschil in lasbaarheid zou verklaard kunnen worden door het verschil in "verwijderbaarheid" van oppervlakteverontreinigingen (oxyden, geadsorbeerd gas, vocht en smeermiddelen). Een eenduidig verband tussen lasbaarheid en materiaaleigenschappen, bijv. hardheid en ductiliteit, zoals in de literatuur wordt gesuggereerd, wordt niet gesteund door de verkregen resultaten.
Een methode om de amplitude van de wisselkracht die door de lastip op de proefstukken werd uitgeoefend, te bepalen, werd ontwikkeld. De grondslag van deze methode werd gevonden in de analyse van het ultrasoon trillend systeem. De amplitude van de wisselkracht bleek in de eerste tientallen milliseconden van de lasperiode toe te nemen tot tenminste 70% van zijn uiteindelijke waarde aan het einde van de lasperiode. De resulterende tangentiele spanningen in het gelaste tussenvlak waren zo groot dat plastische vervorming optrad. Uit deze experimenten bleek dat het reële contactoppervlak na enkele tientallen milliseconden

lassen vrijwel gelijk was aan het uiteindelijk gelaste oppervlak. Dit werd bevestigd door andere experimenten met verruwde plaatjes metaal die in contact worden gebracht met een glas-oppervlak; een ultrasone trilling gedurende enkele milliseconden was voldoende om een aanmerkelijke groei van het reële contactoppervlak te veroorzaken.

Het lassen van een aluminium lastip, rechtstreeks op een aluminium aambeeld, maakte het mogelijk de relatieve trillingsverplaatsing tussen de te lassen delen gedurende het lassen te bepalen. Verdere experimenten toonden aan dat het onderste proefstuk, dat op het aambeeld lag, gedurende het lassen vrijwel in rust was. Het verschil tussen de trillingsamplitude van de lastip en de relatieve trillingsverplaatsing in het lasvlak bleek evenredig te zijn met de dikte van het bovenste plaatje, dat tegen de lastip lag.

Er werd aangetoond, dat subsoon lassen mogelijk was, door toepassing van een aandrukkracht, een relatieve trillingsverplaatsing en een aantal wisselingen, die gelijk waren aan de overeenkomstige parameters bij het ultrasoon lassen. Het enige verschil was de trillingsfrequentie, die 30 Hz bedroeg bij het subsoon lassen en 20.000 Hz bij het ultrasoon lassen.

Er werd een vergelijking tussen de kenmerken van het subsone en het ultrasone lasproces en tussen de met deze processen geproduceerde lassen gemaakt, betreffende:
1. Sterkte van de lassen.
2. Het uiterlijk van het lasvlak; het bestaan van microlassen.
3. Doorsneden van lassen die een plastisch vervormde tussenlaag vertoonden.
4. Het gedrag van de wisselkracht gedurende de twee lasprocessen. De gemiddelde tangentiele spanningen in het lasvlak.
5. De energie-dissipatie per trilling.

Het ultrasoon en het subsoon lasproces bleken op al deze kenmerken zeer verwant te zijn. Hieruit werd geconcludeerd, dat het mechanisme van lasvorming hetzelfde is voor ultrasoon en subsoon lassen. Aangezien het uitgesloten is dat thermische verschijnselen een rol spelen in subsoon lassen, moet ook in ultrasoon lassen de lasvorming door mechanische oorzaken, die resulteren in metaal-adhesie van schoon contactopprvlak (koud lassen), veroorzaakt worden; de mechanische oorzaak is een wisselende kracht, die een plastische vervorming van de contactvlakken veroorzaakt. Er werd aangetoond, dat de flitstemperaturen gedurende deze vervorming enkele graden bedraagt.

Deze waarnemingen maakten het mogelijk om een model van het ultrasoon metaallassen te maken. De aan het model ten grondslag liggende veronderstellingen zijn:
1. Het reële contactoppervlak tussen de te lassen delen neemt, door toedoen van de wisselende tangentiele kracht, toe tot de afmetingen van het te lassen oppervlak, in een periode die kort is vergeleken met de totale lastijd.

2. Locale breuk of verspreiding van de oppervlakte-verontreinigingslaag veroorzaakt contact van schoon metaal in kleine gebieden (afmetingen ~ 10 μm). Deze gebieden lassen door metaal-adhesie en groeien, door wederzijdse deformatie van de contactvlakken, uit tot langwerpige microlassen die enkele honderden μm lang zijn. De vervorming veroorzaakt een voortgaande verbreking van de oppervlaktelagen en daarmee groei van het oppervlak waar metaal-adhesie plaats vindt.
3. Het aantal microlassen dat per eenheid ongelast contactoppervlak wordt gevormd is evenredig met de totale relatieve verplaatsing van de contactoppervlakken. De gemiddelde oppervlakte van de microlassen is onafhankelijk van de lastijd en de trillingsamplitude. De groei van een microlas vindt plaats in een tijdsinterval dat kort is in vergelijking met de totale lastijd.

Uit dit model kan de sterkte van een las, als functie van lastijd en trillingsamplitude, worden afgeleid. De gemaakte veronderstellingen worden gerechtvaardigd door de overeenstemming tussen de uit het model berekende sterkte en de experimenteel gevonden waarden. Het model verklaart tevens de langwerpige vorm van de microlassen. De eindconclusie is dat thermische verschijnselen voor de verklaring van de vorming van een las bij het ultrasoon metaallassen niet noodzakelijk zijn. De las wordt gevormd door adhesie van metaal (koud lassen) op schone contactvlakken.

APPENDICES

A1. Acoustic softening and diffusion under the influence of ultrasound

Acoustic or ultrasonic softening of metals has first been described by Blaha and Langenecker (A.1, 2, 3). They observed that the yield stress of single crystals of Zn, Al and Cd dropped appreciably during irradiation of the specimen by ultrasonic energy; the power intensity being about 2 W/cm^2. Langenecker extended the field of observations to polycrystalline specimens (Al, Be, Ti and steel SAE 1019) (A.4, 5, 6). The stress-strain curve of these materials was determined during irradiation of the samples with ultrasound (power intensity $< 100\ W/cm^2$). The curves measured under irradiation all fell below the normal stress-strain curve. At power intensities between 35 and 100 W/cm^2 the different materials came into a "zero-stress" situation, which means that the static tensile stress, required to deform the specimen, was very small compared with the yield stress of the material without irradiation.
Langenecker points out that the acoustic stresses introduced by ultrasonic irradiation are much smaller than the stress reduction obtained by applying ultrasound. He explains the phenomenon (called acoustic softening) by the hypothesis that ultrasonic energy is preferentially absorbed at dislocations. The dislocations, "activated" by the absorbed energy, can break away from their pinned positions and move through the crystal, thus facilitating plastic deformation. Langenecker estimated the acoustic stresses in the specimen by considering a travelling wave. He did not consider the possibility of a resonant build up of stresses (by which a multiple of the estimated stress value can be reached). His explanation is seriously doubted, by a number of investigators.

Nevill and Botzen (A.7) made observations similar to those of Langenecker. They put forward the hypothesis of superposition of stresses, which means that the real yield stress is reached by adding the static tensile stress and the dynamic (acoustic) stress. They were able to account for their observations by this hypothesis. According to this theory yielding occurs only when the sum of static and dynamic stress exceeds the yield limit.
Further experiments have been carried out by Baker and Carpenter (A.8). They found that the stress reduction by ultrasonic irradiation is always smaller than the dynamic stress amplitude.
Friedrich c.s. (A.9, 10) showed that the reduction in yield stress (caused by ultrasound) was slightly smaller than the applied dynamic stress. They were able to account for this small difference by considering the non-linear relation between yield stress and strain rate. Using this correction the superposition hypothesis explained their observations very well.
Observations of Russian authors (A.11, 12) also agree with the superposition hypothesis. Pohlman and Lehfelt (A.13) explained the reduction of the drawing force in a wire drawing process by superposition of static and dynamic stresses.

Investigators working at the University of Aston in Birmingham could account for the values of stress reduction by ultrasound in a number of metal deformation processes using the superposition principle (A.14, 15).

Acoustic softening as proposed by Langenecker could not be verified by any of the investigators previously mentioned. (Nevertheless it is still advocated by Langenecker (A.16).) Hence the explanation of the ultrasonic metal welding mechanism based on acoustic softening as given by Joshi and Harman (see section 2.5.2) is most unprobable*).

Russian authors (A.17, 18, 19) have introduced the idea of enchanced diffusion to explain joint formation in ultrasonic welding. Experiments concerning the enhancement of diffusion under conditions similar to the high strains and stresses in an ultrasonic weld zone, have not been described in the literererature. The only information on diffusion under the influence of ultrasound follows from experiments where the acoustic stresses are far below the yield stress of the material. Kulemin and Miskevich (A.20) studied diffusion of Cu-Zn, Cu-Al and Fe-Zn. They found that the diffusion coefficient can be enhanced by a factor of 6 under the influence of acoustic irradiation of the specimen.
Similar experiments by Walker et al (A.22) for the diffusion of C and Zn into Ni, did not show a significant change of the diffusion coefficient under the influence of ultrasound. Neither could Attia and Shyne (A.21) detect enhanced diffusion of Zn in their experiments with brass-copper couples. An older review article by Ramshkin (A.23) names 8 authors who report an enchancement of diffusion and 5 studies in which no influence of ultrasound on diffusion could be detected.

As the experimental results are contradictory, the question of the existence of enhancement of diffusion by ultrasonic irradiation is still open to discussion. It is impossible to conclude from the literature whether this phenomenon could be important in ultrasonic welding or not.

---

*) In ultrasonic welding of metals power intensities of 10 to 100 W/mm^2 (10^3 to 10^4 W/cm^2) are normally used. This is 10 to 100 times higher than the intensities reported by Langenecker. In the contact plane between sonotrode and specimen exist acoustic stresses having values in the order of the yield stress of the material. In the case of acoustic softening of the material, one would expect the sonotrode to sink into the sheets to be welded, until the power intensity is reduced (by the growing contact area) to values as mentioned by Langenecker. This, however, does not happen.

A2. Relation between adhesion and physical or chemical properties of metals

Several workers have tried to correlate adhesion properties of metals with the physical or chemical properties of the material. In this appendix we will review literature on this subject.

In order to study the adhesion properties of similar metal couples Sikorski c.s. uses the twist-compression method (A.24, 25, 26, 27, 28). This method can be summarized as follows (A.24)

1. The flat endfaces of a rod and a tube of the material are pressed together. The axes of the two specimens coincide. The clamping force is F_n.
2. One of the specimens is fixed, the other one is rotated 180° around the cylinder axis with the endfaces remain in contact. By this relative movement of the surface the real area of contact is enlarged and contaminating layers are ruptured and dispersed. Consequently adhesion junctions can develop.
3. The two specimens are pulled apart and the adhesion force F_a is measured. The coefficient of adhesion, defined as F_a/F_n, is then calculated.

Altough the values of the coefficient of adhesion show a considerable scatter from test to test, the median coefficient of adhesion, over a number of 99 tests, was found to be reproducible for a specified material. Hence the median coefficient of adhesion is used to characterize the adhesion properties of a metal (A.26).

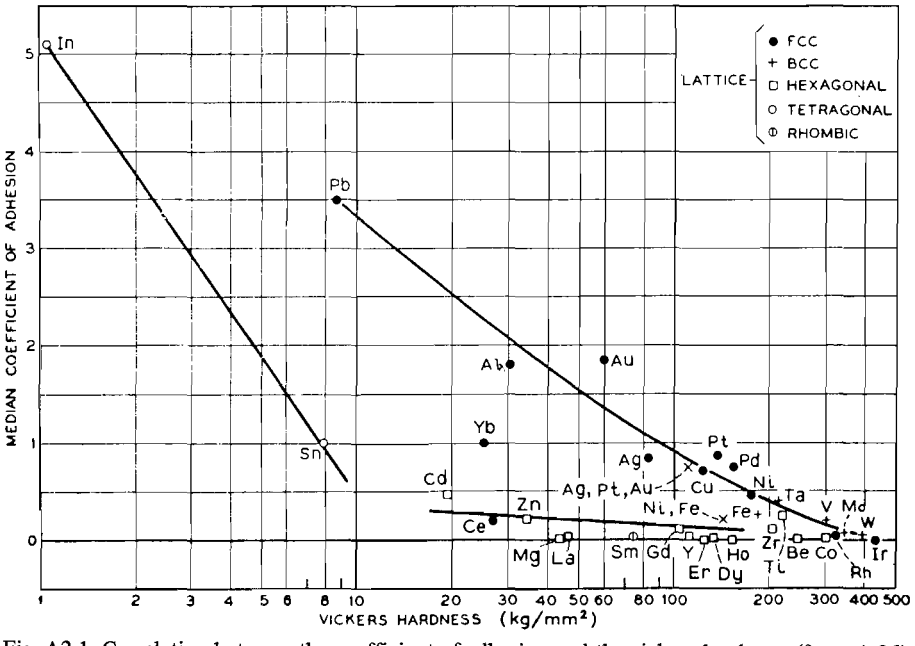

Fig. A2.1. Correlation between the coefficient of adhesion and the vickers hardness. (from A.26)

Fig. A2.1 (from Sikorski (A.26)) summarizes the results of the experiments. The median coefficient of adhesion for a large number of materials has been plotted versus hardness. Sikorsky concludes from these data

1. The higher the hardness of the metal the lower the coefficient of adhesion (this remains valid when modulus of elasticity, surface energy or recrystallization temperature is substituted for hardness).
2. There is a marked difference between metals with a cubic lattice (FCC and BCC) and metals with a hexagonal lattice: the cubic metals show a higher adhesion than the hexagonal metals. Experiments by Buckley (A.29) and Noskovskii (A.30) affirm this conclusion.

A quantitative relation between the coefficient of adhesion and one of the properties mentioned in the first conclusion could not be given *).

Rabinowicz has made an effort to correlate the physico-chemical properties with adhesion-frictional properties and wear of metals (A.31, 32, 33, 34, 35). First the concept energy of adhesion is introduced (A.31). This is the energy which must be applied to separate a unit area of the interface between materials a and b, involving the need to create two surfaces with surface energy γ_a and γ_b respectively, but destroying an interface which had interfacial energy γ_{ab}. Hence

$$W_{ab} = \gamma_a + \gamma_b - \gamma_{ab}$$

For the surface energy of a metal γ_a, the value at the melting point has been chosen **). To account for the variation of the area of real contact with the applied load the hardness p of the metal is used. For dissimilar metal couples p equals the hardness of the softest metal. The quantity W_{ab}/p is used to characterize the physico-chemical properties of the metal contact (A.31, 32, 33).

Rabinowicz has tried to correlate the quantity W_{ab}/p with adhesion and friction properties of metals (A.34). He also tried to find a relation between compatibility (characterized by the mutual solubility of the contacting metals) and adhesion (A.35). The result of these investigations is, that faint general tendencies seem to

---

*) The experiments of Sikorski show a close relationship with ultrasonic welding. A notable difference is that in ultrasonic welding the relative displacement of the sufaces is alternating. Tentatively we can say that a metal with a high median coefficient of adhesion in those experiments has probably a good ultrasonic weldability.

**) This leads to the criticism that adhesion, friction and wear interactions take place at considerably lower temperatures than the melting temperature.

exist; e.g. the higher the degree of compatibility, the higher the coefficient of friction. A calculation of the coefficient of adhesion or the friction coefficent based on the quantity W_{ab}/p could not be made.

This summary from the literature shows that, up to now, no quantitive relationship between the adhesion of a metal and its physical or chemical properties was found; only some general tendencies could be given.

A3. Numerical data for calculation of the alternating force

In order to calculate the real and imaginary part of the load impedance $\bar{Z}_{m1}$ using eqs. (3.28) and (3.29) certain data are required. These are given below.

1. *The electromechanical transformer ration N.*
   This quantity is obtained by measuring the current i through the transducer and the vibrational amplitude ξ at the end face of the transducer. From ξ the velocity v_s (see 3.7) can be calculated. Equation (3.23a) then yields the value of $N = 2.4$ As/m.

2. *The mechanical transformer ratio* M^2.
   This value is calculated using $M = \frac{A_2}{A_1}$, eq. (3.18), where $A_1 = \frac{\pi}{4} D_1^2$ and $A_2 = \frac{\pi}{4} D_2^2$. Hence $M = (\frac{D_2}{D_1})^2$. $D_1 = 22{,}5$ mm; $D_2 = 50.0$ mm (see fig. 3.1).
   Hence $M^2 = 24.3$.

3. *The weighted sum of characteristic impedances B.*
   With $\rho c = 2.17 \times 10^7$ kg m^{-2} s^{-1}; $A_4 \rho c = A_3 \rho c = A_2 \rho c = (A\rho c)_t = 4.25 \times 10^4$ kg s^{-1}; $A_1 \rho c = 8.64 \times 10^3$ kg s^{-1} we obtain using eq (3.21) $B = 33.83 \times 10^4$ kg s^{-1}.
   Next we can substitute these values in eq. (3.29) to obtain $X_{m1} = -1.35\ \Delta\nu_r$.

A4. Estimate of the inertial forces acting on the workpiece contacting the welding tip

It is estimated that only a part of the workpiece in contact with the welding tip (upper workpiece) participates in the vibrational movement. Experiments with both larger and smaller sheets (down to a length of 20 mm) showed that the weld strength was not influenced by the size of the specimens *). Hence we estimate

---

*) Provided that the resonant frequency of the specimens was not close to the ultrasonic vibrational frequency.

that of the strip specimens used in the present experiments (see sec. 4.1) only a part of a 10 mm x 10 mm area particpates in the vibration. This part is called the vibrating mass of the upper specimen. The average vibrational amplitude of the vibrating mass is estimated to be 10 μm.

The inertial force acting on the vibrating mass can be calculated. When welding Al (thickness 0.5 mm: specific gravity 2.7×10^3 kg/m^3) the vibrating mass is 0.14×10^{-3} kg, the vibrational frequency is 2×10^4 Hz, hence the maximum acceleration during the vibrational movement is $(2\pi \times 2 \times 10^4)^2 \times 10^{-5} = 1.6 \times 10^5$ m/sec^2. The inertial force therefore equals 0.14×10^{-3} kg x 1.6×10^5 m/sec^2 = 22 N. This value is small compared to the alternating force F_W exerted by the welding tip, 300-400 N (see table 4.8), therefore the inertial force can be neglected.

A5. Calculation of the energy dissipation in subsonic and ultrasonic welding

Consider the welded interface of two aluminium specimens (medium hard) at the end of the subsonic welding period. During the last oscillations the interfacial layer (estimated thickness for medium hard Al is 30 μm) is deformed plastically. Fig. A5.1 is schematic section through the welding zone, perpendicular to the plane

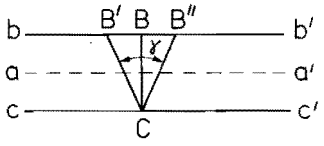

Fig. A5.1. Section through the welding zone, perpendicular to the plane of contact a a'; b b' and c c' are the boundaries of the plastic deformation zone.

of contact. The interfacial layer is situated between the planes bb' and cc', the original contact plane is aa'. Consider point C to be fixed and point B as oscillating between B' and B", thus representing the shear deformation of the interfacial layer. In the present subsonic welding experiments the distance B'B" was estimated as 5 μm, shown by the length of the horizontal parts in the force-parth diagram of fig. 5.3e. Hence the shear angel γ of the interfacial layer amounts to 0.17 radians ($\mathrm{tg}\,\gamma$ = B'B"/CB).

Having estimated the shear angle γ and the thickness of the interfacial layer, we can calculate the energy E, dissipated per unit volume of deformed material per oscillation. The energy dissipation per unit volume, when the effective strain $\bar{\delta}$ increases from 0 to δ equals (4.3)

$$U = \int_0^{\delta} \bar{\sigma}\, d\bar{\delta} \qquad (A.1)$$

The relation, between the effective stress $\bar{\sigma}$ and the effective strain $\bar{\delta}$, is

$$\bar{\sigma} = C\bar{\delta}^m \tag{A.2}$$

where C is a constant, equal to the effective stress when $\bar{\delta} = 1$, and m is the work hardening exponent (see Kobyashi (4.3)). Substitution of eq. (A.2) in eq. (A.1) and integration yields

$$U = \frac{C}{m+1}\delta^{m+1} \tag{A.3}$$

The effective deformation for shearing over a shear angle γ is (A.37)

$$\bar{\delta} = \frac{tg\gamma}{\sqrt{3}} \tag{A.4}$$

Hence the energy dissipation E is found by substitution of eq (A.4) into eq (A.3)

$$E = 2\frac{C}{m+1}\left(\frac{tg\gamma}{\sqrt{3}}\right)^{m+1} \tag{A.5}$$

The factor 2 is included, because deformation over the angle γ occurs twice during one oscillation. Using the data from table 4.2 i.e. $C = 200 \times 10^6$ N/m^2 and $m = 0.3$, together with the estimated value of $\gamma = 0.17$ the following value is obtained for medium hard Al

$E = 1.5 \times 10^7$ J/m^3.

As the estimated thickness of the deformed layer is 30 μm, one mm^2 of welded interface is equivalent to a deformed volume of 3×10^{-11} m^3. Hence the energy dissipated per oscillation per mm^2 welded area in subsonic welding of medium hard Al is $1.5 \times 10^7 \times 3 \times 10^{-11} = 0.45 \times 10^{-3}$ J.

Another estimate to be made is the energy dissipation per oscillation per mm^2 welded area in ultrasonic welding of medium hard Al. In sec. 5.1 it is estimated that the subsonic welding parameters are comparable to the ultrasonic welding parameters represented by point A in fig. 4.1. As there are no measurements for this point A, the energy dissipation mentioned above for the lowest curve of fig. 4.1 will be calculated. In this situation the power P_e delivered by the amplifier is 90 W (see table 4.3) and the electrical resistance R_e (see sec. 3.2.3.3), in which P_e is dissipated, is 500 Ω.
From eq. (3.27)

$$R_e = R_{e1} + R_{et} + R_{ew}$$

R_e is a series connection of
1. The electrical resistance of the vibrating system $R_{et} + R_{ew} = 80\ \Omega$.

2. The electrical resistance equivalent R_{el} of the mechanical load at the welding tip (the load if formed by the workpieces to be welded); $R_{el} = 420\ \Omega$.

Consequently the power dissipated in the load is $(R_{el}/R_e)\ P_e = 76$ W. In this case the average welded area is 7 mm^2, the power dissipation per mm^2 is 11 W/mm^2 and the vibrational frequency is 20 kHz. Therefore the energy dissipation in ultrasonic welding of medium hard Al is 0.55×10^{-3} J per oscillation per mm^2 welded area under conditions comparable to the subsonic experiments.

A6. Temperature in the welding zone

In this appendix consideration will be given to the temperature in the welding zone of an ultrasonic weld. In the first part, an expression for temperature rise, caused by a plane, circular and uniform heat source in an infinite medium, will be derived. Temperature rise will be expressed as a function of intensity of the heat source, time, heat capacity and conductivity of the medium. Next, the magnitude of temperature flashes during ultrasonic and subsonic welding will be estimated. In the final part an estimate of the temperature rise in the ultrasonic welding zone will be made, assuming a uniform heat generation in the whole contact area during welding.

A6.1. Temperature rise caused by a plane circular heat source in an infinite medium

The equation describing the temperature distribution as a function of time in a medium with no internal heat sources distributed over the volume present, is Fourier's equation

$$\alpha \Delta T - \frac{\partial T}{\partial t} = 0 \tag{A.7}$$

where $\alpha = \frac{\lambda}{c}$; λ is the thermal conductivity and c is thermal capacity per unit volume; Δ is the Laplace operator.

A special solution of eq. (A.7) for an instantaneous point source, situated at position (x, y, z) in an infinite medium, supplying an amount of heat dH at time t = o, is

$$dT\,(x', y', z') = \frac{dH}{c\,(4\pi\alpha t)^{3/2}} \exp.\left(-\frac{|\bar{r}' - \bar{r}|^2}{4\alpha t}\right) \tag{A.8}$$

where dT (x', y', z') is the temperature rise in point (x', y', z') due to the heat dH, $\bar{r}$ is the radius vector of the point (x, y, z) and $\bar{r}'$ is the vector of the point (x', y', z') (see (A.38)). We assume that in ultrasonic welding the heat source is coincident with the original circular contact area A, with radius R and having its centre at the origin

of a coordinate system. We assume the original contact plane to be the plane z = o and the intensity W of the heat source to be uniform. The quantity W is the heat generated per unit area in unit time. Hence we can imagine the entire heat source to consist of instantaneous sources having strength dH = W dA dt; where dA is an infinitesimal element of the area A and dt is an infinitesimal element of the time t. The medium is assumed to be infinite.

When the heat source is active from time t = o to t = t_e the temperature rise in a point (x', y', z') can be obtained by integrating eq. (A.8) over the area A and over the time interval o to t_e. Hence

$$T(x',y',z',t_e) = \iint_A \int_0^{t_e} dT = \frac{W}{c\,(4\pi\alpha)^{3/2}} \iint_A dA \int_0^{t_e} t^{-3/2} \exp.\left(-\frac{|\bar{r}' - \bar{r}|^2}{4\alpha t}\right) dt \qquad (A.9)$$

We will limit the calculations to points situated on the line (x = o, y = o, z = z'). This is the line perpendicular to the contact plane in the centre of the heat source area A. Thus $|\bar{r}'| = z'$. Further more the circular heat source area is devided into concentric rings with thickness dr and area dA, as shown in fig. A6.1. Thus dA = 2 π r dr. Integration over the area A then reduces to integration over the radius r

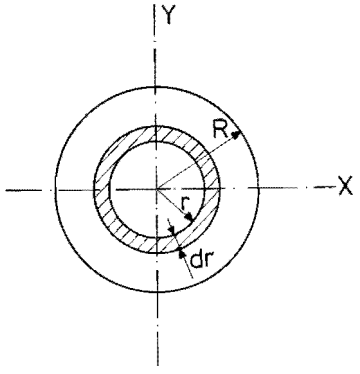

Fig. A6.1. Circular heat source, radius R.

(from 0 to R). Thus eq..(A.9) can be rewritten

$$T(o, o, z', t_e) = \frac{W}{4c\alpha^{3/2}\pi^{1/2}} \int_0^{t_e} t^{-3/2}\, dt \int_0^{R} r \exp.\left(-\frac{|\bar{r}' - \bar{r}|^2}{4\alpha t}\right) dr \qquad (A.10)$$

As $|\bar{r}'| = |z'|$ and $|\bar{r}| = r$, we obtain $|\bar{r}' - \bar{r}|^2 = z'^2 + r^2$. (See fig. A6.2). Equation (A.10) then becomes

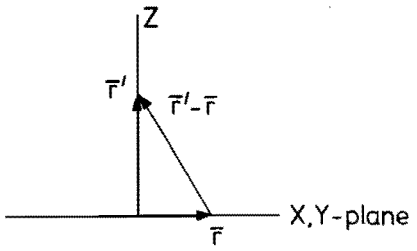

Fig. A6.2. Radius vectors, defined in the text.

$$T(o, o, z', t_e) = \frac{W}{4c\alpha^{3/2}\pi^{1/2}} \int_o^{t_e} t^{-3/2} \exp.\left(-\frac{z'^2}{4\alpha t}\right)dt \int_o^{R} r \exp.\left(-\frac{r^2}{4\alpha t}\right)dr \quad (A.11)$$

Integration over the radius r yields

$$\int_o^{R} r \exp.\left(-\frac{r^2}{4\alpha t}\right)dr = -2\alpha t\left(\exp.\left(-\frac{R^2}{4\alpha t}\right)-1\right) \quad (A.12)$$

Substituting eq. (A.12) in eq. (A.11) we obtain

$$T(o, o, z', t_e) = \frac{W}{2c\alpha^{1/2}\pi^{1/2}}\left[\int_o^{t_e} t^{-1/2} \exp.\left(-\frac{z'^2}{4\alpha t}\right)dt - \int_o^{t_e} t^{-1/2} \exp.\left(-\frac{z'^2+R^2}{4\alpha t}\right)dt\right] \quad (A.13)$$

By partial integration this becomes

$$T(o, o, z', t_e) = \frac{W\, t_e^{1/2}}{(\lambda c\pi)^{1/2}}\left[\exp.\left(-\beta^2\right) + \beta\pi^{1/2}\left\{F(\beta)-1\right\} - \exp.\left(-\beta'^2\right) - \beta'\pi^{1/2}\left\{F(\beta')-1\right\}\right] = \frac{W\, t_e^{1/2}}{(\lambda c\pi)^{1/2}}\,\Phi(z') \quad (A.14)$$

with $\beta = \frac{|z'|}{2\alpha^{1/2}t_e^{1/2}}$, $\beta' = \frac{(z'^2+R^2)^{1/2}}{2\alpha^{1/2}t_e^{1/2}}$ and

$$F(\beta) = \frac{2}{\sqrt{\pi}} \int_o^{\beta} \exp.\left(-x^2\right) d\,x.$$

Equation (A.14) expresses the temperature rise, on a line through the centre of a circular heat source and perpendicular to the plane of the source, as a function of the duration t_e of the heat pulse.

A6.2. Temperature flashes in subsonic and ultrasonic welding

Temperature flashes occur in the contact area of asperities, due to energy dissipation by mutual plastic deformation when the contacting surfaces undergo relative sliding. The mutual deformation is assumed to cause the existence of a plane circular heat source. The radius of heat source R is estimated to be 5 μm, being a typical value for an asperity contact (A.31). The intensity W is estimated using the stress required for plastic deformation τ_n, the relative displacement of the contacting asperities s and the time required to deform the asperity t_1. The relative displacement s is estimated to be equal to the diameter of the asperity contact i.e. 10 μm. The maximum sliding velocity of the surfaces is 0.9 x 10^{-3} m/s in the present welding experiments and 1.5 m/sec. in the ultrasonic welding experiments *). Hence, the time t_1 during which the asperity deformation occurs is about 10^{-2} s in subsonic welding and 7 x 10^{-6} s. in ultrasonic welding. As a measure of the stress at an asperity contact during plastic deformation τ_n is used as defined in sec. 4.2.1.4. The intensity of the heat source can be found from

$$W = \frac{\tau_n \, s}{t_1} \tag{A.15}$$

The resulting values of W are noted in table A6.1.

The maximum temperature rise ΔT in the centre of the contact plane can be calculated using eq. (A.14), with $z' = 0$ and $t_e = t_1$

$$\Delta T = \frac{W \, t_1^{1/2}}{(\lambda c \pi)^{1/2}} \left[\exp.\left(-\beta'^2\right) - 1 - \beta' \, \pi^{1/2} \left\{ F(\beta') - 1 \right\} \right] \tag{A.16}$$

$$\text{with } \beta' = \frac{R}{2\alpha^{1/2} \, t_1^{1/2}}$$

Using the appropriate values of λ and c as given in table A6.1, β' and ΔT can be calculated. The values of ΔT are listed in table A6.1. From these results it appears that in ultrasonic welding the temperature rise ΔT in an asperity contact during

---

*) In subsonic welding the relative displacement amplitude ξ_s is 5 μm. The frequency ν is 30 Hz. Hence the maximum relative velocity is $2\pi\nu \, \xi_s$ = 0,9 x 10^{-3} m/s. In ultrasonic welding ξ_s = 12 μm and ν = 20.000 Hz; hence the maximum relative velocity is 1.5 m/sec.

TABLE A6-1
The magnitude ΔT of temperature flashes in ultrasonic and subsonic welding according to eq. (A.16).

Ultrasonic welding Material	Material stress τ_n *) (N/m^2)	Heat source intensity W **) (W/m^2)	Thermal conductivity λ (W/m °C)	Thermal capacity c (J/m^3 °C)	β'	Calculated temperature rise ΔT (°C)
Al (medium hard)	$80x10^6$	$1.1x10^8$	210	$2.48x10^6$	0.103	1
Al (hard)	$170x10^6$	$2.4x10^8$	168	$2.48x10^6$	0.115	3
Cu	$170x10^6$	$2.4x10^8$	369	$3.40x10^6$	0.091	1
Ni	$440x10^6$	$6.3x10^8$	84	$4.07x10^6$	0.208	12
Subsonic welding Material						
Al	$80x10^6$	$8.1x10^4$	210	$2.48x10^6$	$2.7x10^{-3}$	$6x10^{-4}$

*) according to table 4.2.
**) according to eq. (A.15).

mutual deformation, due to relative sliding of the asperities, in short the temperature flash, is only a few degrees centigrade. In subsonic welding this temperature flash is of the order of 10^{-3} degrees, because the relative sliding velocity is much lower. We conclude that the temperature during the flashes occurs well below the values where melting or recrystallization can be expected.

A6.3. Estimate of the temperature rise in the welding zone during ultrasonic welding

The temperature in the centre of an ultrasonic welding zone can be calculated from the following thermal model: a plane circular heat source, with uniform intensity W, and radius R is situated in the welding area. The source is active during the welding time t. The sheets to be welded have a thickness b and are assumed to be infinite. It is assumed that no heat flows through the surfaces of the sheets, except in the welding area, where the heat source is present. Heat conduction to the anvil and welding tip is neglected. This situation is shown in fig. A6.3a. The mathematical boundary conditions of this problem are indicated in fig. A6.3b. In order to

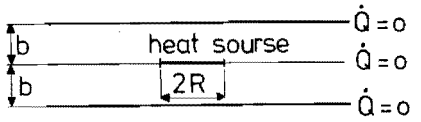

Fig.A6.3a. Thermal model of ultrasonic welding. The circular heat source (radius R; intensity W) is situated in the weld zone between two infinite sheets.

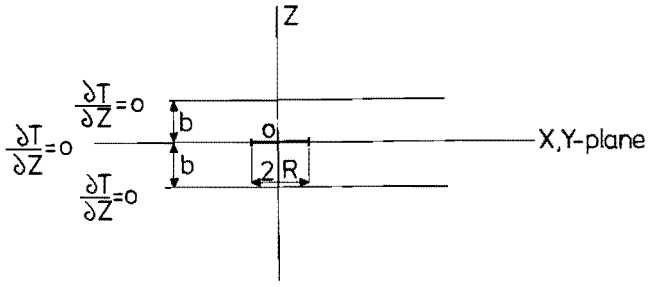

Fig. A6.3b. Mathematical boundary conditions of the arrangement in fig. A6.3a. At the heat source $\left|\frac{\partial T}{\partial z}\right| = \frac{W}{\lambda}$.

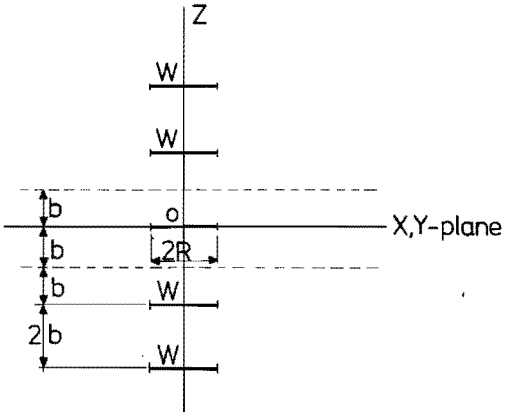

Fig. A6.3c. An infinite series of fictitious heat sources (radius R, intensity W) in an infinite medium. This arrangement satisfies the boundary conditions of fig. A6.3b.

calculate the temperature field as a function of time, the method of fictitious sources is used, see e.g.(A.36) (A.38). According to this method a solution of Fourier's equation (A.7) for specified boundary conditions is the temperature field of a number of (fictitious) point, line or plane sources in an infinite medium. These sources should be arranged in such a way that the boundary conditions of the problem are satisfied. For the present problem an infinite series of plane

circular heat sources (intensity W, radius R) as drawn in fig. A6.3c satisfies the boundary condtions, as seen from the symmetry of the arrangement of sources. The temperature rise in the centre of the welding zone T_c is the sum of temperature rises caused by each member of the series of sources. As the temperature rise on the axis of a single source is determined in sec. A6.1 the calculation of T_c implies a summation of a series of expressions of the type of eq. (A.14).

$$T_c = \frac{W\, t^{1/2}}{(\lambda c \pi)^{1/2}} \sum_{n=-\infty}^{n=+\infty} \Phi\,(z' = 2\,nb). \qquad (A.17)$$

Depending on the convergence of the sum in eq. (A.17), a number of 10 to 30 terms on both sides of the central term (n = o) of the series, was taken into account, to obtain an approximation of the sum, with an accuracy better than 5%.

TABLE A6-2
Temperature rise T_c in the centre of the ultrasonic welding zone, according to eq. (A.17).

Material	Welding time t (ms)	$\frac{W\,t^{1/2}}{(\lambda\, c\, \pi)^{1/2}}$ *) (° C)	$\sum_{n=-\infty}^{n=+\infty} \Phi\,(z' = 2nb)$ **)	Temperature rise T_c (° C)
Al (medium hard)	60	273	1.39	380
Al (hard)	200	556	1.07	590
Cu	1000	717	0.59	420
Ni	1000	1371	0.71	970

*) Using $R = 1.5 \times 10^{-3}$ m; $W = 45 \times 10^6$ W/m^2; λ and c according to values in table A6-1.
**) Accuracy better than 5%; $b = 0{,}5 \times 10^{-3}$ m.

Results of the calculations of T_c are listed in table A6.2. In order to determine W, we assumed all acoustic energy to be dissipated in the contact area of the weld members. As the final welded area in the present experiments varied from 6 to 7 mm^2 (see sec. 6.2.1), a radius of the welds of R = 1.5 mm is used in the calculation of T_c. The electric power P_e, required for making such a weld, is assumed to be nominal power of the generator, i.e. P_e = 400 W. The acoustic power, dissipated in the welding zone, equals $(R_{el}/R_e)\, P_e$ (see appendix A5). Using $R_{el} = 420\ \Omega$

and $R_e = 500\ \Omega$ the intensity of the plane heat source is $W = 45 \times 10^6\ W/m^2$. The calculated temperature rise T_c is listed in the last column of table A6.2 *).

From the results it is concluded that the estimated maximum temperatures are well below the melting temperature of the materials. From experiments with ultrasonic welds in medium hard Al we know that heating at 400°C for 30 minutes did not cause any observable recrystallization (optical microscopy) in the welding zone. Hence the estimated temperature rise is certainly below the recrystallization temp. for medium hard Al. For welds in Cu no recrystallization was detected after heating at 400°C for 30 minutes. Taking into account the short duration of ultrasonic welding ($\leqslant$ 1 sec.) the estimated temperature makes recrystallization during welding of Cu unlikely. For hard Al and Ni the estimated temperatures are above the recrystallization temperature.

---

*) From the detailed calculation of T_c it appears that the temperature rise at a distance of 100 μm from the welded interface ranges from 0.9 T_c to 0.95 T_c. This implies that metallurgical changes, if any, caused by the temperature rise will occur in the entire deformed interfacial zone of an ultrasonic weld.

REFERENCES

(1.1) E.A. Neppiras, Ultrasonics 3, 128-135, 1965
(1.2) A. Coucoulas, Transactions of the Metallurgical Society of AIME 236, 587-589, 1966
(1.3) R. Stemmer, Metallwissenschaft und Technik 22, 1103-1108, 1968
(1.4) A.P. Hulst, Ultrasonics 10, 252-261, 1972;
A.P. Hulst, Proceedings of Ultrasonics International 1973, I.P.C. Guildford 1973.
(1.5) F.R. Meyer, Assembly Engineering, 20-26, March 1968
(1.6) Welding Handbook, sec. 3B, 6th edition, American Welding Society, 1971
(1.7) S.E. Jacke, Proceedings Ultrasonics Symposium 1970, IEEE, New York, 1971
(1.8) G. Maronna, W. Scheel, Schweisstechnik 20, Heft 8, 386-390, 1970
(1.9) G.G. Harman (ed.), Microelectronic Ultrasonic Bonding, Nat. Bureau of Standards, Special Publication no. 400-2, Washington 1974
(1.10) A. Behr, The Metal Industry, 422, Dec. 1943.
(1.11) Siemens-Halske, Patent May/August 1938.
(1.12) H.O. Willrich, Welding 61-66, Febr. 1950.
(1.13) S.W. Neville, British Welding Journal 8, 177-187, 1961
(1.14) J.B. Jones, C.F. de Prisco, F.R. Meyer, Aero projects Inc. Research Report No. 53/77, November 1953.
(1.15) P.L. Hurricks, Wear 15, 389-409, 1970.
(2.1) W.C. Potthoff, Welding Journal 39, 131-138, 1960
(2.2) P. Drews, Schweissen und Schneiden 22, Heft 2, 66-69, 1970.
(2.3) D. Leven, Schweissen und Scheiden 24, Heft 12, 494-497, 1972.
(2.4) R. Pohlman, D. Leven, Schweissen und Schneiden 25, Heft 3, 81-83, 1973.
(2.5) Welding Handbook, American Welding Society, 6th edition, part 3B, London, 1971.
(2.6) N.A. Ol'shanskii, Automatic Welding, 14, nr. 3, 1-8, 1961.
(2.7) L.L. Silin, V.A. Kuznetsov, M.A. El'yaskev, Welding Production, nr. 7, 8-14, 1960.
(2.8) J. Kozianski, Welding Journal 40, 349-358, 1961.
(2.9) C.L. Estes, P.W. Turner, Welding Journal (Research Supplement) 53, 359S-369S, 1973.
(2.10) J.B. Jones, N. Maropis, J.G. Thomas, D. Bancroft, Welding Journal 40, 289S-305S, 1961.
(2.11) B.B. Zolotarev, D. Volkov, U.I. Domaskin, Welding Production no. 9, 65-73, 1962.
(2.12) N.E. Weare, R.E. Monroe, Welding Journal (Research Supplement) 40, 351S-358S, 1961.
(2.13) H.C. Daniels, Ultrasonics 3, 190-196, 1965.
(2.14) T.H. Hazlett, S.M. Ambekar, Welding Journal (Research Supplement) 49, 196S-200S, 1970.
(2.15) H.T. Genscoy, J.A. Adams, Shigeo Shin, Welding Journal (Research Supplement) 46, 145S-153S, 1967.

(2.16) L.L. Silin, V.A. Kuznetsov, G.V. Sysolin, Welding Production no. 3, 19-25, 1960.
(2.17) K.C. Joshi, Welding Journal 50, 840-848, 1971.
(2.18) S.B. Ainbinder, E.K. Tikhomirova, Welding Production no. 9, 34-37, 1962.
(2.19) M. Okada, S. Shin, M. Miyagi, H. Matsuda, Trans. of the Japan Institute of Metal 4, 250-256, 1963.
(2.20) R. Stemmer, Thesis T.H. Aachen, 1971.
(2.21) S.K. Ginzburg, A.M. Miskevich, Yu.G. Nosov, Welding Production no. 5, 83-87, 1967.
(2.22) W. Beyer, Schweisstechnik 19, Heft 1, 16-20, 1969;
W. Beyer, Schweisstechnik 19, Heft 2, 72-75, 1969.
(2.23) J.B. Jones, N. Maropis, J.G. Thomas, D. Bancroft, Fundamentals of Ultrasonic Welding; Aero projects Inc., Research Report, Phase I, RR-59-105, May 1959; Phase II, RR-60-91, Dec. 1960.
(2.24) H. Czichos, K. Kaffanke, VDI-Zeitschrift 112, 1491-1495, 1970; VDI-Zeitschrift 112, 1643-1645, 1970.
(2.25) G.F. Balandin, L.L. Silin, Izvesta AN SSSR, OTN "Metallurgy and fuel" no. 6, p. 42-52, 1960.
(2.26) G.F. Balandin, L.L. Silin, Welding Production no. 12, 1-9, 1961.
(2.27) W. Dippe, Schweisstechnik 20, Heft 3, 108-110, 1970.
(2.28) Yu.V. Kholpov, Automatic Welding 14, no. 6, 20-22, 1971.
(2.29) J.W. Bello, R.W.B. Stephens, British acoustical society; Spring meeting 1972, 5-7 April 1972.
(2.30) M. Beckert, W. Dippe, Schweisstecnik 21, Heft 8, 354-356, 1971.
(2.31) H.D. Wendler, Schweisstechnik 23, Heft 8, 362-364, 1973.
(2.32) B.E. Noltingk, Welding and Metal Fabrication, 260-266, 1960.
(2.33) J.N. Antonovich, IRE Nat. Conv. Rec. Vol. 7, part 6, 204-212, 1959.
(2.34) N.E. Weare, J.N. Antonovich, R.E. Monroe, Welding Journal (Research Supplement) 39, 331S-341S, 1960.
(2.35) G.G. Harman, K.O. Leedy, Proc. of the 10th Conference on Reliability Physics, p. 49-55, Las Vegas, 1972.
(2.36) K.I. Johnson, The Welding Institute Research Bulletin 11, no. 11, 309-313, 1970.
(2.37) W. Lehfelt, Feinwerktechnik 66, Heft 1, 10, 1962.
(2.38) M.V. Bruk, Automatic Welding 15, no. 3, 44-47, 1962.
(2.39) N.A. Cantelajos, G. Cusminsky, Journal of the Inst. of Metals 100, 20-23, 1972
(2.40) A.S. Pranch, Automatic Welding 24, no. 8, 65-68, 1971.
(2.41) J. Frisch, U. Chang, Optimal Strength of Ultrasonically Welded Metals in Vacuum, Final Report No. MD-70-2, University of California, Berkely.
(2.42) U.I. Chang, J. Frisch, Welding Journal (Research Supplement) 53, 24S-35S, 1974.
(2.43) E. Heymann, G. Pusch, Schweisstechnik 19, Heft 12, 542-545, 1969.
(2.44) E. Heymann, G. Heymann, Schweisstechnik 20, Heft 3, 111-113, 1970.
(2.45) P. Drews, Thesis T.H. Aachen, 1966.

(2.46) S.B. Ainbinder, Welding Production no. 12, 10-18, 1959.
(2.47) S.B. Ainbinder, E.F. Dubrovskii, E.F. Rastrigina, Soviet Physics – Doklady 13 no. 4, 339-340, 1968.
(2.48) H. Czichos, Journal of Physics D: Applied Physics 5, 1890-1897, 1972.
(2.49) D.V. Keller, R.G. Aldrich, Journal of Adhesion 1, 142-156, 1969.
(2.50) F.P. Bowden, D. Tabor, The Friction and Lubrication of Solids, Clarendon Press, Oxford; Part I, 1954; Part II, 1964.
(2.51) J.L. McFarlane, D. Tabor, Proc. of the Royal Society A 202, 244-253, 1950
(2.52) J.S. Courtney-Pratt, E. Eisner, Proc. of the Royal Society A 238, 529-550, 1957.
(2.53) N. Gane, P.F. Phaelzer, D. Tabor, Proc. of the Royal Society A 340, 495-517, 1974.
(2.54) K.I. Johnson, D.V. Keller, Journal of Applied Physics 38, 1896-1904, 1967.
(2.55) D.V. Keller, Proc. of the Holm Seminar on Electric Contact Phenomena, Illinois Institute of Technology, Chicago, Illinois, 1971.
(2.56) R.G. Aldrich, D.V. Keller, The Journal of Vacuum Science and Technology 7, no. 6, S82-S89, 1970.
(2.57) K.I. Johnson, D.V. Keller, The Journal of Vacuum Science and Technology 4, no. 3, 115-122, 1967.
(2.58) D.H. Buckley, Proc. of the Conf. on Physics of Adhesion, Karlsruhe, July 14-17, 1969.
(2.59) O.L. Anderson, Wear 3, 253-273, 1960.
(2.60) J.L. Harthoorn, Technical Note. Philips Research Lab., Eindhoven.
(2.61) Welding Handbook, American Welding Society, 6th edition, part 1, London 1969.
(2.62) H.A. Mohamed, J. Washburn, Welding Journal (Research Supplement) 54, 302S-310S, 1975.
(2.63) R. Holm, Electrical contacts, Springer Verlag, Berlin, 1967.
(3.1) A.P. Hulst, Conference proceedings of Ultrasonics International 1973, I.P.C., Guildford 1973.
(3.2) Welding Handbook, sec. 1, 6th edition, American Welding Society, 1968.
(4.1) B.V. Meriin, Yu.V. Kholopov, Welding Production, no. 8, 26-27, 1973.
(4.2) A.H. Cotrell, An introduction to metallurgy, p. 452, London, 1967.
(4.3) S. Kobayashi, E.G. Thomson and C.T. Yang, Mechanics of plastic deformation in metal processing. MacMillan Cy, New York, 1965.
(4.4) P.C. Veenstra, Technische Plasticiteitsleer, Collegedictaat, T.H. Eindhoven, 1969.
(4.5) G. Maronna, B. Weiss, Schweisstechnik 15, Heft 4, 167-171, 1965.
(4.6) Colombier, Hochmann, Stainless and heat resisting steels, London 1967.
(4.7) U.R. Evans, The corrosion and oxidation of metals, London, 1960.
(4.8) E. Rabinowicz, Asle Transactions 10, 400-407, 1967.
(4.9) H. Peeters, J.L. Harthoorn, Technical Note nr. 19/74, Philips Research Laboratories, Eindhoven.

(5.1) J.L. Harthoorn, Ultrasonics International 1973, Conference proceedings p. 43-51, I.P.C. Science and Technology Press Ltd, Guilford, Surrey, 1973.
(6.1) E. Rabinowicz, Friction and wear of metals, chap. 3, p.50, New York, 1965
(6.2) D. Greenwood, D. Tabor, Institute of Mech. Eng.,Conference on Lubrication and Wear, 1957.
(6.3) F.P. Bowden, D. Tabor, Friction and Lubrication of Solids, Part II, p. 353, London 1964.
(6.4) J.F. Archard, W. Hirst, Proc. Roy. Soc. A 236, 397-410, 1956.
(6.5) J.F. Archard, J. of Appl. Physics, 32, no. 8, 1420-1425, 1961.
(6.6) N.P. Suh, Trans. of the ASME, Journal of Lubrication Technology 96F, 631-637, 1974.
(6.7) E.A. Neppiras, Ultrasonics 3, 128-135, 1965.
(6.8) U.I. Chang, J. Frisch, Welding Journal (Research Supplement) 53, 24S-35S, 1974.
(6.9) R.D. Mindlin, W.P. Mason, Proceedings of the first U.S. National Congress on applied mechanics, p. 203-208, 1951.
(6.10) R.D. Mindlin, H. Deresiewicz, Journal of Appl. Mech., p. 327, Sept. 1953.
(6.11) K.L. Johnson, Proc. Royal Soc. A 230, 531-548, 1955.
(6.12) K.L. Johnson, Journal Mech. Eng. Sci., 3/4, 362-368, 1961/62.

(A.1) F. Blaha, B. Langenecker, Naturwissenschaften 20, 556, 1955.
(A.2) F. Blaha, B. Langenecker, Acta Metallurgica 7, 93-100, 1959.
(A.3) F. Blaha, B. Langenecker, Zeitschrift für Metallkunde 51, 636-638, 1960.
(A.4) B. Langenecker, Am. Inst. of Aeronautics and Astronautics, Journal 1, 80-83, 1963.
(A.5) B. Langenecker, SAE Transactions 74, 499-505, 1966.
(A.6) B. Langenecker, IEEE Transactions on Sonics and Ultrasonics, Vol. SU-13 no.1, 1-8, 1966.
(A.7) G.E. Nevill, F.R. Brotzen, Proc. Am. Soc. for Testing Materials 57, 751-758, 1957.
(A.8) G.S. Baker, S.H. Carpenter, Trans. of the Metallurgical Soc. of AIME 236, 700-702, 1966.
(A.9) R. Friedrich, G. Kaiser, W. Pechhold, Zeitschrift für Metallkunde 60, 390-398, 1969.
(A.10) R. Friedrich, U. Engel, Proc. 1st Int. Symp. High-Power Ultrasonics, Graz, Sept. 1970; IPC Business Press, London 1972.
(A.11) E.G. Konovalow, A.L. Skripnichenko, Russian Engineering Journal 46, no. 8, 31-32, 1965.
(A.12) A.L. Skripnichenko, Industrial Laboratories 32, 1180-1190, 1966.
(A.13) P. Pohlman, E. Lehfelt, Ultrasonics 4, 178-185, 1966.
(A.14) G.R. Dawson, C.E. Winsper, D.H. Sansome, Metal Forming, 234-238, 1970; Metal Forming, 254-261, 1970.
(A.15) D.H. Sansome, Proc. of the 1th Int. Symp. High-Power Ultrasonics, Graz 1970, London 1972.

(A.16) B. Langenecker, V.O. Jones, J. Illiewich, Proc. of the 1st Int. Symp. High-Power Ultrasonics, Graz 1970, London 1972.
(A.17) I.L. Gufel'd, M.I. Matveyeva, Physics of Metals and Metallography 17, 141-143, 1964.
(A.18) S.K. Ginzburg, A.M. Miskevich, Yu.G. Nosov, Welding Production, 83-87, no. 5, 1967.
(A.19) A.M. Mitskevich, Ultrasonic Welding of Metals, In: Physical Principles of Ultrasonic Technology, Vol. I, Ed.: L.D. Rozenberg, Plenum Press, New York, London 1973.
(A.20) A.B. Kulemin, A.M. Mitskevich, Proc. of the Seventh International Congress on Acoustics, Budapest, 1971.
(A.21) E.A. Attia, J.C. Shyne, Japanes Journal of Applied Physics 8, 1217-1220, 1969
(A.22) B.F. Walker, V.A. Johnson, W.C. Hahn, J.D. Wood, Trans. of the Metallurgical Society of AIME 242, 1233-1235, 1968.
(A.23) Yu.P. Romashkin, Soviet Physics-Solid State 2, no. 12, 2709-2731, 1961.
(A.24) M.E. Sikorski, Trans. of the ASME: Journal of Basic Engineering 85, 279-305, 1963.
(A.25) M.E. Sikorski, J.S. Courtney-Pratt, ASLE Lubrication Conference, Oct. 1963. ASLE paper no. 63 LC-16.
(A.26) M.E. Sikorski, In: Mechanisms of Solid Friction, ed.: P.J. Bryant, M. Lavic and G. Solomon, Elsevier, Amsterdam, 1964.
(A.27) J.A. Bailey, M.E. Sikorski, Wear 14, 181-192, 1969.
(A.28) J.M. Bradford, M.E. Sikorski, Wear 16, 413-419, 1970.
(A.29) D.H. Buckley, R.L. Johnson, Wear 11, 405-419, 1968.
(A.30) I.G. Nosovskii, E.V. Isaev, B.I. Kostetskii, Soviet Physics – Doklady, 16, 393-395, 1971.
(A.31) E. Rabinowicz, Friction and Wear of Metals, John Wiley and Sons, New York, 1965.
(A.32) E. Rabinowicz, Compatibility Criteria for Sliding Metals; In: Friction and Lubrication in Metal Processing, ed.: Ling, Whiteley: ASME, New York, 1966.
(A.33) E. Rabinowicz, Journal of the Institute of Metals 95, 321-326, 1967.
(A.34) E. Rabinowicz, ASLE Transactions 14, no. 3, 198-205, 1971.
(A.35) E. Rabinowicz, ASLE Transactions 14, no. 3, 206-212, 1971.
(A.36) H.S. Carlslaw, J.C. Jaeger, Conduction of Heat in Solids, Oxford 1959.
(A.37) J.H. Dautzenberg, J.H. Zaat, Wear 23, 9-19, 1973.
(A.38) M. Jakob, Heat Transfer, New York, London 1955.

Het onderzoek dat aan dit proefschrift ten grondslag ligt, werd uitgevoerd op het Centrum voor Fabricagetechnieken (C.F.T.) van de N.V. Philips' Gloeilampenfabrieken te Eindhoven, terwijl ik medewerker van het Natuurkundig Laboratorium was.
Ik dank de directies van genoemde bedrijfsonderdelen voor de vrijheid om dit werk op de hier gepresenteerde wijze af te ronden.
Verder dank ik allen die mij bij dit onderzoek met raad en daad bijstonden.

STELLINGEN

J.L. Harthoorn

14 april 1978

I

Thermische effecten zijn voor de verklaring van de lasvorming bij het ultrasoon metaallassen niet noodzakelijk.

II

De flitstemperaturen die in het contactvlak bij ultrasoon metaallassen optreden bedragen enkele graden Kelvin.

III

Bij wetenschappelijk onderzoek is de keuze van het onderwerp, de te volgen weg en uitwerking sterk afhankelijk van persoonlijke smaak, inzicht en voorgeschiedenis van de betrokken onderzoeker(s); de invloed van deze niet objectieve factoren wordt bij het vastleggen van de resultaten ten onrechte veronachtzaamd.

IV

De overeenkomst, die Ferrante en Smith zien tussen hun berekeningen van de interactie energie van metaaloppervlakken en de door Sikorski gemeten waarden van adhesiekrachten bij Al, Zn en Mg, is zeer aanvechtbaar.

J. Ferrante, J.R. Smith, Surface Science 38, 77 - 92, 1973;
M.E. Sikorski, Wear 7, 144 - 162, 1964.

V

De door internationale organisaties en nationale overheden in het kader van ontwikkelingssamenwerking uitgezonden personen, worden in de voor hun taakvervulling noodzakelijke aanpassing ernstig gehinderd door de hoogte van hun besteedbaar inkomen.

VI

Het is onwaarschijnlijk dat door mensen vervaardigde systemen voor seizoenopslag van zonne-energie in deze eeuw op een schaal van enige betekenings zullen worden toegepast.

VII

In Europa ligt de eerste economisch aantrekkelijke toepassing van warmtepompen in woonhuizen op het gebied van de warmwatervoorziening.

VIII

De experimentele onderzoeker dient erop te letten dat zijn conclusies gebaseerd zijn op experimenten en niet op het menselijk voorstellingsvermogen.

IX

De, in de titel van een door Thalhammer geschreven artikel vervatte, uitspraak: "Elektriciteit voor verwarmingsdoeleinden is verspilling" is in zijn algemeenheid onjuist.

T. Thalhammer, pt/aktueel, 9 februari 1977.

X

De vergelijking die Heinrich Böll maakt tussen de onnauwkeurigheid bij de berekening van een technische constructie en de poëzie is helaas noch voor het begrip van techniek noch voor het begrip van poëzie verhelderend.

Heinrich Böll, Versuch über die Vernunft der Poesie, Nobelvorlesung, Stockholm 1973.

XI

Het gebruik van gele natriumlampen voor verlichting van de weg in de buurt van verkeerslichten kan, met het oog op kleurenblinde weggebruikers, onverantwoord zijn.